

The physics of angular momentum radio

B. Thidé,^{1,*} F. Tamburini,^{2,†} H. Then,³ C. G. Smeda,² and R. A. Ravanelli⁴

¹*Swedish Institute of Space Physics, Ångström Laboratory, P. O. Box 537, SE-75121 Uppsala, Sweden, EU*

²*Twist Off S.R.L., via della Croce Rossa 112, IT-35129 Padova, Italy, EU*

³*University of Bristol, Department of Mathematics, University Walk, Bristol BS8 1TW, England, UK*

⁴*SIAE Microelettronica, 21, via Michelangelo Buonarroti, IT-20093 Cologno Monzese, Milan, Italy, EU*

(Dated: 2015-05-28 19:52:28 +0200 (Thu, 28 May 2015))

To this day, wireless communications, as well as radio astronomy and other radio science and technology applications, have made predominantly use of techniques built on top of the electromagnetic linear momentum physical layer. As a supplement and/or alternative to this conventional approach, techniques rooted in the electromagnetic angular momentum (moment of momentum) physical layer have been advocated, and promising results from proof-of-concept laboratory and real-world angular momentum wireless and fiber communication experiments were recently reported. A physical observable in its own right, albeit much more sparingly used than other electromagnetic observables such as energy and linear momentum, the angular momentum exploits the rotational symmetry of the electromagnetic field and the rotational (spinning and orbiting) dynamics of the pertinent charge and current densities. Here we present a review of the fundamental physical properties of the electromagnetic angular momentum observable, derived from the fundamental postulates of classical electrodynamics (the Maxwell-Lorentz equations), and put it into its context among the other Poincaré symmetry invariants of the electromagnetic field. The multi-mode quantized character and other physical properties that sets the classical electromagnetic angular momentum apart from the electromagnetic linear momentum are pointed out. We give many of the results both in terms of the electric and magnetic field vectors and in terms of the complex Riemann-Silberstein vector formalism (Majorana-Oppenheimer representation of classical electrodynamics) and discuss formal parallels with first quantization formalism. We introduce generalized and symmetrized extensions of the Jefimenko integral formulas for calculating exact expressions for the electric and magnetic fields directly from arbitrary given electric and/or magnetic source distributions and use them for deriving expressions for the volumetric density of the electromagnetic angular momentum radiated from any given arbitrary localized distribution of charges and currents. Our results generalize earlier results, obtained by other authors for certain specific configurations only, and facilitate the modeling and design of angular momentum transducers. They show that the volume integrated angular momentum density, *i.e.*, the total angular momentum emitted by the sources, always tends asymptotically to a constant when the distance from the source volume tends to infinity, proving that a radiation arrow of time exists also for angular momentum, as it does for linear momentum (the volume integrated Poynting vector). Consequently, angular momentum physics (torque action) offers an alternative or a supplement to linear momentum physics (force action) as a means of transferring information wirelessly over very long distances. This finding opens possibilities for, among other things, a more flexible utilization of the radio frequency spectrum and paves the way for the development of new information transfer techniques. We discuss implementation aspects and illustrate them by examples based on analytic and numerical analyses. References are made to experiments demonstrating the feasibility of using angular momentum in real-world applications, and how the vortical beams can be shaped and their divergence controlled. A scenario with angular momentum transducers of new types, including optomechanical ones and those based on the interplay between charge, spin and orbital angular degrees of freedom, heralded by recent advances in spintronics/orbitronics, condensed-matter skyrmion and quantum ring physics and technology, is briefly delineated. Our results can be readily adapted and generalized to other symmetry related radiation phenomena and information transfer scenarios.

PACS numbers: 03.65.Ud,14.70.Bh,42.50.Tx

CONTENTS

I. Introduction	2	A. Electromagnetic fields and observables	8
II. Background	3	1. Purely electric sources	9
III. Physics	8	B. Useful approximations	10
		1. The paraxial approximation	10
		2. The far-zone approximation	11
		IV. Implementation	13
		A. Wireless information transfer with linear momentum	13
		B. Wireless information transfer with angular momentum	14
		1. Spin angular momentum (SAM) vs. orbital angular momentum (OAM)	15
		2. Angular momentum transducers	15

* Electronic address: bt@irfu.se; Home page: www.physics.irfu.se/~bt; Also at: University of Padua, Scuola Galileana di Studi Superiori, via VIII Febbraio 1848 n. 2, IT-35122 Padua, Italy, EU.

† Electronic address: fabrizio.tamburini@unipd.it; Also at: University of Padua, Department of Physics and Astronomy, via Marzolo 8, IT-35131 Padua, Italy, EU.

3. Electric dipoles	16
C. Angular momentum and multi-transducer/space-division techniques	18
V. Summary	19
Acknowledgments	20
A. The ten Poincaré invariants and the corresponding equations of continuity	20
1. Energy	21
2. Linear momentum	21
a. Gauge invariance	22
b. First quantization formalism	23
3. Angular momentum	23
a. Gauge invariance	24
b. First quantization formalism	25
4. Boost momentum	25
B. Hertzian dipoles	26
1. Hertzian dipoles directed along the three Cartesian axes	26
References	28

I. INTRODUCTION

Transferring information wirelessly by means of electromagnetic fields amounts to generating such fields within a spatial volume of finite extent, encoding information onto physical observables carried by these fields, radiating the observables as volumetric densities into the surrounding space, converting them remotely into observables by using volume integrating sensors, and feeding these observables into information-decoding receivers. The volumetric density of each observable is second order (quadratic, bilinear) in the fields, falls off asymptotically in space as the square of the distance from the source, and fulfills a conservation law. Of all physical observables carried by the electromagnetic field, only the linear momentum (volume integrated Poynting vector, “power”) is fully exploited in present-day radio science and communication applications.

A fundamental physical limitation of the linear momentum vectorial observable, which exploits only the *translational* symmetry and the pertinent degrees of freedom of the electromagnetic field, is that it is single-mode in the sense that a linear momentum radio communication link comprising one single transmitting and one single receiving transducer of a conventional type (*e.g.*, a linear half-wave dipole antenna), known as a single-input-single-output (SISO) link, provides only one physical channel per carrier frequency.

In contrast, electromagnetic angular momentum, the pseudo-vectorial physical observable that manifests the *rotational* symmetry of the electromagnetic field, is multi-mode, being a superposition of discrete, mutually independent classical electromagnetic angular momentum eigenmodes, each uniquely identified by the number of 2π that the phase of the field varies

azimuthally during one oscillation period, *i.e.*, by its topological charge. This allows a frequency reuse in the sense that several independent angular momentum channels can co-exist on the same carrier frequency.

Hence, a wireless communication link designed so that the transmitting and receiving ends each are equipped with a single, monolithic transducer, allowing the dynamics of the charges to be two- or three-dimensional, thus enabling the generation and detection of angular momentum modes directly, would constitute an angular momentum SISO link system. The multi-mode property of the angular momentum allows such a system to accommodate multiple physical information transfer channels on a single carrier frequency and within the same frequency bandwidth as that of a single-channel linear momentum SISO system. The actual number of physical angular momentum channels that can be realized in a given application and/or setup is limited classically only by engineering and implementation issues.

The multi-mode capability of systems based on electromagnetic angular momentum is a consequence of the fact that different angular momentum eigenmodes are topologically distinct and linearly independent by virtue of their mutual functional orthogonality in a Hilbert space of denumerably infinite dimension. Even in situations when the different eigenmodes overlap in space, time and frequency, the individual angular momentum eigenmodes are physically independent and separable and can be extracted by using efficient angular momentum mode filtering techniques.

In order to put angular momentum into its proper physical context and on a firm theoretical basis, we first review the conservation/symmetry properties of the electromagnetic field that make wireless information transfer possible. Then we continue with a theoretical presentation of the physics itself, touching upon first quantization quantum-like aspects of classical electrodynamics and its observables.

We derive generic expressions for the angular momentum density and prove that for any system described by the Maxwell equations, the magnitude of the electromagnetic angular momentum always tends to a constant far away from an arbitrary source. This has earlier been shown only for specific source configurations or in certain approximations.

Furthermore, we discuss concepts and issues related to the exploitation of the angular momentum physical layer in practical implementations, both formally and by way of examples. To supplement and support this theoretical approach, we also report experimental results. Both those obtained by using conventional radio and antenna technologies, as well as results from innovative experiments showing how one can shape of angular momentum carrying beams and control their spatial divergence. We also delineate the possibilities for completely new concepts in transducer design and technology that are offered by recent advances in nano- and optomechanics, spintronics and orbitronics.

A theoretical description of electromagnetic angular momentum in the context of the ten Poincaré symmetry invariants and the associated conservation laws is presented in an Appendix where, among other things, exact, gauge-invariant expressions, valid for sources for which the magnetic vector potential falls

off spatially sufficiently rapidly, are derived for both the linear and angular momenta. In another Appendix we derive exact expressions, valid in all space, for the fields from one or more electric Hertzian dipoles, and for second-order field quantities that enters the expressions for the linear and angular momentum densities, as well as other locally conserved quantities, carried by these fields.

II. BACKGROUND

Transferring information electromagnetically is made possible by the fundamental property of the electromagnetic field (\mathbf{E}, \mathbf{B}) to be able to carry physical observables, *i.e.*, directly measurable intrinsic and extrinsic electromagnetic quantities, over long distances through free space, solids, fluids, gases, and plasmas. These observables are generated within a volume of finite spatial extent (the source volume V' ; *e.g.*, a transmitting antenna), propagated in the form of volumetric densities to a remotely located volume of likewise finite spatial extent (the observation volume V ; *e.g.*, a receiving antenna) over which they are volume integrated into observables, allowing the information carried by them to be subsequently extracted and decoded.

The volumetric density of every electromagnetic observable carried by the fields \mathbf{E}, \mathbf{B} is a linear combination of quantities that are second order (quadratic, bilinear) in the fields, such as $\mathbf{E} \cdot \mathbf{E}$, $\mathbf{B} \cdot \mathbf{B}$, $\mathbf{E} \times \mathbf{B}$, $\mathbf{x} \times (\mathbf{E} \times \mathbf{B})$, and/or of derivatives of the fields. These quantities fulfill local equations of continuity, and are therefore conserved. As shown by Noether [1], this conservation is a manifestation of a symmetry of the Maxwell theory [2–4]. In classical physics terms the observables, and their volumetric densities, are viewed as the result of dynamical changes in the charged particle distribution in the source volume V and, causally, in the observation volume V' , as discussed in Appendix A.

In classical electrodynamics the interplay between the microscopic electric charge and current densities $\rho^e(t, \mathbf{x})$ and $\mathbf{j}^e(t, \mathbf{x})$ and the electric and magnetic fields, $\mathbf{E}(t, \mathbf{x})$ and $\mathbf{B}(t, \mathbf{x})$, as well as between the fields themselves, are described by the Maxwell-Lorentz equations. Allowing for magnetic charge and current densities, represented by the pseudoscalar $\rho^m(t, \mathbf{x})$ and the pseudovector $\mathbf{j}^m(t, \mathbf{x})$, respectively, reflecting the dual symmetry of the theory [5–7], these equations can be written in the symmetrical form [8–10]

$$\nabla \cdot \mathbf{E} = \frac{\rho^e}{\epsilon_0} \quad (1a)$$

$$\nabla \cdot \mathbf{B} = \frac{\rho^m}{\epsilon_0 c^2} \quad (1b)$$

$$\nabla \times \mathbf{E} + \frac{\partial \mathbf{B}}{\partial t} = -\frac{1}{\epsilon_0 c^2} \mathbf{j}^m \quad (1c)$$

$$\nabla \times \mathbf{B} - \frac{1}{c^2} \frac{\partial \mathbf{E}}{\partial t} = \frac{1}{\epsilon_0 c^2} \mathbf{j}^e \quad (1d)$$

where c is the speed of light in free space and ϵ_0 is the dielectric permittivity of free space. This set of linear, inhomogeneous, coupled, partial differential equations are the postulates of

Table I. Various second-order products of the Riemann-Silberstein vector $\mathbf{G} = \mathbf{E} + ic\mathbf{B}$ with itself and their meaning in terms of quadratic and bilinear products of the fields \mathbf{E} and \mathbf{B} . An asterisk (*) denotes complex conjugate, and \otimes denotes the tensor (Kronecker, dyadic) product operator.

Complex notation	Real notation
$\mathbf{G} \cdot \mathbf{G}$	$\mathbf{E} \cdot \mathbf{E} - c^2 \mathbf{B} \cdot \mathbf{B} + 2ic\mathbf{E} \cdot \mathbf{B}$
$\mathbf{G} \cdot \mathbf{G}^* = \sqrt{(\mathbf{G} \cdot \mathbf{G})(\mathbf{G} \cdot \mathbf{G}^*)}$	$\mathbf{E} \cdot \mathbf{E} + c^2 \mathbf{B} \cdot \mathbf{B} \equiv E^2 + c^2 B^2$
$\mathbf{G} \times \mathbf{G}$	$\mathbf{0}$
$\mathbf{G}^* \times \mathbf{G} = -\mathbf{G} \times \mathbf{G}^*$	$2ic(\mathbf{E} \times \mathbf{B})$
$\mathbf{G} \otimes \mathbf{G}$	$\mathbf{E} \otimes \mathbf{E} - c^2 \mathbf{B} \otimes \mathbf{B} + ic(\mathbf{E} \otimes \mathbf{B} + \mathbf{B} \otimes \mathbf{E})$
$\mathbf{G}^* \otimes \mathbf{G}^* = (\mathbf{G} \otimes \mathbf{G})^*$	$\mathbf{E} \otimes \mathbf{E} - c^2 \mathbf{B} \otimes \mathbf{B} - ic(\mathbf{E} \otimes \mathbf{B} + \mathbf{B} \otimes \mathbf{E})$
$\mathbf{G} \otimes \mathbf{G}^*$	$\mathbf{E} \otimes \mathbf{E} + c^2 \mathbf{B} \otimes \mathbf{B} - ic(\mathbf{E} \otimes \mathbf{B} - \mathbf{B} \otimes \mathbf{E})$
$\mathbf{G}^* \otimes \mathbf{G} = (\mathbf{G} \otimes \mathbf{G}^*)^*$	$\mathbf{E} \otimes \mathbf{E} + c^2 \mathbf{B} \otimes \mathbf{B} + ic(\mathbf{E} \otimes \mathbf{B} - \mathbf{B} \otimes \mathbf{E})$

classical electrodynamics from which all properties of the classical electromagnetic field, its observables, and interactions can be derived. These postulates are valid for radio and optical wavelengths alike inasmuch as they are scale invariant and are therefore valid for classical wireless information transfer at all frequencies.

It is often convenient to combine the real-valued fields \mathbf{E} and \mathbf{B} into the complex-valued Riemann-Silberstein vector [11–15]

$$\mathbf{G}(t, \mathbf{x}) = \mathbf{E}(t, \mathbf{x}) + ic\mathbf{B}(t, \mathbf{x}), \quad i^2 = -1 \quad (2)$$

some properties of which are listed in Table I. Expressing the charge and current densities in their complex forms

$$\rho(t, \mathbf{x}) = \rho^e(t, \mathbf{x}) + \frac{i}{c} \rho^m(t, \mathbf{x}) \quad (3a)$$

$$\mathbf{j}(t, \mathbf{x}) = \mathbf{j}^e(t, \mathbf{x}) + \frac{i}{c} \mathbf{j}^m(t, \mathbf{x}) \quad (3b)$$

we see that Dirac's symmetrized Maxwell-Lorentz equations (1) become

$$\nabla \cdot \mathbf{G} = \frac{\rho}{\epsilon_0} \quad (4a)$$

$$\nabla \times \mathbf{G} = \frac{i}{c} \frac{\partial \mathbf{G}}{\partial t} + \frac{i}{\epsilon_0 c} \mathbf{j} \quad (4b)$$

Following Białyński-Birula and Białyńska-Birula [16, 17], who instead of \mathbf{G} use a differently normalized complex vector, *viz.* $\mathbf{F} = \mathbf{G} \sqrt{\epsilon_0/2}$, we first introduce the linear momentum operator for the electromagnetic field,

$$\hat{\mathbf{p}}^{\text{field}} = \sum_{i=1}^3 \hat{\mathbf{x}}_i \hat{p}_i^{\text{field}} = \sum_{i=1}^3 \hat{\mathbf{x}}_i \left(-i\hbar \frac{\partial}{\partial x_i} \right) = -i\hbar \nabla \quad (5)$$

where \hbar is the normalized Planck constant. Secondly, we introduce the vector-like symbolic construct

$$\mathbf{S} \equiv \sum_{i=1}^3 S_i \hat{\mathbf{x}}_i \quad (6a)$$

with components

$$S_1 = \begin{pmatrix} 0 & 0 & 0 \\ 0 & 0 & -i \\ 0 & i & 0 \end{pmatrix} \quad S_2 = \begin{pmatrix} 0 & 0 & i \\ 0 & 0 & 0 \\ -i & 0 & 0 \end{pmatrix} \quad S_3 = \begin{pmatrix} 0 & -i & 0 \\ i & 0 & 0 \\ 0 & 0 & 0 \end{pmatrix} \quad (6b)$$

i.e., spin-1 matrices fulfilling the angular momentum commutation rule

$$[S_i, S_j] = -i\epsilon_{ijk}S_k, \quad (6c)$$

where

$$\epsilon_{ijk} = \begin{cases} 1 & \text{if } i, j, k \text{ is an even permutation of } 1, 2, 3 \\ 0 & \text{if at least two of } i, j, k \text{ are equal} \\ -1 & \text{if } i, j, k \text{ is an odd permutation of } 1, 2, 3 \end{cases} \quad (6d)$$

is the totally antisymmetric rank-3 pseudotensor (the Levi-Civita symbol). Thirdly, we introduce the field helicity operator

$$\hat{\Lambda} = \frac{\mathbf{S} \cdot \hat{\mathbf{p}}^{\text{field}}}{|\hat{\mathbf{p}}^{\text{field}}|} \equiv \frac{\sum_{i=1}^3 S_i \hat{p}_i^{\text{field}}}{|\hat{\mathbf{p}}^{\text{field}}|} \quad (7)$$

Using Eqns. (5), (6), and (7), we can write the Maxwell-Lorentz equations (1) in free space and other domains where $\rho^e = \rho^m = 0$ and $\mathbf{j}^e = \mathbf{j}^m = \mathbf{0}$ in the form

$$\hat{\mathbf{p}}^{\text{field}} \cdot \mathbf{G} = 0 \quad (8a)$$

$$i\hbar \frac{\partial \mathbf{G}}{\partial t} = \hat{H}^{\text{field}} \mathbf{G} \quad (8b)$$

where

$$\hat{H}^{\text{field}} = c|\hat{\mathbf{p}}^{\text{field}}|\hat{\Lambda} = c\mathbf{S} \cdot \hat{\mathbf{p}}^{\text{field}} \equiv c \sum_{i=1}^3 S_i \hat{p}_i^{\text{field}} \quad (9)$$

Recalling the quantal relation $\mathbf{p}^{\text{field}} = \hbar\mathbf{k}$, where $\mathbf{k} = k\hat{\mathbf{k}}$ is the wave vector, $k = 2\pi/\lambda$, and λ is the wavelength, we see that the first equation, Eqn. (8a), is the transversality condition, $\mathbf{k} \perp \mathbf{G}$, for electromagnetic waves propagating in free space, whereas the second equation, Eqn. (8b), describes the dynamics of the field and takes the form of a Schrödinger/Pauli/Dirac-like equation where \hat{H}^{field} behaves as a Hamilton operator for the free electromagnetic field. The electromagnetic theory that corresponds to classical mechanics is the geometrical optics (a.k.a. eikonal or “ray optics”) approximation of the Maxwell-Lorentz equations [18].

The solutions of Eqn. (8b) can, in certain aspects, be viewed as first quantization photon wave functions that obey the superposition principle [7, 18–49]. It should be noted, however, that Cohen-Tannoudji *et al.* [50, p. 204] argue against “... suggesting (in spite of warnings) the false idea that the Maxwell waves are the wave functions of the photon.” See also Li [51] and Andrews [52].

For any given, prescribed set of charge and current densities, every electromagnetic observable can be calculated with, in principle, arbitrary accuracy from the first order fields \mathbf{E} and \mathbf{B}

that are solutions of Eqns. (1). As was pointed out by Silberstein [12, 13], it is very convenient to calculate these second order quantities in a formalism based on the use of the complex Riemann-Silberstein vector (2), known as the Majorana-Oppenheimer formalism. This formalism is also convenient for canonical (second) quantization of the electromagnetic field [16, 36].

However, the fields themselves are abstractions in the sense that they cannot be measured directly but have to be estimated from measurements of physical observables that are quadratic or bilinear in the fields. To quote Dyson [53]:

“The modern view of the world that emerged from Maxwell’s theory is a world with two layers. The first layer, the layer of the fundamental constituents of the world, consists of fields satisfying simple linear equations. The second layer, the layer of the things that we can directly touch and measure, consists of mechanical stresses and energies and forces. The two layers are connected, because the quantities in the second layer are quadratic or bilinear combinations of the quantities in the first layer. ... The objects on the first layer, the objects that are truly fundamental, are abstractions not directly accessible to our senses. The objects that we can feel and touch are on the second layer, and their behavior is only determined indirectly by the equations that operate on the first layer. The two-layer structure of the world implies that the basic processes of nature are hidden from our view.”

“The unit of electric field-strength is a mathematical abstraction, chosen so that the square of a field-strength is equal to an energy-density that can be measured with real instruments. ... It means that an electric field-strength is an abstract quantity, incommensurable with any quantities that we can measure directly.”

“It may be helpful for the understanding of quantum mechanics to stress the similarities between quantum mechanics and the Maxwell theory.”

From these considerations it should be clear that it is essential to analyze not only the properties of the fields \mathbf{E} and \mathbf{B} as such but also the properties of the electromagnetic observables, which are second order in these fields or derivatives thereof, in order to satisfactorily assess and optimally exploit the information-carrying capability of the classical electromagnetic field. In Sect. III we will show that for any conceivable distribution of sources of the electromagnetic field, the physical observables (the volume integrated densities) tend to a constant value when they propagate in free space and the distance from the radiation source tends to infinity. This means that there exists no finite distance from the source at which any of these observables tends to zero or beyond which it vanishes globally. Consequently, they can all carry information over arbitrary large distances in free space, albeit subject to engineering limitations (spatial and temporal distribution, transducer geometry, detector sensitivity, integration time, ...).

Of all physical observables that may potentially be used for wireless information transfer, present-day radio science and engineering implementations almost exclusively make full use only of the linear momentum vectorial observable. For instance, a conventional receiving antenna is typically wire-like, *i.e.*, the observation volume V is a very thin cylinder where current-carrying electrons are constrained to move in one dimension, resulting in a scalar, dissipative conduction current flowing along the cylinder axis. The electrons can be viewed as moving relative to a fixed neutralizing background of heavy ions with negligible recoil. Such an antenna, typically with a length L of the order half a wavelength λ , *i.e.*, $L \sim \lambda/2 = \pi/k$, senses a projection of the field linear momentum density vector $\mathbf{p}^{\text{field}}$ and integrates the component of the electric conduction current density vector $\mathbf{j}^e(t, \mathbf{x})$ over L along the axis of the thin, cylindrical antenna into a time-varying, spatially averaged scalar conduction current. This scalar current is fed to the receiver equipment (usually an electronics device) where it is processed and the wirelessly transferred information is extracted. In the process, the vector property of the current density is not exploited and information may therefore be wasted.

Linear momentum wireless information transfer techniques have the advantage of being simple, robust, and easy to implement, but have the drawback that they can be wasteful when it comes to the use of the frequency spectrum. This is because electromagnetic linear momentum is single-mode, permitting only one independent linear-momentum physical channel of information transfer per carrier frequency (per wave polarization, per antenna). The ensuing over-crowding of the radio frequency bands, often referred to as the “spectrum crunch”, has become a serious problem in radio communications. It also imposes limitations on radio astronomy and other radio science applications as well as on fiber optics communications. It is doubtful whether further evolutionary refinements of conventional techniques and methods built on the linear momentum density (*i.e.*, Poynting vector) physics layer alone will, in the long term, suffice to remedy these problems.

This situation has led to the idea of exploiting so far under-utilized physical observables of the electromagnetic field that do not suffer from the inherent information-carrying limitation of present-day radio techniques. The development and exploitation of a new physical layer that provides additional information-carrying capabilities already at the fundamental physics level, before any multi-transducer or other spectral density enhancing techniques are applied at the engineering application layer, will set the stage for new radio paradigms that may enable a wiser exploitation of the radio frequency spectrum resource and for new types of transducers.

Specifically, it has been proposed that the electromagnetic angular momentum (moment of momentum) pseudovectorial observable, discussed already by Maxwell in his writings in the 1860’s [54], studied by other authors since over a century [55–58], and nowadays treated in standard physics textbooks [7, 8, 50, 59–67], be fully exploited in radio science and technology [9, 68–75]. The rationale being that it has been demonstrated in experiments at microwave and optical wavelengths that by exploiting the electromagnetic angular mo-

mentum, one may enhance the information-carrying capability of wireless communications substantially [73, 74, 76–86].

This enhancement is mainly due to the fact that angular momentum is discretized (quantized) already at the classical level. The electric and magnetic fields in a beam that carries a non-integer amount of electromagnetic angular momentum is namely a superposition of discrete angular momentum eigenmodes, *i.e.* vortices [87, 88]. Each eigenmode is characterized by a unique integer that denotes its azimuthal quantum number (mode index), also known as the topological charge.

As an illustration, let us consider a radio or light beam that propagates in free space. Expressed in cylindrical coordinates (ρ, φ, z) and in complex notation, an individual electric field vector $\mathbf{E}(t, \mathbf{x})$ of the beam is assumed to be given by the expression

$$\mathbf{E}(t, \rho, \varphi, z) = R(\rho)\Phi(\varphi)Z(z)T(t)\mathbf{E}_0 \quad (10)$$

where

$$\mathbf{E}_0 = E_0\hat{\mathbf{e}} = |E_0|e^{i\delta_0}\hat{\mathbf{e}} \quad (11)$$

Here E_0 and δ_0 are real-valued scalar constants, but we allow the unit vector $\hat{\mathbf{e}}$ to be complex, *e.g.*, a linear combination of the helical base vectors

$$\hat{\mathbf{x}}_{\pm} = \frac{1}{\sqrt{2}}(\hat{\mathbf{x}} \pm i\hat{\mathbf{y}}) \quad (12)$$

that represent circularly polarized wave fields.

We assume that the field \mathbf{E} has a strongly peaked longitudinal wave vector spectrum containing essentially only one single longitudinal wave vector component k_z , corresponding to the linear momentum z component $p_z = \hbar k_z$ carried by each photon of the beam, and that the z dependence of the field therefore can be written

$$Z(z) = Z_0(\Omega z)e^{ik_z z} \quad (13a)$$

where $Z_0(\Omega z)$ is a slowly varying real-valued envelope function of z , as indicated by the slowness parameter Ω . Likewise, assuming also an essentially single temporal mode, we write

$$T(t) = T_0(\Omega t)e^{-i\omega t} \quad (13b)$$

where $T_0(\Omega t)$ is a slowly varying real-valued function of time t , and ω is the angular frequency, corresponding to the energy $\hbar\omega$ carried by each photon of the beam.

The radial part $R(\rho)$ describes the variation of \mathbf{E} in the radial, ρ , direction, perpendicular to the z direction. Assuming well-behavedness in the usual manner, we can represent R , which is real-valued, as a Fourier integral

$$R(\rho) = \int dk_{\rho} R_{k_{\rho}} e^{ik_{\rho}\rho} \quad (13c)$$

where the complex Fourier amplitudes are

$$R_{k_{\rho}} = \frac{1}{2\pi} \int d\rho R(\rho) e^{-ik_{\rho}\rho} \quad (13d)$$

and k_ρ is the radial (ρ) component of the wave vector.

The azimuthal part $\Phi(\varphi)$ describes the variation of \mathbf{E} in the direction perpendicular to both z and ρ . If Φ is well-behaved enough that it can be represented by a (complex) Fourier series [cf. Yao *et al.* [89, Eqn. (2)], Jha *et al.* [90, Eqns. (1)–(2)], and Jack *et al.* [91, Eqns. (1)–(2)]]

$$\Phi(\varphi) = \sum_{m=-\infty}^{\infty} c_m e^{im\varphi} \quad (13e)$$

where c_m are (constant) Fourier amplitudes, then the electric field \mathbf{E} is a vector sum of discrete angular momentum modes

$$\mathbf{E}(t, \mathbf{x}) = \sum_{m=-\infty}^{\infty} \mathbf{E}_m(t, \rho, \varphi, z) \quad (14a)$$

where

$$\mathbf{E}_m = E_0 Z_0(\Omega z) T_0(t\Omega) R(\rho) e^{i(m\varphi + k_z z - \omega t + \delta_0)} \hat{\mathbf{e}} \quad (14b)$$

$$= E_0 Z_0(\Omega z) T_0(\Omega t) \int dk_\rho R_{k_\rho} e^{i(k_\rho \rho + m\varphi + k_z z - \omega t + \delta_0)} \hat{\mathbf{e}} \quad (14c)$$

In the last step, we used Eqn. (13c).

The $\exp(im\varphi)$ phase factor of the \mathbf{E}_m mode gives the beam a helical phase front and causes a screw dislocation along the z axis. This singularity results in a vanishing linear momentum density (Poynting vector) on the z axis ($\rho = 0$), leading to an annular shape of the linear momentum density. For $m = 0$ the phase front is flat and the field has no phase singularity and the distribution of linear momentum density is not annular.

The smallest radius of the annulus of a beam carrying an OAM $L_z = \hbar m$, $m = \pm 1, \pm 2, \dots$ eigenmode that can be effectively observed is $(|m| - 1/2)\lambda/(2\pi)$ as given by the Bohr-Sommerfeld quantization condition.

If only the φ dependence with $m \neq 0$ is taken into account, then the linear momentum density of the beam would diverge spatially and the radius of the ring-shaped locus of maximum linear momentum density would increase with increasing m as discussed by Padgett *et al.* [92]. However, as can be seen in Eqns. (14), the structure of the amplitude and the phase of \mathbf{E} is determined not only by the azimuthal part Φ , but also by the radial part R and the longitudinal part Z . Hence, by modifying R and Z , which can be done if one uses two- or three-dimensional transducers and/or reflectors, or phased arrays of linear antennas that approximate such transducers, one can structure an OAM-carrying beam. In fact, as has been demonstrated experimentally by Chen *et al.* [93], Ostrovsky *et al.* [94], García-García *et al.* [95], Vaity and Rusch [96], and Li *et al.* [97], it is possible to shape OAM carrying beams so that the radii of the linear momentum annuli do not scale with m .

The quantization of the orbital part of the classical electromagnetic angular momentum is a consequence of the single-valuedness of the electromagnetic fields upon their winding an integer number of 2π in azimuth angle φ around the beam axis z , resulting in a Bohr-Sommerfeld type quantization condition [61, 98–101]. Mathematically the quantization can be understood in terms of the well-known functional space orthogonality condition

$$\frac{1}{2\pi} \int_0^{2\pi} d\varphi (e^{im_1\varphi})^* e^{im_2\varphi} = \delta_{m_1 m_2} \quad (15)$$

where $\delta_{m_1 m_2}$ is the Kronecker delta [68, 77, 102–107]. This mutual orthogonality ensures that different spatially and temporally overlapping L_z^{field} eigenmodes can co-exist on the same carrier frequency ω and in the same polarization state σ without interfering each other, allowing a simultaneous transfer of different information streams independently, without the need for extra frequency bandwidth. In other words, OAM spans a state space of dimension $N = 1, 2, 3, \dots$, and can therefore be regarded as an ‘‘azimuthal (tangential) polarization’’ with arbitrarily many states [78]. This makes it possible, at least in principle, to use OAM to physically encode an unlimited amount of information onto any part of an EM beam, down to the individual photon [108, 109].

Guided by Eqns. (A32), (A52b), and (A53c), we define the expectation value of an observable O^{field} carried by the classical electromagnetic field as

$$\langle O^{\text{field}} \rangle = \langle \mathbf{E}(t, \mathbf{x}) | \hat{O}^{\text{field}} | \mathbf{E}(t, \mathbf{x}) \rangle = \langle \mathbf{G}(t, \mathbf{x}) | \hat{O}^{\text{field}} | \mathbf{G}(t, \mathbf{x}) \rangle \quad (16)$$

The operator for the z component of the orbital angular momentum (OAM) around the z axis is given by Eqn. (A53c). Applying this to the electric field given by expressions (14), we see that

$$\hat{L}_z^{\text{field}} \mathbf{E}(t, \mathbf{x}) = -i\hbar \frac{\partial}{\partial \varphi} \mathbf{E}(t, \mathbf{x}) = \sum_{m=-\infty}^{\infty} c_m m \hbar \mathbf{E}_m(t, \rho, \varphi, z) \quad (17)$$

from which we conclude that in general \mathbf{E} is a weighted vector sum of fields carrying different integer z components OAM. In particular, for a beam that is in an OAM z component eigenstate m ,

$$\hat{L}_z^{\text{field}} \mathbf{E}_m = m \hbar \mathbf{E}_m \quad (18)$$

which means that the z component of the orbital angular momentum of each photon in this beam is $m\hbar$.

In the particular case that the azimuthal part in Eqn. (10) is

$$\Phi(\varphi) = e^{ik_\varphi \rho \varphi} \equiv e^{i\alpha \varphi} \quad (19)$$

where k_φ is the φ (azimuthal) component of the wave vector, and α has a non-integer value [110, 111], the m th Fourier amplitude (13e) is [72, 102, 112]

$$c_m = \frac{\exp(i\pi\alpha) \sin(\pi\alpha)}{\pi(\alpha - m)} \quad (20)$$

and the electric field can be written

$$\mathbf{E}(t, \mathbf{x}) = E_0 Z_0(\Omega z) T_0(\Omega t) R(\rho) e^{i\beta} \hat{\mathbf{e}} \quad (21)$$

where

$$\beta = \alpha \varphi + k_z z - \omega t + \delta_0 = k_\varphi \rho \varphi + k_z z - \omega t + \delta_0 \quad (22)$$

In real-valued notation, the electric field mode under consideration becomes

$$\mathbf{E}(t, \mathbf{x}) = E_0 Z_0(\Omega z) T_0(\Omega t) R(\rho) (\cos \beta \text{Re}\{\hat{\mathbf{e}}\} - \sin \beta \text{Im}\{\hat{\mathbf{e}}\}) \quad (23)$$

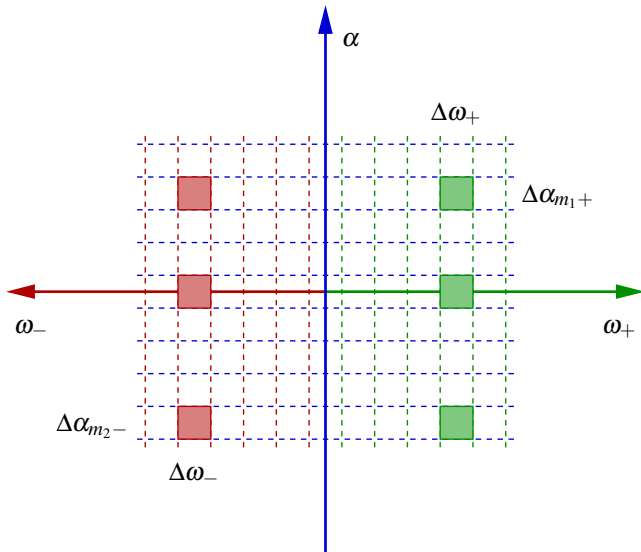


Figure 1. The two-dimensional oscillation/rotation plane spanned by the temporal phase oscillation rate, *i.e.*, the frequency ω (horizontal axis), and the angular phase rotation rate α , *i.e.*, the z component of the orbital angular momentum (OAM) L_z (vertical axis) in units of Planck's normalized constant \hbar . The right-hand, green part of the horizontal axis represents right-hand circular polarization (spin), and the left-hand, red part of the axis represents the opposite, left-hand circular polarization (spin). The α axis is rasterized into rotational frequency bins of azimuthal mode numbers m because of the single-valuedness of the fields that causes a quantization of L_z , and the ω axes are rasterized in terms of bandwidth segments. The solid green squares in the right-hand plane represent different transmission channels on the same carrier frequency ω_+ , with the same frequency bandwidth $\Delta\omega_+$, and in the same spin (polarization) state $\sigma = +1$, but in different rotational frequency bins α_{m_1} and α_{m_2} , corresponding to two different OAM azimuthal quantum numbers m_1 and m_2 , respectively. The solid red squares in the left-hand plane represent transmission channels with the same carrier frequency ($\omega_- = \omega_+$) and frequency bandwidth ($\Delta\omega_- = \Delta\omega_+$) as for the right-hand (green) plane, but in the opposite spin state $\sigma = -1$, still allowing a more optimum use of the frequency spectrum. All possible squares in the (ω_{\pm}, α) plane constitute unique, independent information transfer eigenmode channels $(\omega, \sigma, \alpha_m)$. For instance, the six solid squares in the figure use the same carrier frequency and occupy the same frequency bandwidth. This is therefore an example of a six-fold frequency re-use.

which, of course, is the physically correct form to use when calculating second order quantities such as the densities of the electromagnetic observables that we are discussing here. Alternatively, a description in terms of the Zernike polynomials may be assumed [113–115].

Clearly, an electromagnetic beam carrying an arbitrary amount $\hbar\alpha = \hbar k_{\phi}\rho$ of OAM is a superposition of discrete classical OAM eigenmodes \mathbf{E}_m that are mutually orthogonal in a function space sense and propagate independently of each other in ordinary spacetime [116, 117]. Such a beam therefore exhibits a discrete Fourier spectrum in orbital angular momentum domain α where each angular momentum eigenmode

component occupies a bin

$$\alpha_m \in \{\alpha \in \mathbb{R}; m - 1/2 \leq \alpha < m + 1/2\}, m = 0, \pm 1, \pm 2, \dots \quad (24)$$

This was shown experimentally by Leach *et al.* [118], thus confirming the prediction by Berry [102]; see also Fig. 1, Molina-Terriza *et al.* [119], Jack *et al.* [91], Lavery *et al.* [120], Huang *et al.* [111], and Tamburini *et al.* [72], who used $\alpha = -1.12$.

Orbital angular momentum adds, as it were, an extra dimension of periodic variation, effectively augmenting the one-dimensional ordinary oscillation frequency axis to a two-dimensional frequency plane as outlined graphically in Fig. 1. The horizontal axis represents the usual temporal phase oscillation rate, *i.e.*, the angular frequency $\omega = \partial\beta/\partial t$, whereas the vertical axis represents the angular phase rotation rate, *i.e.*, the orbital angular momentum $\alpha = \partial\beta/\partial\phi$ in a plane perpendicular to the propagation axis of the beam. Since this additional dimension in the frequency is the result of making use of a hitherto largely unexploited physical property of the electromagnetic field, wireless communication based on angular momentum is fundamentally different from present-day wireless engineering techniques. In particular, it does not require arrays of multiple, spaced antennas or other transducers as is the case for spatial division multiplexing techniques, such as the multiple-input-multiple-output (MIMO) technique [121]. Nor does it require massive, power-consuming digital post-processing and has therefore been described as a cost-effective and “green” alternative to MIMO [122] where the algorithms require increasing overheads and the required processing resources scales roughly with M^2 , where M is the mode number [123]. The properties of electromagnetic/photon OAM have been studied for frequencies ranging from low-frequency radio [69] to X-ray [124]. It has been shown that in the optical regime it is possible to generate OAM with an azimuthal mode number of at least $m = 10000$ in free space [125].

From a more fundamental physical point of view, the enhancements made possible by invoking the angular momentum physics layer, compared to systems that are based solely on the linear momentum physics layer, is consistent with the fact that all classical fields carry angular momentum [50, 126, 127] and that the dynamics of a physical system is not completely specified unless both its total linear momentum and its total angular momentum are specified at all instants [128]. Specifying only one of them is not sufficient. Therefore, exploiting only the linear momentum and not the angular momentum of a system of charges, currents and pertinent electromagnetic fields is not exploiting such a system to its full capacity.

From the discussion above, it should be clear that in order to make optimal use of an electromechanical system for radio science and technology, including radio communications, one must, in addition to the one-dimensional translational degrees of freedom represented by the system's linear momentum, invoke also the mechanical and electromagnetic angular momenta of the system [7, 8, 10, 50, 59–65, 67, 129–133], *i.e.*, the rotational degrees of freedom that are necessary to completely and correctly specify the system's two- and three-dimensional dynamics [134–150].

As is the case for electromagnetic linear momentum, elec-

tromagnetic angular momentum can propagate not only in free space, but also in—and interact with—various propagation media [117, 119], including plasmas [9, 151–156]. This includes waveguides [157] and optical fibers [79, 158, 159], where the decay rate, due to absorption, is the same for the propagation of angular momentum as for linear momentum since they are both bilinear in the same electric and magnetic fields.

III. PHYSICS

In this section we introduce symmetrized integral formulas for calculating electromagnetic fields generated by an arbitrary, given distribution of electric and magnetic charges and currents in a volume of finite spatial extent. We then use the results to study the physical properties of the electromagnetic observables carried by these fields. Specifically, we analyze those properties of the electromagnetic angular momentum observable that sets it apart from the electromagnetic linear momentum observable when it comes to information-carrying capacity, within a fixed given frequency bandwidth around a fixed given carrier frequency, for a point-to-point communication link system equipped with single monolithic transducers (“antennas”) at each end of the link. The general formulas derived for the fields are presented in their Majorana-Oppenheimer form and the fields are consistently approximated in both the paraxial and the far-zone approximations, allowing us to derive correctly truncated expressions for the angular momentum density valid in both these approximations.

A. Electromagnetic fields and observables

In classical electrodynamics, different methods are routinely used for calculating electromagnetic fields, and physical observables derived from them, once the sources are given. Commonly the methods amount to solving the Maxwell-Lorentz differential equations (1) in one way or another, or to find the potentials, choose a gauge and then perform the calculations.

Over the past decades, integral equations that allow the immediate calculation of the fields directly from given charge and current distributions have gained increasing attraction; see de Melo e Souza *et al.* [160] and references cited therein. In Chapter VIII of his 1941 textbook, Stratton [161] calculates, without the intervention of potentials, temporal Fourier transform expressions for the retarded electric and magnetic fields, $\mathbf{E}(t, \mathbf{x})$ and $\mathbf{B}(t, \mathbf{x})$, respectively, generated by arbitrary distributions of charge and current densities at rest relative to the observer. In Chapter 14 of the second edition of their textbook on electrodynamics, published in 1962, Panofsky and Phillips [162] present a variant form of these expressions, and give them also in ordinary space-time coordinates. Four years later, Jefimenko published his electrodynamics textbook [163] where the Panofsky and Phillips expressions for the retarded \mathbf{E} and \mathbf{B} fields were given in Chapter 15. These expressions are sometimes referred to as the Jefimenko equations [8, 164], but we propose that they should rather be called the Stratton-Panofsky-Phillips-Jefimenko or the SPPJ equations, a name

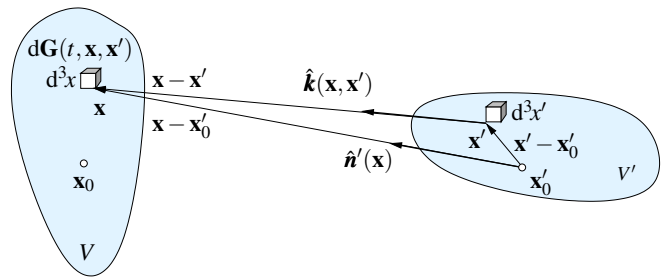


Figure 2. The electric and/or magnetic charges and currents located in the small volume element d^3x' around the point \mathbf{x}' in the source volume V' , with its fixed reference point \mathbf{x}'_0 , give rise to elemental fields in the volume element d^3x around the observation point (field point) \mathbf{x} in the measurement volume V with its fixed reference point \mathbf{x}_0 . In the Figure the volume elements are drawn as small cubes and the fields in d^3x are given in Majorana-Oppenheimer representation by the complex Riemann-Silberstein elemental field vector $d\mathbf{G}(t, \mathbf{x}, \mathbf{x}') = d\mathbf{E}(t, \mathbf{x}, \mathbf{x}') + icd\mathbf{B}(t, \mathbf{x}, \mathbf{x}')$. The elemental fields propagate along the unit vector of $\mathbf{x} - \mathbf{x}'$ that connects \mathbf{x}' with \mathbf{x} , denoted $\hat{\mathbf{k}}(\mathbf{x}, \mathbf{x}')$. If all individual $\hat{\mathbf{k}}(\mathbf{x}, \mathbf{x}')$ from all individual source points \mathbf{x}' in V' that reach \mathbf{x} are almost parallel, for instance if V' has a small lateral extent as seen from \mathbf{x} (as illustrated), all these unit vectors can be approximated by the \mathbf{x}' independent unit vector $\hat{\mathbf{n}}'(\mathbf{x}) \equiv \hat{\mathbf{k}}(\mathbf{x}, \mathbf{x}'_0)$ that connects \mathbf{x}'_0 with \mathbf{x} . This is the paraxial approximation [164].

we will use throughout.

Let us consider a finite (source) volume V' that is located in otherwise empty space (free space) and let V' contain an arbitrary distribution of electric and magnetic charge and current densities $\rho(t', \mathbf{x}')$ and $\mathbf{j}(t', \mathbf{x}')$, given in complex form in Eqns. (3); in conventional radio, V' is the volume in space that is occupied by the transmitting antenna (typically a narrow, straight, electrically conducting cylinder), and $\mathbf{j}^e(t', \mathbf{x}') = \text{Re}\{\mathbf{j}(t', \mathbf{x}')\}$ is the dissipative electric conduction current constrained to oscillate along this essentially one-dimensional transmitting antenna. The fields produced by the sources in V' propagate to a remotely located observer who uses a sensing volume V to integrate (average) the densities of the observables carried by the field in the local volume element d^3x' around the coordinate \mathbf{x} in V . In conventional radio, V comprises the receiving antenna, and $\mathbf{j}^e(t, \mathbf{x}) = \text{Re}\{\mathbf{j}(t, \mathbf{x})\}$ is the dissipative electric conduction current constrained to oscillate along the receiving antenna.

The primary elemental fields $d\mathbf{E}$ and $d\mathbf{B}$ that are set up at time t in d^3x originate from the local dynamics at the retarded time t' of the charges and currents in d^3x' ; see Fig. 2. These elemental fields were emitted at the retarded time

$$t' = t'_{\text{ret}}(t, \mathbf{x}, \mathbf{x}') = t - \frac{|\mathbf{x}(t) - \mathbf{x}'(t')|}{c} \quad (25)$$

and propagated to \mathbf{x} along the local unit vector

$$\hat{\mathbf{k}}(\mathbf{x}, \mathbf{x}') = \frac{\mathbf{x} - \mathbf{x}'}{|\mathbf{x} - \mathbf{x}'|} \quad (26)$$

Choosing a suitable gauge, one can readily calculate exact, closed-form expressions for the electrodynamic scalar and magnetic vector potentials from the electric and magnetic charges

and currents, for a generic source distribution. From these potentials it is possible to derive exact expressions for the corresponding electromagnetic elemental fields—as well as the fields themselves—directly, without the intermediate step of solving the Maxwell-Lorentz equations from first principles or even calculating the explicit potentials themselves [8, 161–164].

If the sources in V' are at rest (*i.e.*, have negligible bulk motion) relative to the observation/field point \mathbf{x} (assumed to be at rest in the lab system), it is possible to express the elemental form of the Riemann-Silberstein vector (2) in terms of a non-covariant complex field vector density Θ as follows:

$$\begin{aligned} d\mathbf{G}(t, \mathbf{x}, \mathbf{x}') &= (d\mathbf{x} \cdot \nabla)\mathbf{G} = d\mathbf{E}(t, \mathbf{x}, \mathbf{x}') + icd\mathbf{B}(t, \mathbf{x}, \mathbf{x}') \\ &= \left(\Theta(t, \mathbf{x}, \mathbf{x}') + \frac{i}{c} \hat{\mathbf{k}}(\mathbf{x}, \mathbf{x}') \times \Theta^*(t, \mathbf{x}, \mathbf{x}') \right) d^3x' \end{aligned} \quad (27)$$

where

$$\Theta(t, \mathbf{x}, \mathbf{x}') = \Theta^e(t, \mathbf{x}, \mathbf{x}') + \frac{i}{c} \Theta^m(t, \mathbf{x}, \mathbf{x}') \quad (28)$$

and the electric charge Θ^e and its magnetic charge dual Θ^m can be written as vector sums [10, 165, 166]

$$\Theta^{e,m}(t, \mathbf{x}, \mathbf{x}') = \sum_{j=1}^4 \mathbf{b}_j^{e,m}(t, \mathbf{x}, \mathbf{x}') \quad (29a)$$

where

$$\mathbf{b}_1^{e,m}(t, \mathbf{x}, \mathbf{x}') = \frac{\rho^{e,m}\left(t - \frac{|\mathbf{x} - \mathbf{x}'|}{c}, \mathbf{x}'\right)}{4\pi\epsilon_0|\mathbf{x} - \mathbf{x}'|^2} \hat{\mathbf{k}}(\mathbf{x}, \mathbf{x}') \quad (29b)$$

$$\mathbf{b}_2^{e,m}(t, \mathbf{x}, \mathbf{x}') = \frac{\mathbf{j}^{e,m}\left(t - \frac{|\mathbf{x} - \mathbf{x}'|}{c}, \mathbf{x}'\right) \cdot \hat{\mathbf{k}}(\mathbf{x}, \mathbf{x}')}{4\pi\epsilon_0c|\mathbf{x} - \mathbf{x}'|^2} \hat{\mathbf{k}}(\mathbf{x}, \mathbf{x}') \quad (29c)$$

$$\mathbf{b}_3^{e,m}(t, \mathbf{x}, \mathbf{x}') = \frac{\mathbf{j}^{e,m}\left(t - \frac{|\mathbf{x} - \mathbf{x}'|}{c}, \mathbf{x}'\right) \times \hat{\mathbf{k}}(\mathbf{x}, \mathbf{x}')}{4\pi\epsilon_0c|\mathbf{x} - \mathbf{x}'|^2} \times \hat{\mathbf{k}}(\mathbf{x}, \mathbf{x}') \quad (29d)$$

$$\mathbf{b}_4^{e,m}(t, \mathbf{x}, \mathbf{x}') = \frac{\frac{\partial \mathbf{j}^{e,m}\left(t - \frac{|\mathbf{x} - \mathbf{x}'|}{c}, \mathbf{x}'\right)}{\partial t} \times \hat{\mathbf{k}}(\mathbf{x}, \mathbf{x}')}{4\pi\epsilon_0c^2|\mathbf{x} - \mathbf{x}'|} \times \hat{\mathbf{k}}(\mathbf{x}, \mathbf{x}') \quad (29e)$$

An appealing feature of this representation is that the expressions for the four vectors $\mathbf{b}_j^{e,m}$ do not involve any spatial derivatives. As pointed out by Heras [167], this is an advantage as this avoids some mathematical subtleties associated with the retardation that mixes space and time [see Eqn. (25)]. Furthermore, $|\mathbf{b}_j^{e,m}|$, $j = 1, 2, 3$, all have a $1/|\mathbf{x} - \mathbf{x}'|^2$ spatial fall-off, whereas $|\mathbf{b}_4^{e,m}|$ falls off as $1/|\mathbf{x} - \mathbf{x}'|$ and therefore dominates over the other three at very long distances $|\mathbf{x} - \mathbf{x}'|$ from the source volume V' .

Formulas (27) are generalized (and symmetrized) elemental field versions of the SPPJ equations [8, 161–164] and clearly show that interesting geometric relations exist between the elemental fields. For instance, for purely electric sources and for purely magnetic sources $d\mathbf{E}$ is always and everywhere perpendicular to $d\mathbf{B}$. The new representation (27) has also proved to be economical and in other ways advantageous to use in practical computations.

1. Purely electric sources

From now on, we consider only electric charges and currents, *i.e.* we set $\Theta^m = \mathbf{0}$. However, as is well known, magnetic currents that manifest the duality of electrodynamics [168] and are useful in practical applications such as modeling electric slot antennas. Formulas for this case can be readily derived following the recipes given below.

We shall frequently decompose a vector \mathbf{v} into its component \mathbf{v}_{\parallel} parallel to a unit vector $\hat{\mathbf{e}}$, and its component \mathbf{v}_{\perp} transverse to $\hat{\mathbf{e}}$, according to the following scheme:

$$\mathbf{v} = \mathbf{v}_{\parallel} + \mathbf{v}_{\perp} \quad (30a)$$

where

$$\mathbf{v}_{\parallel} = v_{\parallel} \hat{\mathbf{e}} = (\mathbf{v} \cdot \hat{\mathbf{e}}) \hat{\mathbf{e}} \quad (30b)$$

$$\mathbf{v}_{\perp} = \mathbf{v} - \mathbf{v}_{\parallel} = \mathbf{v} - (\mathbf{v} \cdot \hat{\mathbf{e}}) \hat{\mathbf{e}} \quad (30c)$$

We shall use this decomposition several times in the following and start with Θ^e that we write as a sum of one longitudinal component, Θ_{\parallel}^e , parallel to the unit vector $\hat{\mathbf{k}}(\mathbf{x}, \mathbf{x}')$, and one transverse component, Θ_{\perp}^e , perpendicular to $\hat{\mathbf{k}}(\mathbf{x}, \mathbf{x}')$, *i.e.*,

$$\Theta^e = \Theta_{\parallel}^e + \Theta_{\perp}^e \quad (31a)$$

where

$$\Theta_{\parallel}^e = \mathbf{b}_1^e + \mathbf{b}_2^e \quad (31b)$$

$$\Theta_{\perp}^e = \mathbf{b}_3^e + \mathbf{b}_4^e \quad (31c)$$

This representation of Θ^e is very convenient when one wishes to calculate and analyze electromagnetic field quantities that are second order in the field vectors.

The local field vectors at a field point \mathbf{x} in the observation volume V , $\mathbf{E}(t, \mathbf{x})$ and $\mathbf{B}(t, \mathbf{x})$, are obtained by integrating the contributions from the entire source volume V' to the field vector density Θ^e , *i.e.*, from Eqns. (27) and (29) for purely electric charges and currents, taking vector perpendicularity into account. The result is

$$\begin{aligned} \mathbf{E}(t, \mathbf{x}) &= \int_{V'} d\mathbf{E} = \int_{V'} d^3x' \Theta^e = \int_{V'} d^3x' (\Theta_{\parallel}^e + \Theta_{\perp}^e) \\ &= \sum_{j=1}^4 \int_{V'} d^3x' \mathbf{b}_j^e(t, \mathbf{x}, \mathbf{x}') \end{aligned} \quad (32a)$$

$$\begin{aligned} \mathbf{B}(t, \mathbf{x}) &= \int_{V'} d\mathbf{B} = \frac{1}{c} \int_{V'} d^3x' (\hat{\mathbf{k}} \times \Theta^e) = \frac{1}{c} \int_{V'} d^3x' (\hat{\mathbf{k}} \times \Theta_{\perp}^e) \\ &= \frac{1}{c} \sum_{j=3}^4 \int_{V'} d^3x' \hat{\mathbf{k}}(\mathbf{x}, \mathbf{x}') \times \mathbf{b}_j^e(t, \mathbf{x}, \mathbf{x}') \end{aligned} \quad (32b)$$

Interestingly, Θ^e behaves as a volumetric super-density, that, when integrated, yields exact expressions for the fields from which one can, in turn, calculate exact expressions for volumetric densities of the observables that are generated by the sources in V' .

B. Useful approximations

The vector density Θ^e as given by Eqns. (31) has one component, represented by the vectors \mathbf{b}_1^e and \mathbf{b}_2^e defined by Eqns. (29b) and (29c), respectively. This component is parallel to the unit vector $\hat{\mathbf{k}}(\mathbf{x}, \mathbf{x}')$ from a point \mathbf{x} in the source volume V' to a point \mathbf{x}' in the observation volume V over which the observables are integrated (the longitudinal field component). The other component, represented by the vectors \mathbf{b}_3^e and \mathbf{b}_4^e in Eqns. (29d) and (29e), is perpendicular to $\hat{\mathbf{k}}(\mathbf{x}, \mathbf{x}')$ (the transverse field component).

1. The paraxial approximation

In a configuration where all the source points \mathbf{x}' in V' are observed at \mathbf{x} in V such that $\hat{\mathbf{k}}(\mathbf{x}, \mathbf{x}')$ are all nearly parallel, the paraxial approximation, illustrated in Fig. 2, can be applied. This amounts to setting

$$\hat{\mathbf{k}}(\mathbf{x}, \mathbf{x}') \approx \hat{\mathbf{k}}(\mathbf{x}, \mathbf{x}_0) \equiv \hat{\mathbf{n}}'(\mathbf{x}) \quad (33)$$

i.e., approximating the unit vector from \mathbf{x}' to \mathbf{x} with the \mathbf{x} -ward pointing normal unit vector of a sphere centered on a fixed reference point \mathbf{x}_0 in V' . When we introduce this approximation into the exact expressions for the vectors \mathbf{b}_j^e in Eqns. (29), we obtain the paraxially approximate vectors

$$\mathbf{b}_1^{e\text{parax}}(t, \mathbf{x}, \mathbf{x}') = \frac{\rho^e\left(t - \frac{|\mathbf{x} - \mathbf{x}'|}{c}, \mathbf{x}'\right)}{4\pi\epsilon_0|\mathbf{x} - \mathbf{x}'|^2} \hat{\mathbf{n}}'(\mathbf{x}) \quad (34a)$$

$$\mathbf{b}_2^{e\text{parax}}(t, \mathbf{x}, \mathbf{x}') = \frac{\mathbf{j}^e\left(t - \frac{|\mathbf{x} - \mathbf{x}'|}{c}, \mathbf{x}'\right) \cdot \hat{\mathbf{n}}'(\mathbf{x})}{4\pi\epsilon_0c|\mathbf{x} - \mathbf{x}'|^2} \hat{\mathbf{n}}'(\mathbf{x}) \quad (34b)$$

$$\mathbf{b}_3^{e\text{parax}}(t, \mathbf{x}, \mathbf{x}') = \frac{\mathbf{j}^e\left(t - \frac{|\mathbf{x} - \mathbf{x}'|}{c}, \mathbf{x}'\right) \times \hat{\mathbf{n}}'(\mathbf{x})}{4\pi\epsilon_0c|\mathbf{x} - \mathbf{x}'|^2} \times \hat{\mathbf{n}}'(\mathbf{x}) \quad (34c)$$

$$\mathbf{b}_4^{e\text{parax}}(t, \mathbf{x}, \mathbf{x}') = \frac{\frac{\partial \mathbf{j}^e\left(t - \frac{|\mathbf{x} - \mathbf{x}'|}{c}, \mathbf{x}'\right)}{\partial t} \times \hat{\mathbf{n}}'(\mathbf{x})}{4\pi\epsilon_0c^2|\mathbf{x} - \mathbf{x}'|} \times \hat{\mathbf{n}}'(\mathbf{x}) \quad (34d)$$

These expressions can be further simplified with the help of standard vector identities, with the result that the field vector density given by Eqns. (31) can be approximated by

$$\Theta^{e\text{parax}} = \Theta_{\parallel}^{e\text{parax}} + \Theta_{\perp}^{e\text{parax}} \quad (35)$$

where

$$\Theta_{\parallel}^{e\text{parax}} = \frac{c\rho^e \hat{\mathbf{n}}'}{4\pi\epsilon_0c|\mathbf{x} - \mathbf{x}'|^2} + \frac{(\mathbf{j}^e \cdot \hat{\mathbf{n}}') \hat{\mathbf{n}}'}{4\pi\epsilon_0c|\mathbf{x} - \mathbf{x}'|^2} \quad (36a)$$

$$\begin{aligned} &\equiv \frac{c\rho^e \hat{\mathbf{n}}'}{4\pi\epsilon_0c|\mathbf{x} - \mathbf{x}'|^2} + \frac{\mathbf{j}_{\parallel}^e}{4\pi\epsilon_0c|\mathbf{x} - \mathbf{x}'|^2} \\ \Theta_{\perp}^{e\text{parax}} &= \frac{(\mathbf{j}^e \cdot \hat{\mathbf{n}}') \hat{\mathbf{n}}' - \mathbf{j}^e}{4\pi\epsilon_0c|\mathbf{x} - \mathbf{x}'|^2} + \frac{(\mathbf{j}^e \cdot \hat{\mathbf{n}}') \hat{\mathbf{n}}' - \mathbf{j}^e}{4\pi\epsilon_0c^2|\mathbf{x} - \mathbf{x}'|} \\ &\equiv -\frac{\mathbf{j}_{\perp}^e}{4\pi\epsilon_0c|\mathbf{x} - \mathbf{x}'|^2} - \frac{\mathbf{j}_{\perp}^e}{4\pi\epsilon_0c^2|\mathbf{x} - \mathbf{x}'|} \end{aligned} \quad (36b)$$

For compactness, introduced the overdot ($\dot{}$) notation

$$\mathbf{j}^e \equiv \left(\frac{\partial \mathbf{j}^e}{\partial t} \right)_{t=t'} = \frac{\partial \mathbf{j}^e\left(t - \frac{|\mathbf{x} - \mathbf{x}'|}{c}, \mathbf{x}'\right)}{\partial t} \quad (37)$$

in the last equation and also suppressed obvious arguments.

Using the above expressions (36), we conclude that in the paraxial approximation the formulas (32) can be approximated by

$$\begin{aligned} \mathbf{E}^{\text{parax}}(t, \mathbf{x}) &= \mathbf{E}_{\parallel}^{\text{parax}}(t, \mathbf{x}) + \mathbf{E}_{\perp}^{\text{parax}}(t, \mathbf{x}) \\ &= \int_{V'} d^3x' \Theta_{\parallel}^{e\text{parax}}(t, \mathbf{x}, \mathbf{x}') + \int_{V'} d^3x' \Theta_{\perp}^{e\text{parax}}(t, \mathbf{x}, \mathbf{x}') \end{aligned} \quad (38a)$$

$$\begin{aligned} \mathbf{B}^{\text{parax}}(t, \mathbf{x}) &= \mathbf{B}_{\perp}^{\text{parax}}(t, \mathbf{x}) = \frac{1}{c} \hat{\mathbf{n}}'(\mathbf{x}) \times \int_{V'} d^3x' \Theta_{\perp}^{e\text{parax}}(t, \mathbf{x}, \mathbf{x}') \\ &= \frac{1}{c} \hat{\mathbf{n}}'(\mathbf{x}) \times \mathbf{E}_{\perp}^{\text{parax}}(t, \mathbf{x}) = \frac{1}{c} \hat{\mathbf{n}}'(\mathbf{x}) \times \mathbf{E}^{\text{parax}}(t, \mathbf{x}) \end{aligned} \quad (38b)$$

Whereas $\mathbf{E}^{\text{parax}}$ has two mutually perpendicular components, $\mathbf{B}^{\text{parax}}$ has only one component. This component is perpendicular both to $\hat{\mathbf{n}}$ and to the component of $\mathbf{E}^{\text{parax}}$ that, in turn, is perpendicular to $\hat{\mathbf{n}}$. These geometrical properties always hold in the paraxial approximation, even if the far-zone approximation is not applicable. On the other hand, sufficiently far away from a source volume of finite extent, such as an antenna array, the paraxial approximation is always applicable.

A consistently truncated paraxial approximation expression for the electromagnetic linear momentum density is obtained by inserting the paraxially valid approximate expressions (38) for the fields into the exact expression (A10). The result is

$$\mathbf{g}^{\text{fieldparax}}(t, \mathbf{x}) = \mathbf{g}_{\perp}^{\text{fieldparax}}(t, \mathbf{x}) + \mathbf{g}_{\parallel}^{\text{fieldparax}}(t, \mathbf{x}) \quad (39a)$$

where

$$\mathbf{g}_{\perp}^{\text{fieldparax}}(t, \mathbf{x}) = \epsilon_0 \mathbf{E}_{\parallel}^{\text{parax}}(t, \mathbf{x}) \times \mathbf{B}_{\perp}^{\text{parax}}(t, \mathbf{x}) \quad (39b)$$

$$\mathbf{g}_{\parallel}^{\text{fieldparax}}(t, \mathbf{x}) = \epsilon_0 E_{\perp}^{\text{parax}}(t, \mathbf{x}) B_{\perp}^{\text{parax}}(t, \mathbf{x}) \hat{\mathbf{n}}'(\mathbf{x}) \quad (39c)$$

The angular momentum density carried by (\mathbf{E}, \mathbf{B}) with respect to the fixed moment point \mathbf{x}_m is given by the exact expression (A37). Inserting the paraxially valid approximate expressions (38) for the fields into (A37), we obtain

$$\begin{aligned} \mathbf{h}^{\text{fieldparax}}(t, \mathbf{x}; \mathbf{x}_m) &= (\mathbf{x} - \mathbf{x}_m) \times \mathbf{g}^{\text{fieldparax}}(t, \mathbf{x}) \\ &= \mathbf{h}^{\text{fieldparax}}(t, \mathbf{x}; \mathbf{0}) - \mathbf{x}_m \times \mathbf{g}^{\text{fieldparax}}(t, \mathbf{x}) \end{aligned} \quad (40)$$

where the first term in the second RHS is the angular momentum around the origin $\mathbf{x} = \mathbf{0}$

$$\begin{aligned} \mathbf{h}^{\text{fieldparax}}(t, \mathbf{x}; \mathbf{0}) &= \epsilon_0 \mathbf{x} \times (\mathbf{g}_{\perp}^{\text{fieldparax}}(t, \mathbf{x}) + \mathbf{g}_{\parallel}^{\text{fieldparax}}(t, \mathbf{x})) \\ &= \epsilon_0 (\mathbf{B}_{\perp}^{\text{parax}}(t, \mathbf{x}) \cdot \mathbf{x}) \mathbf{E}_{\parallel}^{\text{parax}}(t, \mathbf{x}) \\ &\quad - \epsilon_0 (\mathbf{E}_{\parallel}^{\text{parax}}(t, \mathbf{x}) \cdot \mathbf{x}) \mathbf{B}_{\perp}^{\text{parax}}(t, \mathbf{x}) \\ &\quad + \epsilon_0 E_{\perp}^{\text{parax}}(t, \mathbf{x}) B_{\perp}^{\text{parax}}(t, \mathbf{x}) \mathbf{x} \times \hat{\mathbf{n}}'(\mathbf{x}) \end{aligned} \quad (41)$$

as follows from Eqns. (39) and the ‘bac-cab’ vector identity. Recalling that, by definition, the radius vector \mathbf{x} from the source, located at the origin, to the field point is $\mathbf{x} = |\mathbf{x}|\hat{\mathbf{n}}'$, we note that $\mathbf{B}_\perp \cdot \mathbf{x} = 0$ and $\mathbf{x} \times \hat{\mathbf{n}}' = 0$, which simplifies Eqn. (41) to

$$\mathbf{h}^{\text{fieldparax}}(t, \mathbf{x}; \mathbf{0}) = -\varepsilon_0 |\mathbf{x}| E_\parallel^{\text{parax}} \mathbf{B}_\perp^{\text{parax}} \quad (42)$$

which, in a spherical polar coordinate system (r, ϑ, φ) where $\mathbf{x} = r\hat{\mathbf{r}}$ and $\hat{\mathbf{r}} = \hat{\mathbf{n}}'$, becomes

$$\mathbf{h}^{\text{fieldparax}}(t, r, \vartheta, \varphi; \mathbf{0}) = -\varepsilon_0 r E_r^{\text{parax}} \mathbf{B}_\perp^{\text{parax}} \quad (43)$$

This shows that in cases when the paraxial approximation can be applied, the angular momentum density with respect to the origin is always proportional to the product of the distance r from the source, the amplitude of the near-zone longitudinal (radial) component of the electric field vector, which goes like r^{-2} , and the amplitude of the transverse component of the magnetic field vector, which goes like r^{-1} , so that the whole expression goes as r^{-2} as it should. For a single frequency component ω , the angular momentum density (pseudo)vector has one DC component and one component that oscillates along the magnetic field (pseudo)vector at twice the oscillation frequency ω . The cycle average of the latter component vanishes.

Using the paraxial relation (38b) and simple vector algebra, we can express the result in Eqn. (42) entirely in terms of the electric field in the following way:

$$\mathbf{h}^{\text{fieldparax}}(t, \mathbf{x}; \mathbf{0}) = \frac{\varepsilon_0}{c} (\mathbf{x} \cdot \mathbf{E}_\parallel^{\text{parax}}(t, \mathbf{x}) \otimes \mathbf{E}_\perp^{\text{parax}}(t, \mathbf{x}) \times \hat{\mathbf{n}}'(\mathbf{x})) \quad (44)$$

where \otimes is the dyadic product operator. When the paraxial approximation is not applicable, there exists a certain angular spread in the wave vectors that may require corrections to the geometrical factors.

2. The far-zone approximation

In the far-zone approximation, the integrands (31) and (36) can be consistently approximated in order to further simplify the integrals (32) and (38), respectively. With reference to Fig. 2, and with the choice of the reference point \mathbf{x}'_0 as the origin of the spherical polar coordinate used, implying that

$$\mathbf{x} - \mathbf{x}'_0 = \mathbf{r} = r\hat{\mathbf{r}} \quad (45a)$$

$$\mathbf{x}' - \mathbf{x}'_0 = \mathbf{r}' = r'\hat{\mathbf{r}}' \quad (45b)$$

the identity

$$\frac{1}{|\mathbf{x} - \mathbf{x}'|} = \frac{1}{|(\mathbf{x} - \mathbf{x}'_0) - (\mathbf{x}' - \mathbf{x}'_0)|} = \frac{1}{|\mathbf{r} - \mathbf{r}'|} \quad (46)$$

holds. For configurations such that the shortest distance between V' and V is large, or, more precisely, when

$$\sup r' = \sup |\mathbf{x}' - \mathbf{x}'_0| \ll \inf |\mathbf{x} - \mathbf{x}'_0| = \inf r \quad (47)$$

the Taylor expansion

$$\begin{aligned} \frac{1}{|\mathbf{x} - \mathbf{x}'|} &= \frac{1}{|\mathbf{r} - \mathbf{r}'|} \\ &= \frac{1}{r} - (\mathbf{r}' \cdot \nabla) \frac{1}{r} - \frac{1}{2} (\mathbf{r}' \cdot \nabla)^2 \frac{1}{r} + \dots \\ &= \frac{1}{r} + \frac{\mathbf{r}' \cdot \hat{\mathbf{r}}}{r^2} + \frac{1}{2} \frac{\hat{\mathbf{r}} \cdot (3\mathbf{r}' \otimes \mathbf{r}' - \mathbb{1}_3 r'^2) \cdot \hat{\mathbf{r}}}{r^3} + \mathcal{O}(r^{-4}) \end{aligned} \quad (48)$$

converges rapidly. This allows us to set $1/|\mathbf{x} - \mathbf{x}'| \approx 1/r$ in Eqns. (36). As a result, the un-truncated expressions for the longitudinal and transverse components of the field density vector in the combined paraxial and far-zone approximations can be written

$$\Theta_\parallel^{\text{e paraxfar}} = \frac{c\rho^{\text{e}} \hat{\mathbf{n}}'}{4\pi\varepsilon_0 c r^2} + \frac{\mathbf{j}_\parallel^{\text{e}}}{4\pi\varepsilon_0 c r^2} \quad (49a)$$

$$\Theta_\perp^{\text{e paraxfar}} = -\frac{\mathbf{j}_\perp^{\text{e}}}{4\pi\varepsilon_0 c r^2} - \frac{\mathbf{j}_\perp^{\text{e}}}{4\pi\varepsilon_0 c^2 r} \quad (49b)$$

Accordingly, the integrals in Eqns. (38) simplify considerably.

Following Tamburini *et al.* [74] and Thidé *et al.* [165], we introduce the following shorthand notations:

$$q^{\text{e}}(t') \equiv \int_{V'} d^3x' \rho^{\text{e}}(t', \mathbf{x}') \quad (50a)$$

$$\mathbf{I}^{\text{e}}(t') \equiv \int_{V'} d^3x' \mathbf{j}^{\text{e}}(t', \mathbf{x}') \quad (50b)$$

$$\begin{aligned} \dot{\mathbf{I}}^{\text{e}}(t') &\equiv \int_{V'} d^3x' \dot{\mathbf{j}}^{\text{e}}(t', \mathbf{x}') \\ &\equiv \int_{V'} d^3x' \frac{\partial \mathbf{j}^{\text{e}}(t - \frac{|\mathbf{x} - \mathbf{x}'|}{c}, \mathbf{x}')}{\partial t} \end{aligned} \quad (50c)$$

Then, under the assumption of paraxial as well as far-zone approximation, we can write the perpendicular and parallel components of the fields as follows:

$$\mathbf{E}_\perp^{\text{paraxfar}}(t, \mathbf{x}) = -\frac{\mathbf{I}_\perp^{\text{e}}(t')}{4\pi\varepsilon_0 c r^2} - \frac{\dot{\mathbf{I}}_\perp^{\text{e}}(t')}{4\pi\varepsilon_0 c^2 r} \quad (51a)$$

$$\mathbf{E}_\parallel^{\text{paraxfar}}(t, \mathbf{x}) = \frac{q^{\text{e}}(t') \hat{\mathbf{n}}'(\mathbf{x})}{4\pi\varepsilon_0 r^2} + \frac{\mathbf{I}_\parallel^{\text{e}}(t')}{4\pi\varepsilon_0 c r^2} \quad (51b)$$

$$\mathbf{B}_\perp^{\text{paraxfar}}(t, \mathbf{x}) = \frac{\mathbf{I}_\perp^{\text{e}}(t') \times \hat{\mathbf{n}}'(\mathbf{x})}{4\pi\varepsilon_0 c r^2} + \frac{\dot{\mathbf{I}}_\perp^{\text{e}}(t') \times \hat{\mathbf{n}}'(\mathbf{x})}{4\pi\varepsilon_0 c^2 r} \quad (51c)$$

Evaluating the linear momentum density formula (A10) in the paraxial approximation, keeping all terms and approximating each one of them in a consistent way, we see that far away from the source the linear momentum density is

$$\mathbf{g}^{\text{fieldparaxfar}} = \mathbf{g}_\perp^{\text{fieldparaxfar}} + \mathbf{g}_\parallel^{\text{fieldparaxfar}} \quad (52a)$$

where

$$\mathbf{g}_\perp^{\text{fieldparaxfar}} = \frac{1}{16\pi^2 \varepsilon_0 c^2 r^3} (c q^{\text{e}} + I_\parallel^{\text{e}}) \left(\frac{\mathbf{I}_\perp^{\text{e}}}{r} + \frac{\dot{\mathbf{I}}_\perp^{\text{e}}}{c} \right) \quad (52b)$$

$$\mathbf{g}_\parallel^{\text{fieldparaxfar}} = \frac{1}{16\pi^2 \varepsilon_0 c^2 r^2} \left(\frac{\mathbf{I}_\perp^{\text{e}}}{r} + \frac{\dot{\mathbf{I}}_\perp^{\text{e}}}{c} \right) \cdot \left(\frac{\mathbf{I}_\perp^{\text{e}}}{r} + \frac{\dot{\mathbf{I}}_\perp^{\text{e}}}{c} \right) \hat{\mathbf{n}}' \quad (52c)$$

If we express this result in terms of the explicit integrals in Eqns. (50), we find that as the distance r from the source tends to infinity, the linear momentum density vector is given by the consistently truncated expression

$$\begin{aligned} \mathbf{g}^{\text{fieldparaxfar}}(t, \mathbf{x}) = & \frac{1}{16\pi^2\epsilon_0 c^4 r^3} \int_{V'} d^3x' (c\rho^e + j_{\parallel}^e + \mathcal{O}(r^{-1})) \int_{V'} d^3x' \mathbf{j}_{\perp}^e \\ & + \frac{1}{16\pi^2\epsilon_0 c^4 r^2} \left(\int_{V'} d^3x' \mathbf{j}_{\perp}^e \cdot \int_{V'} d^3x' \mathbf{j}_{\perp}^e + \mathcal{O}(r^{-1}) \right) \hat{\mathbf{n}}' \end{aligned} \quad (53)$$

To leading order in r the magnitude of this vector is the scalar

$$\left| \mathbf{g}^{\text{fieldparaxfar}}(t, \mathbf{x}) \right| = \frac{1}{16\pi^2\epsilon_0 c^4 r^2} \left| \int_{V'} d^3x' \mathbf{j}_{\perp}^e \right|^2 + \mathcal{O}(r^{-3}) \quad (54)$$

that exhibits the well-known r^{-2} asymptotic fall-off.

Starting from the exact expression for the angular momentum density, Eqn. (A37), and using the un-truncated paraxially approximate expressions (52), noticing that $\mathbf{x} = r\hat{\mathbf{n}}'$, we see that the un-truncated paraxially approximate expression for the angular momentum density is

$$\mathbf{h}^{\text{fieldparaxfar}}(t, \mathbf{x}; \mathbf{0}) = \frac{c q^e(t') + I_{\parallel}^e(t')}{16\pi^2\epsilon_0 c^2 r^2} \hat{\mathbf{n}}' \times \left(\frac{\mathbf{I}_{\perp}^e}{r} + \frac{\mathbf{j}_{\perp}^e}{c} \right) \quad (55)$$

Expressing this result explicitly in the integrals in Eqns. (38), and truncating consistently, we obtain

$$\begin{aligned} \mathbf{h}^{\text{fieldparaxfar}}(t, \mathbf{x}; \mathbf{0}) = & -\frac{1}{16\pi^2\epsilon_0 c^3 r^2} \int_{V'} d^3x' \rho^e \int_{V'} d^3x' \mathbf{j}_{\perp}^e \times \hat{\mathbf{n}}' \\ & - \frac{1}{16\pi^2\epsilon_0 c^4 r^2} \int_{V'} d^3x' j_{\parallel}^e \int_{V'} d^3x' \mathbf{j}_{\perp}^e \times \hat{\mathbf{n}}' + \mathcal{O}(r^{-3}) \end{aligned} \quad (56)$$

In the first integral in the first term we may, with the help of the continuity equation, formally express ρ^e in \mathbf{j}^e as follows

$$\int_{V'} d^3x' \rho^e(t', \mathbf{x}') = - \int_{V'} dt' \int_{V'} d^3x' \nabla' \cdot \mathbf{j}^e(t', \mathbf{x}') \quad (57)$$

which, by introducing the shorthand notation

$$\tilde{\mathbf{j}}^e(\mathbf{x}') = \int_{V'} dt' \mathbf{j}^e(t', \mathbf{x}') \quad (58)$$

allows us to write

$$\int_{V'} d^3x' \rho^e(t', \mathbf{x}') = - \int_{V'} d^3x' \nabla' \cdot \tilde{\mathbf{j}}^e(\mathbf{x}') \quad (59a)$$

$$= - \oint_{S'} d^2x' \hat{\mathbf{n}}' \cdot \tilde{\mathbf{j}}^e(\mathbf{x}') \quad (59b)$$

where, in the last step, the divergence theorem was applied. We note that we can, in the same vein, formally write Eqn. (50a) as

$$q^e(t') \equiv - \int_{V'} d^3x' \nabla' \cdot \int_{V'} dt' \mathbf{j}^e(t', \mathbf{x}') \quad (60a)$$

$$= - \int_{V'} dt' \int_{V'} d^3x' \nabla' \cdot \mathbf{j}^e(t', \mathbf{x}') \quad (60b)$$

Recalling formula (40) and using expression (53), we conclude that for an arbitrary source distribution (ρ^e, \mathbf{j}^e) located in a volume V' of finite extent, the angular momentum density with respect to an arbitrary fixed moment point \mathbf{x}_m in the paraxial, far-zone approximation is

$$\begin{aligned} \mathbf{h}^{\text{fieldparaxfar}}(t, \mathbf{x}; \mathbf{x}_m) = & \frac{1}{16\pi^2\epsilon_0 c^4 r^2} \int_{V'} d^3x' (c\nabla' \cdot \tilde{\mathbf{j}}^e - j_{\parallel}^e) \int_{V'} d^3x' \mathbf{j}_{\perp}^e \times \hat{\mathbf{n}}' \\ & + \frac{1}{16\pi^2\epsilon_0 c^4 r^2} \left| \int_{V'} d^3x' \mathbf{j}_{\perp}^e \right|^2 \mathbf{x}_m \times \hat{\mathbf{n}}' + \mathcal{O}(r^{-3}) \end{aligned} \quad (61a)$$

or, since $\hat{\mathbf{n}}' \cdot \tilde{\mathbf{j}}^e = \tilde{j}_{\parallel}^e$,

$$\begin{aligned} \mathbf{h}^{\text{fieldparaxfar}}(t, \mathbf{x}; \mathbf{x}_m) = & \frac{1}{16\pi^2\epsilon_0 c^3 r^2} \oint_{S'} d^2x' \tilde{j}_{\parallel}^e \int_{V'} d^3x' \mathbf{j}_{\perp}^e \times \hat{\mathbf{n}}' \\ & - \frac{1}{16\pi^2\epsilon_0 c^4 r^2} \int_{V'} d^3x' j_{\parallel}^e \int_{V'} d^3x' \mathbf{j}_{\perp}^e \times \hat{\mathbf{n}}' \\ & + \frac{1}{16\pi^2\epsilon_0 c^4 r^2} \left| \int_{V'} d^3x' \mathbf{j}_{\perp}^e \right|^2 \mathbf{x}_m \times \hat{\mathbf{n}}' + \mathcal{O}(r^{-3}) \end{aligned} \quad (61b)$$

Sufficiently far away from V' , the paraxial approximation is trivially fulfilled. Therefore, Eqns. (61) show that the magnitude of the angular momentum density always has an r^{-2} asymptotic fall-off. See also Table II, Tamburini *et al.* [74] and Thidé *et al.* [165]). Eqns. (61) generalize the proof, published by Abraham [57] for the special case that the source is a single electric Hertzian dipole and the moment point is the origin, to hold for any conceivable combination of charge and current densities, located inside a source volume V' of finite extent, and for an arbitrary moment point \mathbf{x}_m .

We note from Eqns. (32) for \mathbf{E} and \mathbf{B} that far away from V' , the dominating contribution to the magnitude of the linear momentum density (the Poynting vector) comes from the asymptotic approximation of the far-zone \mathbf{b}_4^e term, *i.e.*, the transverse component of the time rate of change of the current density, whereas the dominating contribution to the magnitude of the angular momentum in the same region comes from both the *far-zone* \mathbf{b}_4^e term for \mathbf{B} and the *near-zone* \mathbf{b}_1^e and \mathbf{b}_2^e terms for \mathbf{E} , *i.e.*, from both the perpendicular component of the time rate change of the current density vector and the (time integrated) divergence and the longitudinal component of the current density itself. Hence, the far-zone \mathbf{E} field has in general no direct, primary influence on the far-zone angular momentum; see, however, formula (44). This may at first seem like a paradox but is a fact that was established more than a century ago [57]; see also Tamburini *et al.* [74], Then and Thidé [145], and Thidé *et al.* [165].

Equations (61) can be used for designing transducers that can generate beams with a coherent superposition of angular momentum eigenmodes that can be sensed, resolved and analyzed far away from the source volume V' . It is important that the volume V used for integrating the angular momentum density is chosen appropriately and that the angular momentum measurements are made in an optimum way, so that the r^{-2} fall-off is judiciously exploited.

IV. IMPLEMENTATION

For many reasons, not least to mitigate the problems of growing frequency congestion and increasing energy consumption in radio science, radar, and wireless and fiber optic communication applications, it is desirable to strive for a more resource-conserving, efficient and flexible use of the electromagnetic field than is offered by the prevalent linear-momentum techniques. In this Section we discuss physical issues that are essential to consider when developing and implementing angular momentum techniques in the radio domain. These results are of interest not only for radio but also for other wavelengths, since, as was pointed out by Thidé *et al.* [69], it is often more convenient to perform fundamental studies of electromagnetic radiation, including those addressed in this article, in radio than in optics. One reason being that it is relatively easy to vary the frequency and to control the phase of radio waves and beams made from them. They can therefore be produced with a very high degree of coherence and spectral purity. Furthermore, the fact that it is possible to use with digitally controlled transmitters, receivers and antenna arrays that enables experiments to be completely software defined, adds considerable flexibility and versatility compared to the typical experiment at optical wavelength, something that further the serendipity factor.

Let us consider a spatially limited source volume V' from which an electromagnetic beam is emitted into free space where there is no creation or annihilation of neither linear nor angular field momentum. The emission takes place during a finite time interval Δt_0 , thus forming a signal “pulse” that after a sufficiently long time t_0 after the end of the emission will be propagating radially outward with speed c into the surrounding free space as discussed in Sect. III. This signal “pulse” will then be located in a finite volume V_0 between two concentric spherical shells, one with radius $r_0 = ct_0$ relative to the reference point \mathbf{x}'_0 in V' (see Fig. 2), and another with radius $r_0 + \Delta r_0$ where $\Delta r_0 = c\Delta t_0$ [7]. According to the conservation laws (A22) and (A49), the cycle averaged field momentum $\mathbf{p}^{\text{field}}$ and angular momentum $\mathbf{J}^{\text{field}}$ contained in this spatially limited volume do not fall off asymptotically at large distances from the source, but tend to constant values.

Consequently, both linear and angular electromagnetic field momenta can propagate—and be used for information transfer—over in principle arbitrarily long distances. Of course, the magnitude and angular distribution of the respective momentum densities depend on the specific spatio-temporal properties of the actual radiating and receiving transducers (“antennas”) used. Some transducers, such as one-dimensional linear dipole antennas used in radio today, are effective radiators and sensors of linear momentum, whereas well-defined coherent superpositions of angular momentum eigenmodes are more optimally radiated and sensed by transducers that make full use of two- or three-dimensional current distributions.

A. Wireless information transfer with linear momentum

If we identify the individual terms in the global law of conservation of linear momentum in a closed volume, (A22), we

can rewrite this equation as a balance equation between the time rate change of mechanical linear momentum, *i.e.*, the force on the matter (the charged mechanical particles) in V , the time rate change of field linear momentum in V , and the flow of field linear momentum into V , across the surface S bounding V , as follows:

$$\underbrace{\int_V d^3x \mathbf{f}}_{\text{Force on the matter}} + \frac{d}{dt} \underbrace{\int_V d^3x \epsilon_0 (\mathbf{E} \times \mathbf{B})}_{\text{Field momentum}} + \underbrace{\oint_S d^2x \hat{\mathbf{n}} \cdot \mathbf{T}}_{\text{Linear momentum flow}} = \mathbf{0} \quad (62)$$

Hence, electric charges that are subject to an oscillating electromotive force, *e.g.*, a current fed into an antenna from a transmitter via a transmission line, experience a mechanical force that sets the charges into translational oscillatory motion and therefore gives rise to a time-varying linear conduction current density $\mathbf{j}^e(t', \mathbf{x}')$ in V' . The conservation law (A22) also shows that $\mathbf{j}^e(t', \mathbf{x}')$ is accompanied by the simultaneous emission of a time-varying electromagnetic field linear momentum $\mathbf{p}^{\text{field}}(t)$ that propagates in free space away from V' in the form of the linear momentum density $\mathbf{g}^{\text{field}}(t, \mathbf{x}')$, as described in earlier Sections and in Appendix A.

For illustrative purposes, let us consider an electromechanical system comprising an electromagnetic field that interacts with point charges q_i , $i = 1, 2, \dots, j, \dots, n$, located at \mathbf{x}_i at time t_i . All charges have the same charge q and same mass m . The charge density ρ_j^e representing the j th point charge q_j at \mathbf{x}_j can be described in the form of the Dirac delta distribution

$$\rho_j^e = q\delta(\mathbf{x} - \mathbf{x}_j) \quad (63)$$

According to the balance equation (62), the Lorentz force acting on q_j due to the imposed linear momentum flow (the Maxwell stresses) is

$$\begin{aligned} \mathbf{F}_j &\equiv \mathbf{F}(t_j, \mathbf{x}_j) = \int_V d^3x \mathbf{f} = \int_V d^3x \rho_j^e (\mathbf{E} + \mathbf{v}^{\text{mech}} \times \mathbf{B}) \\ &= q\mathbf{E}(t_j, \mathbf{x}_j) + q\mathbf{v}^{\text{mech}}(t_j, \mathbf{x}_j) \times \mathbf{B}(t_j, \mathbf{x}_j) \\ &\equiv q\mathbf{E}_j + q\mathbf{v}_j^{\text{mech}} \times \mathbf{B}_j = q\mathbf{E}_j + \mathbf{j}_j^e \times \mathbf{B}_j \end{aligned} \quad (64)$$

Expressed in the mechanical linear momentum of particle j , $\mathbf{p}_j^{\text{mech}}$, this can be written

$$\frac{d\mathbf{p}_j^{\text{mech}}}{dt} - \frac{q}{m}\mathbf{p}_j^{\text{mech}} \times \mathbf{B}_j = q\mathbf{E}_j \quad (65)$$

This illustrates that the process of estimating the fields from the measured current in a linear antenna of finite one-dimensional extent where the charges experience a holonomic constraint due to their cylindrically symmetric axial confinement, is difficult and can only be projective. The situation gets worse if we also include self-interaction effects, re-radiation, pre-acceleration and related complications. For a detailed discussion see Rohrlich [67, Supplement].

In a remote sensing volume V , the conservation law (A22) shows that the reverse process takes place in that (a part of) the flow of field linear momentum density $\mathbf{g}^{\text{field}}(t, \mathbf{x})$ emitted from V' is integrated in V into a field linear momentum $\mathbf{p}^{\text{field}}(t)$ that is accompanied by a mechanical linear momentum $\mathbf{p}^{\text{mech}}(t)$. This gives rise to a translational motion of the

charges and, hence, a translational (non-rotational) conduction current. If V is a very thin cylindrical conductor, as in typical radio communications scenarios, this is a one-dimensional, scalar, (Ohmic) dissipative conduction current, known as the antenna current, that is fed to the receiving equipment. Clearly, a single translational symmetric receiving antenna cannot sense the electromagnetic angular momentum, manifesting rotational symmetry, carried by the same beam.

Let us calculate the amount of linear momentum $\mathbf{p}^{\text{field}}$ carried by the electromagnetic field generated by an arbitrary source that is localized in a volume V' , *e.g.*, a typical transmitting antenna. This is most readily done by evaluating the integral in the right-hand member of Eqn. (A19) that expresses the field linear momentum in a volume away from V' , in a spherical polar coordinate system (r, ϑ, φ) with its origin at the center of the source region, *e.g.*, the antenna phase center. One finds that the total linear momentum carried by such an electromagnetic “pulse” of finite duration $\Delta t = \Delta r_0/c$ is

$$\mathbf{p}^{\text{field}}(t) = \int_{r_0}^{r_0+\Delta r_0} dr r^2 \int_0^{2\pi} d\varphi \int_0^\pi d\vartheta \sin \vartheta \mathbf{g}^{\text{field}}(t, r, \vartheta, \varphi) \quad (66)$$

when it propagates in free space [7].

The integration over the angular domain (the two last integrals) yields a function of r (and t) that, for very large $r_0 = ct_0$, becomes proportional to r^{-2} as shown by expressions (52) and (53). Taking into account that this function shall in the remaining (*i.e.*, first) integral in the right-hand member of Eqn. (66) be first multiplied by r^2 and thereafter integrated over the finite radial interval $[r_0, r_0 + \Delta r_0] \equiv [ct_0, c(t_0 + \Delta t_0)]$, we see that $|\mathbf{p}^{\text{field}}|$ tends to a constant when r_0 tends to infinity. This asymptotic independence of distance from a localized source, allowing the field linear momentum generated by this source to be transported all the way to infinity without radial fall-off and therefore be irreversibly lost there, is the celebrated arrow of radiation asymmetry (see Eddington [169, pp. 328–329], Jackson [8, Chap. 6], Zeh [170], Rohrlich [67, Chap. 9], and Wheeler and Zurek [171]).

The angular distribution in the far zone of the magnitude of the linear momentum density, $|\mathbf{g}^{\text{field far}}|$ and, consequently, of the Poynting vector $|\mathbf{S}|$ [see relation (A12)], is commonly referred to as “the radiation pattern” or, in the case of antenna engineering, “the antenna pattern” or “antenna diagram”.

B. Wireless information transfer with angular momentum

As the global law of conservation of angular momentum in a closed volume, Eqn. (A49), shows, the electric charges in a source volume V' that are subject to a time-varying surface integrated angular momentum flux \mathbf{M} suffer a change in their total mechanical (matter) angular momentum \mathbf{h}^{mech} , *i.e.*, they experience a mechanical torque $\boldsymbol{\tau}^{\text{mech}}$. This torque sets the charges into two- or three-dimensional rotational motion that causes the emission of a superposition of electromagnetic angular momentum eigenmodes that propagates in free space away from V' in the form of the angular momentum density $\mathbf{h}^{\text{field}}$ as described in earlier Sections and in Appendix A.

The angular momentum conservation law (A49) can be written in the form of a balance equation between the time rate change of mechanical torque on the matter (the charged mechanical particles) in V , the time rate change of field angular momentum and the flow of angular momentum across the surface S , which encloses V , as follows:

$$\underbrace{\int_V d^3x \boldsymbol{\tau}(\mathbf{x}_m)}_{\text{Torque}} + \frac{d}{dt} \underbrace{\int_V d^3x (\mathbf{x} - \mathbf{x}_m) \times \varepsilon_0 (\mathbf{E} \times \mathbf{B})}_{\text{Field angular momentum}} + \underbrace{\oint_S d^2x \hat{\mathbf{n}} \cdot \mathbf{M}(\mathbf{x}_m)}_{\text{Angular momentum flow}} = \mathbf{0} \quad (67)$$

For illustrative purposes let us consider the j th charge q_j in a system of n point charges $q_i, i = 1, 2, \dots, j, \dots, n$, each carrying the charge q . The charge density can be represented by the Dirac delta distribution as given by Eqn. (63). Then we find that the mechanical torque on q_j is

$$\begin{aligned} \boldsymbol{\tau}_j(\mathbf{x}_m) &\equiv \boldsymbol{\tau}(t_j, \mathbf{x}_j; \mathbf{x}_m) = \int_V d^3x (\mathbf{x} - \mathbf{x}_m) \times \mathbf{f} \\ &= \int_V d^3x (\mathbf{x} - \mathbf{x}_m) \times (\rho_j^e \mathbf{E} + \mathbf{j}^e \times \mathbf{B}) \\ &= (\mathbf{x}_j - \mathbf{x}_m) \times \mathbf{F}_j \end{aligned} \quad (68)$$

where \mathbf{F}_j is the Lorentz force on q_j , given by Eqn. (64).

In a remote observation volume V where the charges are not constrained to move along a line but can move freely in two or three dimensions, the reverse process takes place in that (a sufficient amount of) the flow of field angular momentum density emitted from V' is intercepted and integrated into a mechanical angular momentum \mathbf{J}^{mech} . This gives rise to a rotational motion of the charges and, hence, to a two- or three-dimensional rotational (non-translational) current density in V . Applications that exploit the rotational symmetry of the fields, *i.e.*, make use of the angular momentum degrees of freedom, must therefore be implemented in techniques that are based on the angular momentum physical layer.

The field angular momentum about the origin, $\mathbf{J}^{\text{field}}(\mathbf{0})$, contained in the “pulse” emitted from the same localized source and volume as described by equation (66), is

$$\mathbf{J}^{\text{field}}(t, \mathbf{0}) = \int_{r_0}^{r_0+\Delta r_0} dr r^2 \int_0^{2\pi} d\varphi \int_0^\pi d\vartheta \sin \vartheta \mathbf{h}^{\text{field}}(t, r, \vartheta, \varphi) \quad (69)$$

The expressions (55) and (56) explicitly show that the angular momentum density $\mathbf{h}^{\text{field}}$ emitted from any electromagnetic radiation source has precisely the same asymptotic r^{-2} radial fall-off in all directions as the linear momentum density $\mathbf{g}^{\text{field}}$. Hence, it is clear that also $|\mathbf{J}^{\text{field}}|$ tends asymptotically to a constant value and is irreversibly lost when the “pulse” approaches infinity. This is the angular momentum analog of the well-known linear momentum arrow of radiation.

We point out that for one and the same radiating device (“antenna”), the angular distribution of the radiated *angular*

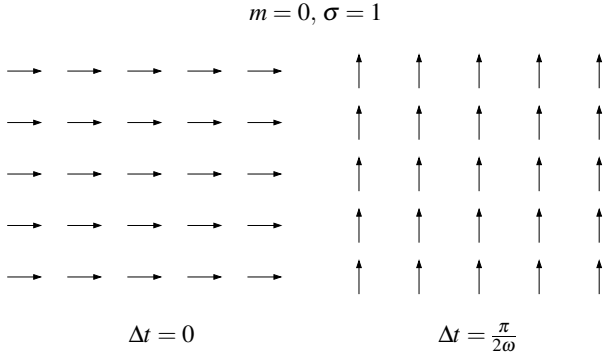


Figure 3. Schematic plot of the instantaneous directions of the field vectors in a right-hand circular polarized cylindrical beam (SAM $\sigma = 1$), projected onto the phase plane perpendicular to the z axis (pointing out of the figure). The right-hand panel shows the situation $1/4$ period later than the left-hand panel. The beam does not carry OAM so the directions of the field vectors vary only with time and rotate in unison.

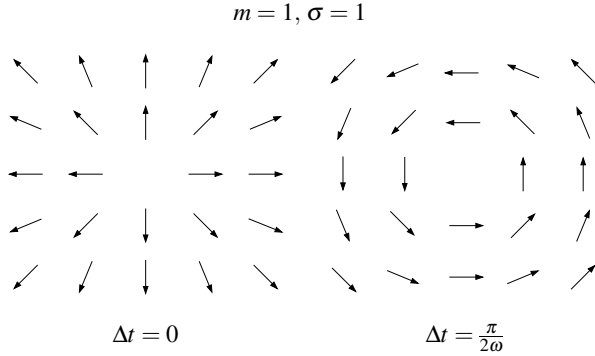


Figure 4. Same as Fig. 3, but for the case that the beam also carries a z component of OAM, L_z , with azimuthal quantum number (mode index) $m = 1$, corresponding to a phase variation $e^{i\varphi}$ of the field where φ is the azimuth angle around the z axis. As a result, the instantaneous direction of the field vector depends on φ in addition to varying with time due to SAM.

momentum density $|\mathbf{h}^{\text{field}}|$ is different from the angular distribution of the radiated *linear* momentum density, $|\mathbf{g}^{\text{field}}|$, *i.e.*, the “antenna pattern”; see Eqns. (52) and (55), Thidé *et al.* [9], and Then and Thidé [145].

1. Spin angular momentum (SAM) vs. orbital angular momentum (OAM)

It is shown in Subsection A 3 in Appendix A, that if the vector potential \mathbf{A} fulfills the criteria for Helmholtz decomposition, it is possible to separate the analytic expression for the total field angular momentum, $\mathbf{J}^{\text{field}}$, into two exact, gauge independent expressions. One that is not dependent of the moment point, Σ^{field} , *viz.*, expression (A51a), and one that is, $\mathcal{L}^{\text{field}}$, *viz.*, expression (A51b). In radio communication scenarios these expressions can be identified with the spin and orbital angular momentum, respectively, of the radio beam.

Figure 3 illustrates how the intrinsic spin part of the angular momentum (SAM), Σ^{field} , manifests itself as left- or right-hand circular polarization, *i.e.*, as a unison rotation in time of the field vectors such that they all have one and the same direction across the phase front of the beam at given time t , and all have rotated into another direction (modulo 2π in oscillation frequency phase ωt) in each point at time $t + \Delta t$. Hence, the measurement of SAM (polarization) requires temporal coherence.

A common technique to observe and exploit SAM in radio is to use two co-located linear dipole antennas arranged orthogonally to each other and to determine the polarization state by comparing the phases of the antenna currents induced in the two antennas by using interferometry. In antenna engineering such antennas are known as turnstile antennas [141, 150, 172]. Another technique is to use longitudinal mode helical antennas; see Someda [173, example 12.7.1, p. 461].

In contrast to SAM, the orbital part of the electrodynamic angular momentum, the orbital angular momentum (OAM) $\mathcal{L}^{\text{field}}$, is an extrinsic (coordinate dependent) property. Figure 4 illustrates how OAM manifests itself as a rotation in space of the field vectors such that they at any given instant have different directions (modulo 2π in oscillation frequency phase ωt) for different azimuth angles positions φ and $\varphi + \Delta\varphi$ around the z (beam) axis in the phase plane. Hence, the measurement of OAM requires spatial coherence.

We emphasize that whereas the spin angular momentum (SAM) is an intrinsic property of the photon, both its linear and orbital angular momenta are extrinsic properties.

2. Angular momentum transducers

As the conservation law (A49) shows, angular momentum modes cannot be radiated and measured by single, monolithic transducers that work solely on the principle of force, *e.g.*, are based on (Ohmically) dissipative conduction currents flowing along a line, as is the case for linear dipole-type antennas commonly used today. Instead, these modes should be radiated and measured by transducers (actuators, sensors, “antennas”) that work on the principle of rotational degrees of freedom and torque, thus being capable of exploiting the angular momentum directly [134–150, 174, 175].

In general, angular momentum transducers must support—and be able to control and sense—the three-dimensional dynamics of the charges. If, however, the rotation is confined to a single plane, it suffices that the transducers are effectively two-dimensional. Such transducers can be realized by equipping single linear-momentum antennas with two-dimensional azimuthally dependent reflectors, lenses or phase plates [72, 85, 176–182] or by employing helicoidal parabolic antennas [73, 183]. Other examples are the flat plate transducer developed by Bennis *et al.* [184] and the screen detector used by Krenn *et al.* [185].

Interesting possibilities for innovative monolithic transducers are offered by developments in nano- and optomechanics [150, 186–193], and by atomic Bose-Einstein condensates [194]. Recent research into spintronics and orbitron-

ics herald the arrival of transducers that are based on the interplay between charge, spin and orbital degrees of freedom and that may be realized with dissipation-less non-charge currents [195–209], including antennas realized with condensed-matter skyrmions (magnetic vortex structures) [87, 210–212] and quantum rings [213–215].

However, monolithic multi-dimensional “antennas” that make direct use of the angular momentum degree of freedom for the radio frequency range are not yet readily available. Until they are, one may use existing phased arrays of linear-momentum antennas of the type that are used in today’s radio astronomy and wireless communications. This is because these multi-transducer arrays, including MIMO arrays, sample a radio beam with transducers, essentially in the form of a finite set of integrating cylindrical volumes $V_n, n = 1, 2, \dots, M$ deployed at discrete points distributed over a certain region in space, thereby approximating, within the limitations and constraints set by the sampling theorem, [216–218], the properties of a single, monolithic two- and three-dimensional transducer that samples the field in a continuous manner [9, 69, 145, 219–237]. The fact that it is *possible* to use arrays of conventional linear-momentum antennas (*e.g.*, dipole antennas) to exploit (a subset of approximate) angular momentum modes, does of course not imply that it is *necessary* to use such arrays. Maxwell’s equations allow any number and combination of sources ρ and \mathbf{j} with any spatio-temporal and topological properties in the source volume V' . And the currents do not have to be conduction currents in the usual sense [192].

Within the limitations just mentioned, it is possible to use arrays of linear antennas and currently available radio equipment and techniques for experimental investigations of certain properties of a finite subset of (approximate) OAM eigenmodes and coherent superpositions of them. This will provide useful insights into the properties of OAM information transfer and therefore pave the way for the development of future innovative angular momentum radio concepts based on single transducers.

These experimental investigations typically amount to measuring the phase of the currents sampled at the feedpoints of spatially distributed individual 1D antenna elements, *i.e.*, a spatial sampling of one component of the linear momentum of the charges, and then performing a phase gradient analysis [9, 101, 120, 133, 184, 238–241] and post-processing the data so that the approximate (possibly aliased) spectrum of the z component of the angular momentum, L_z can be estimated. This way, approximations of individual OAM eigenmodes may be extracted and an approximation of the correct spectrum of individual OAM eigenmodes and the information they carry be decoded. It should be emphasized that this way of estimating L_z is based on the application of the operator defined by formula (A53c) on the electric (or magnetic) field. However, as was discussed in Sect. II, fields are, strictly speaking, not directly observable.

Proof-of-concept experiments where existing conventional radio technology was employed have shown that it is indeed possible to use the total angular momentum, *i.e.*, the SAM+OAM physical observable, as a new physical layer for radio science and technology exploitation. These studies include numerical experiments [69] showing that it is fea-

sible to utilize OAM in radio; controlled laboratory experiments [72, 77, 85, 242] verifying that it is possible to generate and transmit radio beams carrying non-integer OAM and to measure their OAM spectra in the form of weighted superpositions of different integer OAM eigenmodes each with its own quantum number (mode index), also known as topological charge; and outdoor experiments [73, 110, 243], verifying that in real-world settings different signals, physically encoded in different OAM modes and overlapping each other in space and time and subject to reflection, can be transmitted wirelessly to a receiver located in the (linear momentum) far zone and be individually extracted and decoded there.

We stress that for EM beams of the kind used in radio astronomy, radar investigations, radio communications and similar applications, OAM is distinctively different from—and independent of—SAM (wave polarization). If such a beam is already N -fold OAM encoded, utilizing also SAM will double the information transfer capacity by virtue of the fact that the dimension of the state space then doubles from N to $2N$.

3. Electric dipoles

An antenna type that is commonly used in today’s radio is the half-wavelength dipole antenna. Many qualitative as well as quantitative characteristics of this antenna are fairly accurately approximated by an electric Hertzian dipole, *i.e.*, an antenna whose length L is much shorter than the wavelength λ of its emitted (nearly monochromatic) field, $L \ll \lambda$, so that the phase variations over L of the antenna current can be neglected, a condition that simplifies the theoretical analysis considerably. We have found it convenient for our study to calculate analytically the linear and angular momentum densities emitted by a single Hertzian dipole and combinations of such dipoles. We choose a Cartesian coordinate system (x_1, x_2, x_3) where the x_3 axis coincides with the polar axis of a spherical polar coordinate system (r, ϑ, φ) and let the two systems have the same origin $\mathbf{x}' = \mathbf{0}$.

a. A single Hertzian dipole along the polar axis The properties of Hertzian dipoles are described in many textbooks [8, 10, 50] and explicit formulas are derived in Appendix B.

According to Eqn. (B17) for $\mathbf{E}_3 \times \mathbf{B}_3$ the electromagnetic linear momentum density, $\mathbf{g}_3^{\text{field}} = \epsilon_0 \mathbf{E}_3 \times \mathbf{B}_3$, emitted from a single Hertzian dipole $\mathbf{d}_3(\mathbf{0})$ located at the origin and directed along the x_3 axis, has nine different vector components. Five of them are longitudinal ($\parallel \hat{\mathbf{r}}$) and four of them are transverse ($\perp \hat{\mathbf{r}}$). It follows trivially from Planck’s relation, Eqn. (A12), that the same is also true for the Poynting vector \mathbf{S} . However, the different components have different fall-offs, implying that

far away from the dipole the following approximation holds:

$$\begin{aligned} \mathbf{g}_3^{\text{fieldfar}}(t, r, \vartheta, \varphi) &= \frac{k^4 d_3^2}{32\pi^2 \epsilon_0 c} \left(\frac{1 + \cos[2(kr - \omega t + \delta_3)]}{r^2} + \mathcal{O}(r^{-3}) \right) \sin^2 \vartheta \hat{\mathbf{r}} \\ &+ \frac{k^3 d_3^2}{32\pi^2 \epsilon_0 c} \left(\frac{\sin[2(kr - \omega t + \delta_3)]}{r^3} + \mathcal{O}(r^{-4}) \right) \cos 2\vartheta \hat{\boldsymbol{\vartheta}} \end{aligned} \quad (70)$$

To the same degree of approximation, the cycle (temporal) average of the Poynting vector in the far zone is, to leading order,

$$\langle \mathbf{S}_3^{\text{far}} \rangle_t = c^2 \mathbf{g}_3^{\text{fieldfar}} \approx \frac{\omega^4 d_3^2}{32\pi^2 \epsilon_0 c^3} \left(\frac{1}{r^2} + \mathcal{O}(r^{-3}) \right) \sin^2 \vartheta \hat{\mathbf{r}} \quad (71)$$

where we used the fact that $k = \omega/c$ and that

$$\langle \sin[2(kr - \omega t + \delta_3)] \rangle_t = \langle \cos[2(kr - \omega t + \delta_3)] \rangle_t = 0 \quad (72)$$

This is a well-known result that can be found in most textbooks.

To calculate the electromagnetic angular momentum density around $\mathbf{x}_m = \mathbf{0}$ we use Eqn. (A37), Eqn. (B17), and the fact that $\mathbf{x} = r\hat{\mathbf{r}}$ and $\hat{\mathbf{r}} \times \hat{\boldsymbol{\vartheta}} = \hat{\boldsymbol{\varphi}}$ to obtain the exact expression

$$\begin{aligned} \mathbf{h}_3^{\text{field}}(t, r, \vartheta, \varphi; \mathbf{0}) &= r\hat{\mathbf{r}} \times \mathbf{g}_3^{\text{field}} = \frac{d_3^2}{8\pi^2 \epsilon_0 c} r [f_1(\delta_3)f_2(\delta_3) \\ &- f_2^2(\delta_3) + f_1(\delta_3)f_3(\delta_3) - f_2(\delta_3)f_3(\delta_3)] \sin \vartheta \cos \vartheta \hat{\boldsymbol{\varphi}} \end{aligned} \quad (73)$$

where the functions f_n are given by Eqns. (B12).

At very long distances from a Hertzian dipole located at the origin and oscillating along the x_3 axis we can use the approximation in Eqn. (70) for $\mathbf{g}_3^{\text{field}}$. Because of the geometry, only the transverse part ($\perp \hat{\mathbf{r}}$) of the linear momentum density, where the dominating part is $\mathcal{O}(r^{-3})$, contributes to the linear momentum density in the far zone. The radial component ($\parallel \hat{\mathbf{r}}$) of the linear momentum density (Poynting vector), which is $\mathcal{O}(r^{-2})$ does not contribute to the angular momentum density. If it would, then expression (69) for the total angular momentum at very large distances of a ‘‘pulse’’ would grow without bounds as the ‘‘pulse’’ propagates, thus violating fundamental laws of physics. See the detailed, clarifying discussion about this by Abraham [57]; an English translation of the essential part of this discussion is included in Tamburini *et al.* [74]. This almost paradoxical fact is also discussed by Low [244]. Therefore, in the far zone, the angular momentum density is

$$\begin{aligned} \mathbf{h}_3^{\text{fieldfar}}(t, r, \vartheta, \varphi; \mathbf{0}) &\approx \frac{d_3^2}{16\pi^2 \epsilon_0 c} r f_1(\delta_3) f_2(\delta_3) \sin \vartheta \cos \vartheta \hat{\boldsymbol{\varphi}} \\ &= -\frac{k^3 d_3^2}{64\pi^2 \epsilon_0 r^2 c} \sin[2(kr - \omega t + \delta_3)] \sin 2\vartheta \hat{\boldsymbol{\varphi}} \end{aligned} \quad (74)$$

This result shows that $\mathbf{h}_3^{\text{fieldfar}}$ has the expected r^{-2} fall off, has no z component, and oscillates at 2ω along $-\hat{\boldsymbol{\varphi}}$. This causes an electric charge in the far zone but not located at

$\vartheta = n\pi/2, n \in \mathbb{Z}$, to rotate around its own center of mass in the osculating plane normal to $\hat{\boldsymbol{\varphi}}$. However, the temporal (cycle) average of $\mathbf{h}_3^{\text{fieldfar}}$ is zero, which makes it nontrivial to measure this rotational motion. It is tempting to relate this and similar double-frequency terms to photon *Zitterbewegung* [42, 245–247].

b. Two co-located crossed Hertzian dipoles in the azimuthal plane We now want to calculate the field linear and angular momenta emitted from a system of two co-located monochromatic Hertzian dipoles, one spatially rotated from the other by $\pi/2$, fed at the same frequency but with different temporal phase shifts. For this purpose we chose the two Hertzian dipoles $\mathbf{d}_j, j = 1, 2$ with their generated fields described by Eqns. (B14). Since the total field is a superposition of the fields from the two individual dipoles, the total linear momentum density $\mathbf{g}_{1\&2}^{\text{field}}$ emitted by the two dipoles is

$$\begin{aligned} \mathbf{g}_{1\&2}^{\text{field}} &= \epsilon_0 (\mathbf{E}_1 + \mathbf{E}_2) \times (\mathbf{B}_1 + \mathbf{B}_2) \\ &= \epsilon_0 \mathbf{E}_1 \times \mathbf{B}_1 + \epsilon_0 \mathbf{E}_2 \times \mathbf{B}_2 + \epsilon_0 \mathbf{E}_1 \times \mathbf{B}_2 + \epsilon_0 \mathbf{E}_2 \times \mathbf{B}_1 \\ &= \mathbf{g}_1^{\text{field}} + \mathbf{g}_2^{\text{field}} + \mathbf{g}_{12}^{\text{field}} + \mathbf{g}_{21}^{\text{field}} \end{aligned} \quad (75)$$

We see that in addition to the vector sum of the two linear momentum densities from the individual dipoles \mathbf{d}_1 and \mathbf{d}_2 , the total linear momentum contains two interference terms $\mathbf{g}_{12}^{\text{field}}$ and $\mathbf{g}_{21}^{\text{field}}$ which appear due to the fact that the total electromagnetic field is the superposition of the fields from each dipole. Using Eqns. (B15)–(B16) and (B18)–(B19), we can calculate the exact expression for $\mathbf{g}_{1\&2}^{\text{field}}$, and from that, using Eqn. (A37), the exact expression for the total angular momentum density $\mathbf{h}_{1\&2}^{\text{field}}$. If the two dipole moments have equal amplitudes, $d_1 = d_2 = d$, and are in phase quadrature relative each other, $\delta_1 = 0$ and $\delta_2 = \pi/2$, we find that the exact expression for the z component of the angular momentum density $h_{1\&2}^{\text{field}}$, valid in all of space outside the dipoles, is

$$\begin{aligned} h_{1\&2z}^{\text{field}}(t, r, \vartheta, \varphi; \mathbf{0}) &= \frac{d^2(\mathbf{0})k}{8\pi^2 \epsilon_0 c} \left(\frac{k^2}{r^2} \{ \sin^2 \varphi \cos^2(kr - \omega t) \right. \\ &+ \cos^2 \varphi \sin^2(kr - \omega t) + \sin \varphi \cos \varphi \sin[2(kr - \omega t)] \} \\ &+ \frac{k}{r^3} \{ 2 \sin \varphi \cos \varphi [\cos^2(kr - \omega t) - \sin^2(kr - \omega t)] \\ &- (\sin^2 \varphi - \cos^2 \varphi) \sin[2(kr - \omega t)] \} \\ &+ \frac{1}{r^4} \{ \cos^2 \varphi \cos^2(kr - \omega t) + \sin^2 \varphi \sin^2(kr - \omega t) \\ &\left. - \sin \varphi \cos \varphi \sin[2(kr - \omega t)] \} \right) \sin^2 \vartheta \end{aligned} \quad (76)$$

To turn the z component of the angular momentum density, $h_{1\&2z}^{\text{field}}$, radiated from two co-located Hertzian dipoles, arranged perpendicular to each other and oscillating in quadrature phase, into the observable z component of the total field angular momentum, $J_z^{\text{field}}(\mathbf{0})$, we must integrate (76) over an observation volume V . Choosing V as in Eqn. (69), *i.e.*, as the region between two spherical shells with radii r_0 and $r_0 + \Delta r_0$, repre-

senting the radial extent of the “pulse” emitted, we obtain

$$J_{1\&2z}^{\text{field}}(t, \mathbf{0}) = \int_{r_0}^{r_0+\Delta r_0} dr r^2 \int_{\vartheta_1}^{\vartheta_2} d\vartheta \sin \vartheta \int_{\varphi_1}^{\varphi_2} d\varphi h_{1\&2z}^{\text{field}}(\mathbf{0}) \quad (77)$$

where $h_{1\&2z}^{\text{field}}(\mathbf{0})$ is given by Eqn. (76).

If we integrate over all azimuth angles φ from $\varphi_1 = 0$ to $\varphi_1 = 2\pi$, and also use the well-known identities

$$\int_0^{2\pi} d\varphi \sin^2 \varphi = \int_0^{2\pi} d\varphi \cos^2 \varphi = \pi \quad (78a)$$

$$\int_0^{2\pi} d\varphi \sin \varphi \cos \varphi = 0 \quad (78b)$$

$$\sin^2(kr - \omega t) + \cos^2(kr - \omega t) = 1 \quad (78c)$$

we obtain

$$J_{1\&2z}^{\text{field}}(t, \mathbf{0}) = \frac{d^2(\mathbf{0})k}{8\pi\epsilon_0 c} \int_{r_0}^{r_0+\Delta r_0} dr \left(k^2 + \frac{1}{r^2} \right) \int_{\vartheta_1}^{\vartheta_2} d\vartheta \sin^3 \vartheta \quad (79)$$

If we now integrate over all polar angles ϑ from $\vartheta_1 = 0$ to $\vartheta_2 = \pi$, we obtain the explicit, closed-form expression

$$J_{1\&2z}^{\text{field}}(t, \mathbf{0}) = \frac{d^2(\mathbf{0})k}{6\pi\epsilon_0 c} \left(k^2 \Delta r_0 + \frac{\Delta r_0}{k^2 r_0 (r_0 + \Delta r_0)} \right) \quad (80)$$

where the only time dependence comes from the duration of the emitted “pulse” $\Delta t = \Delta r_0/c$. When the distance r_0 that the “pulse” has propagated is very large so that the $1/r_0^2$ contribution can be neglected, the z component of the field angular momentum can be approximated by

$$J_{1\&2z}^{\text{field far}}(t, \mathbf{0}) = \frac{d^2(\mathbf{0})k}{6\pi\epsilon_0 c} k^2 \Delta r_0 = \frac{d^2(\mathbf{0})k^3}{6\pi\epsilon_0} \Delta t \quad (81)$$

which propagates without radial fall-off as expected.

If the observation volume V , *i.e.*, the angular momentum sensing transducer, is a very thin circular ring with radius r_0 , located in the azimuthal (xy) plane ($\vartheta = \pi/2$), centered on the dipoles, and subtending the small polar angular interval $\vartheta_2 - \vartheta_1$ around the azimuthal plane, the integrals in Eqn. (77) are trivial and the result is

$$J_{1\&2z}^{\text{field}}(t, \mathbf{0}) = \frac{d^2(\mathbf{0})k}{8\pi\epsilon_0 c} \left(k^2 + \frac{1}{r_0^2} \right) (\vartheta_2 - \vartheta_1) \quad (82)$$

A torsion pendulum experiment that is a kind of radio analog of the celebrated Einstein-de Haas experiment [248], first suggested by Vul’fson [141], was performed in the microwave radio regime by Emile *et al.* [150]. The results was found to agree with the prediction in Eqn. (82). However, comparing this equation with Eqn. (4) in [150], shows, that the latter is in error: there is a factor of 2π missing which explains the factor of ~ 6 discrepancy mentioned.

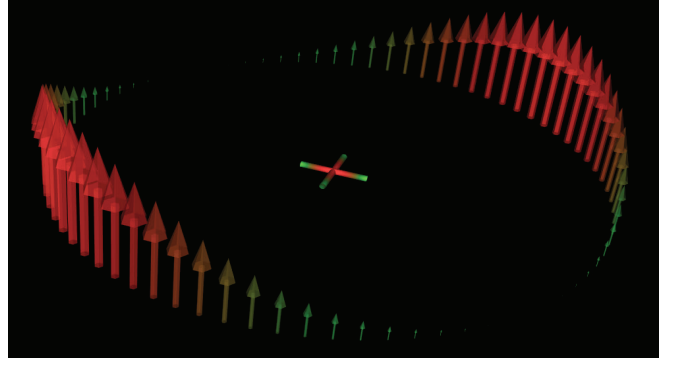


Figure 5. Snapshot of the distribution of the angular momentum density pseudovector $\mathbf{J}^{\text{field}}(t, \mathbf{0})$ on a circle in the plane around the centers of two crossed half-wave dipole antennas, co-located at the origin $\mathbf{x}' = \mathbf{0}$, arranged perpendicular to each other, and fed with equal-amplitude currents at one an the same frequency but $\pi/2$ out of phase with each other.

c. Two co-located crossed half-wave dipole antennas
The analytic results for two monochromatic crossed Hertzian dipoles in quadrature phase derived above are in fair qualitative agreement with the results obtained for the same configuration using two half-wave dipole antennas. Since the analytic treatment for the latter configuration is a bit complicated, we resorted to a direct numerical evaluation of the exact formulas (32) and (A37). We found that our results were in excellent agreement with those obtained with two enterprise-grade Maxwell solvers but with five times shorter compute time. Graphical snapshots of the time evolution of the angular momentum density $\mathbf{h}^{\text{field}}(\mathbf{0})$ from the two crossed half-wave dipole antennas, fed $\pi/2$ out of phase relative to each other, measured along a circle in the x_1x_2 plane, is displayed in Fig. 5. We see that $\mathbf{h}^{\text{field}}(\mathbf{0})$ is positively directed along the entire circle. The total field angular momentum, $\mathbf{J}^{\text{field}}(\mathbf{0})$, obtained by integrating $\mathbf{h}^{\text{field}}(\mathbf{0})$ along this circle, is therefore always directed in the x_3 axis, representing rotation around this axis. As mentioned above, this mechanical rotation caused by the angular momentum carried by the microwave beam was verified experimentally [150].

C. Angular momentum and multi-transducer/space-division techniques

The multi-antenna technique for enhancing the capacity of a link using linear momentum that goes by the name multiple-input-multiple-output (MIMO) is a space-division method that amounts to utilizing the fact that the EM linear momentum $\mathbf{p}^{\text{field}}$ emitted from an ordinary antenna—typically a linear dipole—is a vector quantity. Dividing this EM linear momentum vector up into M equal components such that

$$\mathbf{p}^{\text{field}} = \sum_{n=1}^M \mathbf{p}_n^{\text{field}} \quad (83)$$

letting each $\mathbf{p}_n^{\text{field}}$ be emitted from one of M linear momentum antennas and propagate along different paths to the receiving

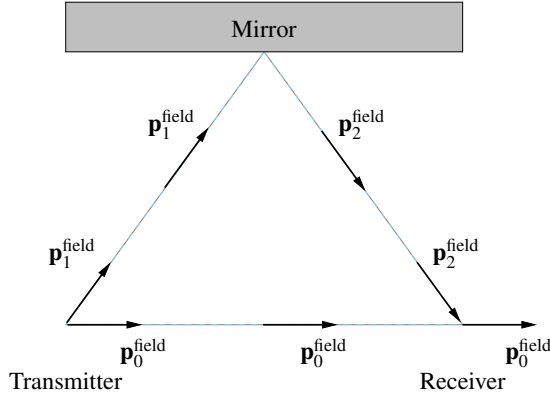


Figure 6. Communicating with electromagnetic linear momentum $\mathbf{p}^{\text{field}}$ in the presence of a reflective surface. In the two-dimensional plane of the figure, the vector $\mathbf{p}_0^{\text{field}}$ propagates directly along the straight path to the receiver, while the vector $\mathbf{p}_1^{\text{field}}$ is reflected off the mirror without recoil and produces the vector $\mathbf{p}_2^{\text{field}}$ at the receiver. Since $\mathbf{p}^{\text{field}}$ is a constant of the motion and preserves its parity upon reflection, the full 3D structure of the EM linear momentum can be obtained by post-processing. This is used in present MIMO schemes for enhancing the spectral density of linear-momentum radio communications in reflective environments.

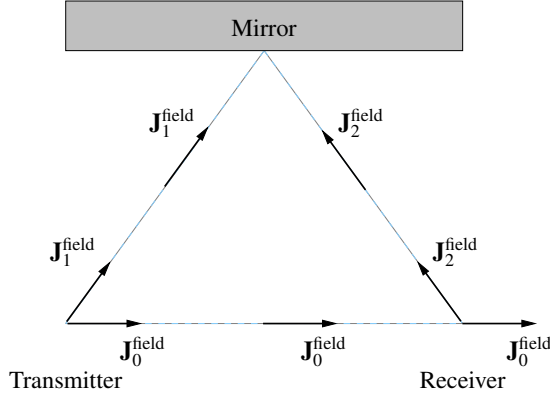


Figure 7. Communicating with electromagnetic angular momentum $\mathbf{J}^{\text{field}}$ in the presence of a reflecting surface. Angular momentum is a pseudovector and therefore $\mathbf{J}^{\text{field}}$ suffers a parity change when it is reflected off a dense medium. Taking this parity change into account properly, the reflected pseudovector can be used in MIMO-type schemes for enhancing the spectral density of angular-momentum radio communications, over and above the enhancement offered by the multi-state capability of angular momentum relative to the single-state linear momentum.

end where the individual EM linear momenta $\mathbf{p}_n^{\text{field}}$ are combined vectorially by digital signal post-processing, the spectral efficiency and/or the signal-to-noise-ratio (SNR) can, under certain circumstances be increased.

A MIMO-like enhancement of the radio spectral capacity can be achieved by the alternative technique of letting a beam of linear momentum $\mathbf{p}^{\text{field}}$ emitted from an antenna be reflected off a wall, say. This works because the linear momentum density (Poynting) vector is an ordinary (polar) vector and therefore does not suffer any parity change upon reflection.

This is illustrated schematically in Fig. 6; see also Fig. 1 in Andrews *et al.* [249] where the authors plot a vector which, in physics terms, is the (approximate) far-field electric field vector but the authors call “polarization,”

For this to work, the Heisenberg uncertainty relation for momentum must be fulfilled. If λ denotes the wavelength, then $p_n^{\text{field}} = \hbar/\lambda$ is the x component of the linear momentum of each photon of the monochromatic radio beam emitted from the n th antenna and this relation becomes

$$\Delta p_n^{\text{field}} \Delta x \geq \hbar/2$$

Hence the spatial separation Δx between the linear momenta must be at least $\lambda/2$ in order to be statistically independent. In practical radio implementations this means that the distance between one (translational current carrying) antenna and another one must fulfill the inequality

$$\Delta x \geq \lambda/2$$

Consequently, the space-time distance between each individual linear-momentum MIMO antenna must be at least half a wavelength; in practical implementations the separation must be much larger. This may limit the usefulness of the MIMO technique in practice. Furthermore, MIMO often requires substantial post-processing and this may limit its usefulness even further [122, 250, 251].

As described earlier, when wireless communication is based on the angular momentum physics layer, it is possible, in an ideal case, to N -tuple the capacity within a fixed frequency bandwidth of a SISO system using single monolithic transducers at both the transmitting and the receiving ends. Furthermore, replacing the single transducer by M transmitting and receiving transducers in order to split the orbital angular momentum (OAM) pseudovector into M equal units $\mathbf{L}_n^{\text{field}}$

$$\mathbf{L}^{\text{field}} = \sum_{n=1}^M \mathbf{L}_n^{\text{field}} \tag{84}$$

it should be possible to achieve an $N \times M$ -fold increase in capacity. Using, in addition to this OAM MIMO technique, also wave polarization (spin angular momentum, SAM), the total capacity will be $2N \times M$ higher than for a linear-momentum SISO channel. As illustrated in Figure 7, the exploitation of the angular momentum technique in a reflective environment requires that the parity of $\mathbf{J}^{\text{field}}$ can be taken properly into account. Experiments have shown that this is feasible [252].

V. SUMMARY

We have presented a review of those fundamental physical principles that comprise the foundation for radio science and technology. We have clarified that in electromagnetic experiments and applications such as wireless communications, one has to rely on the existence and judicious use of electromagnetic observables and have emphasized the fact that by exploiting the angular momentum observable, in addition to the linear momentum observable used today, many advantages can be achieved.

Table II. Similarities and differences between the EM linear momentum density, $\mathbf{g}^{\text{field}}(t, \mathbf{x})$, the Poynting vector $\mathbf{S}(t, \mathbf{x})$, and the EM angular momentum density around a moment point \mathbf{x}_m , $\mathbf{h}^{\text{field}}(t, \mathbf{x}, \mathbf{x}_m)$, carried by a classical electromagnetic field $[\mathbf{E}(t, \mathbf{x}), \mathbf{B}(t, \mathbf{x})]$ in the presence of matter (particles) with mechanical linear momentum density $\mathbf{g}^{\text{mech}}(t, \mathbf{x})$ and mechanical angular momentum density $\mathbf{h}^{\text{mech}}(t, \mathbf{x}, \mathbf{x}_m)$.

Property	Linear momentum density	Angular momentum density
Definition	$\mathbf{g}^{\text{field}} = \epsilon_0 \mathbf{E} \times \mathbf{B} = \mathbf{S}/c^2$	$\mathbf{h}^{\text{field}} = (\mathbf{x} - \mathbf{x}_m) \times (\epsilon_0 \mathbf{E} \times \mathbf{B})$
SI unit	N s m^{-3} ($\text{kg m}^{-2} \text{s}^{-1}$)	$\text{N s m}^{-2} \text{rad}^{-1}$ ($\text{kg m}^{-1} \text{s}^{-1} \text{rad}^{-1}$)
Spatial fall off at large distances r	$\sim r^{-2} + \mathcal{O}(r^{-3})$	$\sim r^{-2} + \mathcal{O}(r^{-3})$
Typical phase factor	$\exp\{i(kz - \omega t)\}$	$\exp\{i(\alpha\varphi + kz - \omega t)\}$
C (charge conjugation) symmetry	Even	Even
P (spatial inversion) symmetry	Even (polar vector, ordinary vector)	Odd (axial vector, pseudovector)
T (time reversal) symmetry	Odd	Odd

The similarities and differences between linear momentum and angular momentum based techniques in radio science and communication applications are summarized in Table II and in the following list:

1. The conventional techniques based on the linear momentum degrees of freedom of an electromechanical system exploits the translational degrees of freedom of the EM field and the associated particles.

- (a) The linear momentum $\mathbf{p}^{\text{field}}(t)$ can be measured remotely—and thereby be utilized in applications—by employing a conduction current based device that integrates the local linear momentum density $\mathbf{g}^{\text{field}}(t, \mathbf{x})$ over a one-dimensional volume V , typically a very thin cylinder as is the case for the ubiquitous linear electric dipole antenna.

From such a nonlocal measurement one can estimate the (weighted) average of the primary EM field over V but not determine the exact field (within instrumental errors).

2. Novel techniques based on the angular momentum degrees of freedom of an electromechanical system exploits the rotational degrees of freedom of the EM field and the associated particles.

- (a) The angular momentum $\mathbf{J}^{\text{field}}(t)$ can be measured remotely—and thereby utilized in applications—by using a conduction current based device, or a spin- and/or orbit current based device, that integrates the local angular momentum density $\mathbf{h}^{\text{field}}(t, \mathbf{x})$ over a two- or three-dimensional volume.

- (b) In a beam situation typical for radio communication links, radio astronomy observations, and radar applications, the spin and angular parts of the angular momentum, $\mathbf{\Sigma}^{\text{field}}$ and $\mathbf{J}^{\text{field}}$ respectively, can be separated or, alternatively, both the helicity and the total angular momentum of the beam can be measured [253]. The main differences between the two parts of the angular momenta are:
 - i. The spin part of the angular momentum (SAM, polarization), $\mathbf{\Sigma}^{\text{field}}$, manifests itself as a rotation in time of the field vectors such that they

have different directions (oscillation phase) modulo 2π at one position \mathbf{x} in the phase front at different times t and $t + \Delta t$. Hence, the measurement of SAM (polarization) requires temporal coherence.

- ii. The orbital part of the angular momentum (OAM, twist), $\mathbf{L}^{\text{field}}$, manifests itself as a rotation in space of the field vectors such that they have different directions (oscillation phase) modulo 2π at different azimuthal angles φ and $\varphi + \Delta\varphi$ in the phase plane at a given instant t . Hence, the measurement of OAM (twist) requires spatial coherence.

ACKNOWLEDGMENTS

The authors gratefully acknowledge useful discussions with professor Iwo Białynicki-Birula, professor Anton Zeilinger, and professor Markus Aspelmeyer. We also thank professor Göran Fäldt, Uppsala, for reminding us about the excellent treatment by Truesdell [128] on the fundamental properties of angular momentum, and professor Olle Eriksson, Uppsala, for comments on skyrmions.

B. T. thanks the Institute for Quantum Optics and Quantum Information (IQOQI), Vienna, where part of this work was done, for very generous hospitality during repeated visits.

B. T. was financially supported by the Swedish National Space Board (SNSB) and the Swedish Research Council (VR) under the contract number 2012-3297. H. T. acknowledges support from EPSRC grant EP/H005188/1 and, for the early stage of the work, from the Centre for Dynamical Processes and Structure Formation, Uppsala University, Sweden.

Appendix A: The ten Poincaré invariants and the corresponding equations of continuity

If all conserved quantities (constants of motion) of an integrable physical system are known, the system dynamics can be obtained trivially by formulating it in terms of action-angle variables. All in all the electromagnetic field has 84 constants of motion [3]. In this Appendix we discuss the ten conserved elec-

tromagnetic observables that correspond to the ten-dimensional Poincaré symmetry group $P(10)$, *i.e.*, the ten Poincaré invariants and their associated equations of continuity. They are the scalar quantity energy, the three components of the linear momentum vector, the three components of the angular momentum pseudovector, and the three components of the energy center position vector. Only a small subset of these observables are currently used in radio science, optics, and wireless communications.

Electromagnetic conservation laws can be viewed as constraints on the field dynamics and, in this sense, every conserved quantity is physically significant. The information contained in the conserved quantities corresponds one-to-one to the information contained in the Maxwell-Lorentz postulates [254].

1. Energy

The energy density $u^{\text{field}}(t, \mathbf{x})$ carried by the fields generated by the sources in V' is

$$u^{\text{field}} = \frac{\epsilon_0}{2} (\mathbf{E} \cdot \mathbf{E} + c^2 \mathbf{B} \cdot \mathbf{B}) \quad (\text{A1a})$$

which, according to Eqns. (2) and Table I, can be written

$$u^{\text{field}} = \frac{\epsilon_0}{2} \mathbf{G} \cdot \mathbf{G}^* = \frac{\epsilon_0}{2} |\mathbf{G}|^2 = \frac{\epsilon_0}{2} \sqrt{(\mathbf{G} \cdot \mathbf{G})(\mathbf{G} \cdot \mathbf{G}^*)} \quad (\text{A1b})$$

Outside the source volume V' , the field energy in a certain observation volume V can be measured with an appropriate energy sensor, *e.g.*, a calorimeter or bolometer, that integrates u^{field} over V .

With the energy flux vector (Poynting vector) $\mathbf{S}(t, \mathbf{x})$ given by the formula

$$\mathbf{S} = \epsilon_0 c^2 \mathbf{E} \times \mathbf{B} \quad (\text{A2a})$$

or, using Eqns. (2) and Table I,

$$\mathbf{S} = i \frac{\epsilon_0 c}{2} \mathbf{G} \times \mathbf{G}^* \quad (\text{A2b})$$

the energy density balance equation, which follows straightforwardly from the Maxwell-Lorentz equations (1), takes the form

$$\frac{\partial u^{\text{field}}}{\partial t} + \nabla \cdot \mathbf{S} = -\mathbf{j}^e \cdot \mathbf{E} \quad (\text{A3})$$

i.e., a local continuity equation for the field energy density with a sink (loss) term $\mathbf{j}^e \cdot \mathbf{E}$. By using Eqns. (2), (A1b), and (A2b), we can write this as

$$\frac{\partial (\mathbf{G} \cdot \mathbf{G}^*)}{\partial t} + i c \nabla \cdot (\mathbf{G} \times \mathbf{G}^*) = -\frac{1}{\epsilon_0} \mathbf{j}^e \cdot (\mathbf{G} + \mathbf{G}^*) \quad (\text{A4})$$

If $\rho^{\text{mech}}(t', \mathbf{x}')$ denotes the local mechanical mass density field and $\mathbf{v}^{\text{mech}}(t', \mathbf{x}')$ the local mechanical velocity field of

the charged particles at a point in V' , then, in the approximation where statistical mechanics as well as relativistic and quantum physics effects are negligible, the electric current density $\mathbf{j}^e(t', \mathbf{x}')$ carried by the charged particles can be written as $\mathbf{j}^e = \rho^e \mathbf{v}^{\text{mech}}$ and the loss term in Eqn. (A3) can therefore be identified as the increase in mechanical energy density of the particles [7, 8]:

$$\frac{\partial u^{\text{mech}}}{\partial t} = \mathbf{j}^e \cdot \mathbf{E} = \mathbf{v}^{\text{mech}} \cdot \rho^e \mathbf{E} \quad (\text{A5})$$

representing dissipation due to Ohmic losses, *i.e.*, transfer of field energy density to mechanical energy density of the current-carrying particles.

This identification makes it possible to introduce the total energy density of the electromechanical system under study (charged particles and their associated fields)

$$u^{\text{sys}}(t, \mathbf{x}) = u^{\text{field}}(t, \mathbf{x}) + u^{\text{mech}}(t, \mathbf{x}) \quad (\text{A6})$$

and to put Eqn. (A3) in the form of an equation of continuity where there are no sources or sinks (losses) [7, 8]:

$$\frac{\partial u^{\text{sys}}}{\partial t} + \nabla \cdot \mathbf{S} = 0 \quad (\text{A7})$$

We let $U(t)$ denote energy (volume integrated energy density). Then, in obvious notation, the system energy is the sum of the energy of the particles and the energy of the field:

$$U^{\text{sys}}(t) = \int_V d^3x u^{\text{sys}}(t, \mathbf{x}) = U^{\text{field}}(t) + U^{\text{mech}}(t) \quad (\text{A8})$$

Volume integrating the local continuity equation (A7) and using the divergence theorem, the corresponding global continuity equation can be written

$$\frac{dU^{\text{sys}}}{dt} + \oint_S d^2x \hat{\mathbf{n}} \cdot \mathbf{S} = 0 \quad (\text{A9})$$

This is the Poynting theorem, also known as the energy theorem in Maxwell's theory. It is utilized, for instance, in radiometry. The field energy itself is utilized in simple, broadband "on-off" signaling as was used in Marconi's first radio experiments and also in optical fiber communications. The conservation of energy as described by (A9) is a manifestation of the temporal translation invariance symmetry of electrodynamics and describes the kinematics of the system.

2. Linear momentum

The electromagnetic linear momentum density $\mathbf{g}^{\text{field}}(t, \mathbf{x})$ radiated from V' is [7–9, 65]

$$\mathbf{g}^{\text{field}} = \epsilon_0 \mathbf{E} \times \mathbf{B} \quad (\text{A10})$$

or, using Eqns. (2),

$$\mathbf{g}^{\text{field}} = i \frac{\epsilon_0}{2c} \mathbf{G} \times \mathbf{G}^* \quad (\text{A11})$$

and is, in free space, simply related to the Poynting vector (A2) by the Planck relation

$$\mathbf{S} = c^2 \mathbf{g}^{\text{field}} \quad (\text{A12})$$

Let us introduce the electromagnetic linear momentum flux tensor $\mathbf{T}(t, \mathbf{x})$ as the negative of Maxwell's stress tensor [7, 9]

$$\mathbf{T} = u^{\text{field}} \mathbb{1}_3 - \epsilon_0 (\mathbf{E} \otimes \mathbf{E} + c^2 \mathbf{B} \otimes \mathbf{B}) \quad (\text{A13a})$$

or, using Eqns. (2),

$$\mathbf{T} = \frac{\epsilon_0}{2} [\mathbf{G} \cdot \mathbf{G}^* \mathbb{1}_3 - (\mathbf{G} \otimes \mathbf{G}^* + \mathbf{G}^* \otimes \mathbf{G})] \quad (\text{A13b})$$

where $\mathbb{1}_3$ is the rank-3 unit tensor and \otimes the tensor (Kronecker, dyadic) product operator. Then the balance equation for linear momentum density that follows from the Maxwell-Lorentz equations (1) can be written [7–9]

$$\frac{\partial \mathbf{g}^{\text{field}}}{\partial t} + \nabla \cdot \mathbf{T} = -\mathbf{f} \quad (\text{A14a})$$

where

$$\mathbf{f}(t, \mathbf{x}) = \rho^e(t, \mathbf{x}) \mathbf{E}(t, \mathbf{x}) + \mathbf{j}^e \times \mathbf{B}(t, \mathbf{x}) \quad (\text{A14b})$$

This polar vector \mathbf{f} is the Lorentz force density[255] that behaves like a loss of field linear momentum density.

By using Eqns. (2), (A11), and (A13b) we can write this local equation of continuity for linear momentum density as

$$\begin{aligned} & \frac{\partial (\mathbf{G} \times \mathbf{G}^*)}{\partial t} - i c \nabla \cdot (\mathbf{G} \cdot \mathbf{G}^* \mathbb{1}_3 - \frac{1}{\epsilon_0} (\mathbf{G} \otimes \mathbf{G}^* + \mathbf{G}^* \otimes \mathbf{G})) \\ & = -i \frac{c}{\epsilon_0} [\rho^e (\mathbf{G} + \mathbf{G}^*) - \epsilon_0 \mathbf{j}^e \times (\mathbf{G} - \mathbf{G}^*)] \end{aligned} \quad (\text{A15})$$

In an electromechanical system of charged, massive particles and pertinent fields, *e.g.*, a transmitting antenna, the mechanical linear momentum density the particles is

$$\mathbf{g}^{\text{mech}}(t, \mathbf{x}) = \rho^{\text{mech}}(t, \mathbf{x}) \mathbf{v}^{\text{mech}}(t, \mathbf{x}) \quad (\text{A16})$$

The local equation of continuity of linear momentum of an electromechanical system, directly derivable from Maxwell's equations, can therefore be written [7–9, 67]

$$\frac{\partial \mathbf{g}^{\text{sys}}}{\partial t} + \nabla \cdot \mathbf{T} = \mathbf{0} \quad (\text{A17})$$

where

$$\mathbf{g}^{\text{sys}}(t, \mathbf{x}) = \mathbf{g}^{\text{field}}(t, \mathbf{x}) + \mathbf{g}^{\text{mech}}(t, \mathbf{x}) \quad (\text{A18})$$

is the system linear momentum density.

The classical electromagnetic field linear momentum $\mathbf{p}^{\text{field}}$ that is localized inside a volume V embedded in free space is obtained by volume integrating the linear momentum density $\mathbf{g}^{\text{field}}$ over V [8, 9, 67]

$$\mathbf{p}^{\text{field}}(t) = \int_V d^3x \mathbf{g}^{\text{field}}(t, \mathbf{x}) = \epsilon_0 \int_V d^3x [\mathbf{E}(t, \mathbf{x}) \times \mathbf{B}(t, \mathbf{x})] \quad (\text{A19})$$

This integration can be done by using an appropriate volume integrating linear momentum sensor, *e.g.*, a linear dipole antenna.

The mechanical linear momentum in V is

$$\mathbf{p}^{\text{mech}}(t) = \int_V d^3x \mathbf{g}^{\text{mech}}(t, \mathbf{x}) = \int_V d^3x \rho^{\text{mech}}(t, \mathbf{x}) \mathbf{v}^{\text{mech}}(t, \mathbf{x}) \quad (\text{A20})$$

which means that the total linear momentum of the system of particles and fields in V is

$$\mathbf{p}^{\text{sys}}(t) = \mathbf{p}^{\text{field}}(t) + \mathbf{p}^{\text{mech}}(t) \quad (\text{A21})$$

It fulfills the global conservation law [7, 8, 10]

$$\frac{d\mathbf{p}^{\text{sys}}}{dt} + \oint_S d^2x \hat{\mathbf{n}} \cdot \mathbf{T} = \mathbf{0} \quad (\text{A22})$$

This is the linear momentum theorem in Maxwell's theory. It demonstrates that not only the mechanical particles (charges) but also the electromagnetic field itself carries linear momentum (translational momentum) that couples to the mechanical linear momentum of the matter (charged particles) and thereby to the conduction current carried by the charged particles.

a. Gauge invariance

It is common practice to investigate the properties of the electromagnetic observables that we consider here, by expressing the fields in terms of their potentials [256]. If the vector potential $\mathbf{A}(t, \mathbf{x})$ is twice continuously differentiable in space, it is well known that it fulfills the vector analytic identity (see, *e.g.*, Thidé [10])

$$\begin{aligned} \mathbf{A}(t, \mathbf{x}) &= -\nabla \int_{V'} d^3x' \frac{\nabla' \cdot \mathbf{A}(t, \mathbf{x}')}{4\pi |\mathbf{x} - \mathbf{x}'|} \\ &+ \nabla \times \int_{V'} d^3x' \frac{\nabla' \times \mathbf{A}(t, \mathbf{x}')}{4\pi |\mathbf{x} - \mathbf{x}'|} \\ &- \oint_{S'} d^2x' \hat{\mathbf{n}}' \cdot \left(\frac{\mathbf{A}(t, \mathbf{x}') \otimes (\mathbf{x} - \mathbf{x}')}{|\mathbf{x} - \mathbf{x}'|^3} \right) \end{aligned} \quad (\text{A23})$$

The last integral, to be evaluated over a surface S' enclosing the entire volume V' within which $\mathbf{A} \neq \mathbf{0}$ is localized, vanishes if it is evaluated at very large distances and the expression within the big parentheses falls off faster than $1/|\mathbf{x} - \mathbf{x}'|^2 = 1/r^2$, or if it is perpendicular to the normal unit vector $\hat{\mathbf{n}}'$, or if it has certain (a)symmetry properties [257]. Then, Helmholtz's decomposition is applicable, allowing us to write

$$\mathbf{A}(t, \mathbf{x}) = \mathbf{A}^{\text{irrot}}(t, \mathbf{x}) + \mathbf{A}^{\text{rotat}}(t, \mathbf{x}) \quad (\text{A24})$$

where $\mathbf{A}^{\text{irrot}}$ is the irrotational part of \mathbf{A} , fulfilling $\nabla \times \mathbf{A}^{\text{irrot}} = \mathbf{0}$, and $\mathbf{A}^{\text{rotat}}$ is the rotational part, fulfilling $\nabla \cdot \mathbf{A}^{\text{rotat}} = 0$. Since $\mathbf{A}^{\text{rotat}}$ is gauge invariant by definition, it follows that in this case

$$\mathbf{B}(t, \mathbf{x}) = \nabla \times \mathbf{A}(t, \mathbf{x}) = \nabla \times \mathbf{A}^{\text{rotat}}(t, \mathbf{x}) \quad (\text{A25})$$

If we take (A19) as a starting point, and assume that not only the vector potential \mathbf{A} can be Helmholtz decomposed, but also \mathbf{E} is so well-behaved that it can be decomposed as

$$\mathbf{E}(t, \mathbf{x}) = \mathbf{E}^{\text{irrot}}(t, \mathbf{x}) + \mathbf{E}^{\text{rotat}}(t, \mathbf{x}) \quad (\text{A26})$$

then the electromagnetic linear (translational) momentum can be represented by the gauge invariant expression

$$\begin{aligned} \mathbf{p}^{\text{field}}(t) &= \varepsilon_0 \int_V d^3x \mathbf{E}^{\text{irrot}} \times (\nabla \times \mathbf{A}^{\text{rotat}}) \\ &+ \varepsilon_0 \int_V d^3x \mathbf{E}^{\text{rotat}} \times (\nabla \times \mathbf{A}^{\text{rotat}}) \end{aligned} \quad (\text{A27})$$

Using straightforward vector analysis, we obtain the following result [10]

$$\begin{aligned} \mathbf{p}^{\text{field}}(t) &= \int_V d^3x \rho^e \mathbf{A}^{\text{rotat}} - \varepsilon_0 \int_V d^3x \mathbf{A}^{\text{rotat}} \times (\nabla \times \mathbf{E}^{\text{rotat}}) \\ &- \varepsilon_0 \oint_S d^2x \hat{\mathbf{n}} \cdot \mathbf{E}^{\text{rotat}} \otimes \mathbf{A}^{\text{rotat}} \end{aligned} \quad (\text{A28})$$

Whenever Eqns. (A24) and (A26) hold, this gauge invariant expression for $\mathbf{p}^{\text{field}}$ is exact. If the electric field is such that it cannot be Helmholtz decomposed, every occurrence of $\mathbf{E}^{\text{irrot}}$ and $\mathbf{E}^{\text{rotat}}$ in Eqn. A27 and Eqn. A28 has to be replaced by \mathbf{E} but would still be exact and gauge independent.

If the expression within the big parentheses in the integrand of the last integral in Eqn. (A23) is such that this surface integral grows without bounds at very large distances, it is not possible to decompose the vector potential as described by Eqn. (A24) and $\mathbf{A}^{\text{rotat}}$ and $\mathbf{E}^{\text{rotat}}$ in Eqn. A27 and Eqn. A28 would have to be replaced by \mathbf{A} and \mathbf{E} .

b. First quantization formalism

If we restrict ourselves to consider a single temporal Fourier component of the rotational ('transverse') component of \mathbf{E} in a region where $\rho^e = 0$, we find that in complex representation

$$\mathbf{E}^{\text{rotat}} = -\frac{\partial \mathbf{A}^{\text{rotat}}}{\partial t} = i\omega \mathbf{A}^{\text{rotat}} \quad (\text{A29})$$

which allows us to replace $\mathbf{A}^{\text{rotat}}$ by $-i\mathbf{E}^{\text{rotat}}/\omega$, yielding,

$$\begin{aligned} \langle \mathbf{p}^{\text{field}} \rangle_t &= \text{Re} \left\{ -i \frac{\varepsilon_0}{2\omega} \int_V d^3x (\nabla \otimes \mathbf{E}^{\text{rotat}}) \cdot (\mathbf{E}^{\text{rotat}})^* \right\} \\ &+ \text{Re} \left\{ i \frac{\varepsilon_0}{2\omega} \oint_S d^2x \hat{\mathbf{n}} \cdot \mathbf{E}^{\text{rotat}} \otimes (\mathbf{E}^{\text{rotat}})^* \right\} \end{aligned} \quad (\text{A30})$$

If the tensor (dyadic) $\mathbf{E} \otimes (\mathbf{E}^{\text{rotat}})^*$ is regular and falls off sufficiently rapidly at large distances or if $\hat{\mathbf{n}} \cdot \mathbf{E} = 0$, we can discard the surface integral term and find that the cycle averaged linear momentum carried by the rotational components of the fields, $\mathbf{E}^{\text{rotat}}$ and $\mathbf{B}^{\text{rotat}} \equiv \mathbf{B} = \nabla \times \mathbf{A}^{\text{rotat}}$, is

$$\langle \mathbf{p}^{\text{field}} \rangle_t = \text{Re} \left\{ -i \frac{\varepsilon_0}{2\omega} \int_V d^3x (\nabla \otimes \mathbf{E}^{\text{rotat}}) \cdot (\mathbf{E}^{\text{rotat}})^* \right\} \quad (\text{A31})$$

In complex tensor notation this can be written

$$\begin{aligned} \langle \mathbf{p}^{\text{field}} \rangle_t &= -i \frac{\varepsilon_0}{2\omega} \sum_{i,j=1}^3 \int_V d^3x (E_i^{\text{rotat}})^* (\hat{\mathbf{x}}_j \partial_j E_i^{\text{rotat}}) \\ &= -i \frac{\varepsilon_0}{2\omega} \sum_{i=1}^3 \int_V d^3x (E_i^{\text{rotat}})^* \nabla E_i^{\text{rotat}} \end{aligned} \quad (\text{A32})$$

Making use of the field linear momentum operator, Eqn. (5), we can write the expression for the linear momentum of the electromagnetic field in terms of this operator as

$$\langle \mathbf{p}^{\text{field}} \rangle_t = \frac{\varepsilon_0}{2\hbar\omega} \sum_{i=1}^3 \int_V d^3x (E_i^{\text{rotat}})^* \hat{\mathbf{p}}^{\text{field}} E_i^{\text{rotat}} \quad (\text{A33})$$

If we introduce the vector

$$\Psi = \sum_{i=1}^3 \Psi_i \hat{\mathbf{x}}_i = \sqrt{\frac{\varepsilon_0}{2\hbar\omega}} \mathbf{E}^{\text{rotat}} = \sqrt{\frac{\varepsilon_0}{2\hbar\omega}} \sum_{i=1}^3 E_i^{\text{rotat}} \hat{\mathbf{x}}_i \quad (\text{A34})$$

we can write

$$\langle \mathbf{p}^{\text{field}} \rangle_t = \sum_{i=1}^3 \int_V d^3x \Psi_i^* \hat{\mathbf{p}}^{\text{field}} \Psi_i \quad (\text{A35})$$

or, if we assume Einstein's summation convention,

$$\langle \mathbf{p}^{\text{field}} \rangle_t = \langle \Psi_i | \hat{\mathbf{p}}^{\text{field}} | \Psi_i \rangle \quad (\text{A36})$$

Thus we can represent the cycle (temporal) averaged linear momentum carried by a monochromatic electromagnetic field as a sum of diagonal quantal matrix elements (expectation values) where the rotational ('transverse') component of the (scaled) electric field vector behaves as a kind of vector wavefunction.

Methods based on electromagnetic linear momentum are used for radio science and radar applications, and for wireless communications.

3. Angular momentum

The volumetric density of the electromagnetic field angular momentum, radiated from V' is [65, Sect. 10.6], [7, 10]

$$\mathbf{h}^{\text{field}}(t, \mathbf{x}; \mathbf{x}_m) = (\mathbf{x} - \mathbf{x}_m) \times \mathbf{g}^{\text{field}} = \varepsilon_0 (\mathbf{x} - \mathbf{x}_m) \times (\mathbf{E} \times \mathbf{B}) \quad (\text{A37})$$

where $\mathbf{x}_m = \sum_{i=1}^3 x_{mi} \hat{\mathbf{x}}_i$ is a regular but otherwise arbitrary point (the moment point). Using Eqns. (2), we can write this in complex notation as

$$\mathbf{h}^{\text{field}}(t, \mathbf{x}; \mathbf{x}_m) = i \frac{\varepsilon_0}{2c} (\mathbf{x} - \mathbf{x}_m) \times (\mathbf{G} \times \mathbf{G}^*) \quad (\text{A38})$$

The mechanical angular momentum density of the charged particles around \mathbf{x}_m is

$$\begin{aligned} \mathbf{h}^{\text{mech}}(t, \mathbf{x}; \mathbf{x}_m) &= (\mathbf{x} - \mathbf{x}_m) \times \mathbf{g}^{\text{mech}}(t, \mathbf{x}) \\ &= (\mathbf{x} - \mathbf{x}_m) \times \rho^{\text{mech}}(t, \mathbf{x}) \mathbf{v}^{\text{mech}}(t, \mathbf{x}) \end{aligned} \quad (\text{A39})$$

As emphasized by Truesdell [128], angular momentum (also known as moment of momentum) is a physical observable in its own right, in general independent of and not derivable from linear momentum[258]. Therefore, as is well known, the knowledge of one of these two observables does not automatically imply a knowledge of the other. This also follows from Noether's theorem [1, 259].

Let us introduce the electromagnetic angular momentum flux pseudotensor

$$\mathbf{M}(\mathbf{x}_m) = (\mathbf{x} - \mathbf{x}_m) \times \mathbf{T} \quad (\text{A40})$$

where \mathbf{T} is defined by formula (A13), and the physically observable the Lorentz torque density pseudovector (axial vector) around the moment point \mathbf{x}_m is

$$\boldsymbol{\tau}(t, \mathbf{x} - \mathbf{x}_m) = (\mathbf{x} - \mathbf{x}_m) \times \mathbf{f}(t, \mathbf{x}) \quad (\text{A41})$$

where \mathbf{f} is the Lorentz force density defined by formula (A14b). Then the following local conservation law can be derived from Maxwell's equations [7, 8, 10, 260]

$$\frac{\partial \mathbf{h}^{\text{field}}(\mathbf{x}_m)}{\partial t} + \nabla \cdot \mathbf{M}(\mathbf{x}_m) = -\boldsymbol{\tau} \quad (\text{A42})$$

Hence, there is a loss of field angular momentum density to the mechanical angular momentum density, in the form of Lorentz torque density $\boldsymbol{\tau}$, showing that the angular momentum of the electromagnetic field and the rotational dynamics of the charges and currents are coupled to each other.

By using Eqns. (2), (A38), and (A13b) we can write this local equation of continuity for angular momentum density as

$$\begin{aligned} & \frac{\partial [(\mathbf{x} - \mathbf{x}_m) \times (\mathbf{G} \times \mathbf{G}^*)]}{\partial t} \\ & - ic \nabla \cdot \left[(\mathbf{x} - \mathbf{x}_m) \times \left(\mathbf{G} \cdot \mathbf{G}^* \mathbf{1}_3 - \frac{1}{\epsilon_0} (\mathbf{G} \otimes \mathbf{G}^* + \mathbf{G}^* \otimes \mathbf{G}) \right) \right] \\ & = -i \frac{c}{\epsilon_0} (\mathbf{x} - \mathbf{x}_m) \times [\rho^e (\mathbf{G} + \mathbf{G}^*) - \epsilon_0 \mathbf{j}^e \times (\mathbf{G} - \mathbf{G}^*)] \end{aligned} \quad (\text{A43})$$

Recalling the definition (A39) of the mechanical angular momentum density, and that the angular momentum density of the system is

$$\mathbf{h}^{\text{sys}}(t, \mathbf{x}; \mathbf{x}_m) = \mathbf{h}^{\text{field}}(t, \mathbf{x}; \mathbf{x}_m) + \mathbf{h}^{\text{mech}}(t, \mathbf{x}; \mathbf{x}_m) \quad (\text{A44})$$

the continuity equation (A42) can be written

$$\frac{\partial \mathbf{h}^{\text{sys}}(t, \mathbf{x}; \mathbf{x}_m)}{\partial t} + \nabla \cdot \mathbf{M}(\mathbf{x}_m) = \mathbf{0} \quad (\text{A45})$$

This shows that a volume containing an arbitrary distribution of charge density $\rho^e(t', \mathbf{x}')$ and current density $\mathbf{j}^e(t', \mathbf{x}')$ does not only radiate linear momentum density (Poynting vector) but also angular momentum density into the surrounding free space; see also [165]. However, since angular momentum describes rotations, it cannot be sensed by a single linear dipole or similar one-dimensional linear-momentum sensing antenna.

The total classical electromagnetic angular momentum around an arbitrary moment point \mathbf{x}_m carried by the electromagnetic field in a volume V is [see also Mandel and Wolf

[65]]

$$\begin{aligned} \mathbf{J}^{\text{field}}(t; \mathbf{x}_m) &= \int_V d^3x \mathbf{h}^{\text{field}}(t, \mathbf{x}; \mathbf{x}_m) \\ &= \epsilon_0 \int_V d^3x \mathbf{x} \times [\mathbf{E}(t, \mathbf{x}) \times \mathbf{B}(t, \mathbf{x})] \\ &\quad - \mathbf{x}_m \times \epsilon_0 \int_V d^3x [\mathbf{E}(t, \mathbf{x}) \times \mathbf{B}(t, \mathbf{x})] \\ &= \mathbf{J}^{\text{field}}(t; \mathbf{0}) - \mathbf{x}_m \times \mathbf{p}^{\text{field}}(t) \end{aligned} \quad (\text{A46})$$

where, in the last step, Eqn. (A19) was used.

The mechanical angular momentum in V is

$$\begin{aligned} \mathbf{J}^{\text{mech}}(t; \mathbf{x}_m) &= \int_V d^3x \mathbf{h}^{\text{mech}}(t, \mathbf{x}; \mathbf{x}_m) \\ &= \int_V d^3x (\mathbf{x} - \mathbf{x}_m) \times \rho^{\text{mech}}(t, \mathbf{x}) \mathbf{v}^{\text{mech}}(t, \mathbf{x}) \\ &= \mathbf{J}^{\text{mech}}(t; \mathbf{0}) - \mathbf{x}_m \times \mathbf{p}^{\text{mech}}(t) \end{aligned} \quad (\text{A47})$$

where, in the last step, Eqn. (A20) was used.

Hence, the total angular momentum of the system of particles and fields in V is

$$\begin{aligned} \mathbf{J}^{\text{sys}}(t; \mathbf{x}_m) &= \mathbf{J}^{\text{field}}(t; \mathbf{x}_m) + \mathbf{J}^{\text{mech}}(t; \mathbf{x}_m) \\ &= \mathbf{J}^{\text{sys}}(t; \mathbf{0}) - \mathbf{x}_m \times \mathbf{p}^{\text{sys}}(t) \end{aligned} \quad (\text{A48})$$

Clearly, if $\mathbf{p}^{\text{sys}} \neq \mathbf{0}$, then it is always possible to find a moment point \mathbf{x}_m that makes the total system angular momentum vanish. If, on the other hand, $\mathbf{p}^{\text{sys}} = \mathbf{0}$, then the total system angular momentum is independent of moment point \mathbf{x}_m .

The total angular momentum of the system of charges, currents and fields fulfills the global conservation law [7, 9, 67]

$$\frac{d\mathbf{J}^{\text{sys}}(\mathbf{x}_m)}{dt} + \oint_S d^2x \hat{\mathbf{n}} \cdot \mathbf{M}(\mathbf{x}_m) = \mathbf{0} \quad (\text{A49})$$

i.e., a continuity equation without sources and sinks showing that for a constant angular momentum flux (including zero) the system's angular momentum is a constant of motion. This is the angular momentum theorem in Maxwell's theory. It shows that not only the mechanical particles (charges) but also the electromagnetic field itself carries angular momentum (rotational momentum) that couples to the mechanical angular momentum of the matter (charged particles) and thereby to the conduction current carried by the charged particles.

We see that the conservation law (A49) describes the angular momentum analogs of the linear momentum processes described by the conservation law (A22) and shows that the use of single monolithic antenna devices based on torque action will allow an alternative way of transferring information but with the added benefit of higher information density offered by the inherent quantized multi-state property of the classical electromagnetic angular momentum.

a. Gauge invariance

If the vector potential can be decomposed as in Subsect. A 2 a and if one uses several vector analytic identities

and employing partial integration, it is possible to derive an exact, manifestly gauge invariant expression for the total field angular momentum $\mathbf{J}^{\text{field}}$ that is the sum of two pseudovectors, one independent and one dependent of the moment point \mathbf{x}_m . The result is [10]

$$\mathbf{J}^{\text{field}}(t, \mathbf{x}_m) = \boldsymbol{\Sigma}^{\text{field}}(t) + \mathbf{L}^{\text{field}}(t, \mathbf{x}_m) \quad (\text{A50})$$

where

$$\boldsymbol{\Sigma}^{\text{field}}(t) = \varepsilon_0 \int_V d^3x \mathbf{E}(t, \mathbf{x}) \times \mathbf{A}^{\text{rotat}}(t, \mathbf{x}) \quad (\text{A51a})$$

and

$$\begin{aligned} \mathbf{L}^{\text{field}}(t, \mathbf{x}_m) &= \int_V d^3x (\mathbf{x} - \mathbf{x}_m) \times \rho^e(t, \mathbf{x}) \mathbf{A}^{\text{rotat}}(t, \mathbf{x}) \\ &+ \varepsilon_0 \int_V d^3x (\mathbf{x} - \mathbf{x}_m) \times ([\nabla \otimes \mathbf{A}^{\text{rotat}}(t, \mathbf{x})] \cdot \mathbf{E}(t, \mathbf{x})) \\ &- \varepsilon_0 \oint_S d^2x \hat{\mathbf{n}} \cdot [\mathbf{E}(t, \mathbf{x}) \otimes (\mathbf{x} - \mathbf{x}_m) \times \mathbf{A}^{\text{rotat}}(t, \mathbf{x})] \quad (\text{A51b}) \end{aligned}$$

The last integral vanishes if the integrand is regular and falls off sufficiently rapidly, becomes perpendicular to $\hat{\mathbf{n}}$, or otherwise causes the surface integral to go to zero at very large distances. However, if the vector potential \mathbf{A} is not regular and/or does not fall off faster than $1/r$ as r tends to infinity, the separation of $\mathbf{J}^{\text{field}}$ into $\boldsymbol{\Sigma}^{\text{field}}$ and $\mathbf{L}^{\text{field}}$ is not gauge invariant and, hence, not unique; *cf.* Leader [261] and Białyński-Birula and Białyńska-Birula [262]. See also Keller [36, Sect. 7].

b. First quantization formalism

Let us now assume that \mathbf{A} is so well-behaved that the conditions for Helmholtz's decomposition (A24) are fulfilled and, furthermore, that ρ^e vanishes in the region of interest. Particularizing to a single temporal Fourier component of the field $\propto \exp(-i\omega t)$, we can then write $\mathbf{E} = -\partial\mathbf{A}/\partial t = i\omega\mathbf{A}$ and obtain the following expressions for the cycle averages of $\boldsymbol{\Sigma}^{\text{field}}$ and $\mathbf{L}^{\text{field}}$ in complex notation:

$$\langle \boldsymbol{\Sigma}^{\text{field}} \rangle_t = -i \frac{\varepsilon_0}{2\omega} \int_V d^3x (\mathbf{E}^* \times \mathbf{E}) \quad (\text{A52a})$$

$$\begin{aligned} \langle \mathbf{L}^{\text{field}}(\mathbf{x}_m) \rangle_t &= -i \frac{\varepsilon_0}{2\omega} \sum_{i=1}^3 \int_V d^3x E_i^* [(\mathbf{x} - \mathbf{x}_m) \times \nabla] E_i \\ &= \frac{\varepsilon_0}{2\hbar\omega} \sum_{i=1}^3 \int_V d^3x E_i^* (-i\hbar\mathbf{x} \times \nabla) E_i \\ &\quad - \frac{\varepsilon_0}{2\hbar\omega} \mathbf{x}_m \times \sum_{i=1}^3 \int_V d^3x E_i^* (-i\hbar\nabla) E_i \\ &= \langle \mathbf{L}^{\text{field}}(\mathbf{0}) \rangle_t - \mathbf{x}_m \times \langle \mathbf{p}^{\text{field}} \rangle_t \quad (\text{A52b}) \end{aligned}$$

We note that if the cycle averaged electromagnetic field linear momentum $\langle \mathbf{p}^{\text{field}} \rangle_t \neq \mathbf{0}$, it is always possible to choose the moment point \mathbf{x}_m such that $\langle \mathbf{L}^{\text{field}}(\mathbf{x}_m) \rangle_t = \mathbf{0}$. But if $\langle \mathbf{p}^{\text{field}} \rangle_t = \mathbf{0}$, *i.e.*, if the cycle average of the linear momentum of the

monochromatic field in question vanishes in a volume V , then the cycle averaged OAM, $\langle \mathbf{L}^{\text{field}} \rangle_t$, is independent of \mathbf{x}_m in V . In a beam geometry the quantity $\boldsymbol{\Sigma}^{\text{field}}$ can often to a good approximation be identified with the spin angular momentum (SAM) carried by the field, and $\mathbf{L}^{\text{field}}$ with its orbital angular momentum (OAM).

The fact that we can express the temporal averages $\langle \mathbf{p}^{\text{field}} \rangle_t$ and $\langle \mathbf{L}^{\text{field}} \rangle_t$ in terms of expectation values with the quantal operators for linear and angular momentum, $\hat{\mathbf{p}}^{\text{field}} = -i\hbar\nabla$ and $\hat{\mathbf{L}}^{\text{field}} = -i\hbar\mathbf{x} \times \nabla$, respectively, hints to the first-quantization character of the Maxwell-Lorentz equations.

As is well known from quantum mechanics, but true also for classical fields, the Cartesian components of $\hat{\mathbf{L}}$ expressed in cylindrical coordinates (ρ, φ, z) are

$$\hat{L}_x^{\text{field}} = -i\hbar \left[\sin\varphi \left(z \frac{\partial}{\partial\rho} - \rho \frac{\partial}{\partial z} \right) + \frac{z}{\rho} \cos\varphi \frac{\partial}{\partial\varphi} \right] \quad (\text{A53a})$$

$$\hat{L}_y^{\text{field}} = -i\hbar \left[\cos\varphi \left(z \frac{\partial}{\partial\rho} - \rho \frac{\partial}{\partial z} \right) - \frac{z}{\rho} \sin\varphi \frac{\partial}{\partial\varphi} \right] \quad (\text{A53b})$$

$$\hat{L}_z^{\text{field}} = -i\hbar \frac{\partial}{\partial\varphi} \quad (\text{A53c})$$

duly recalling that \hbar should be divided out; *cf.* formula (A52b). The magnitude squared of the orbital angular momentum operator is

$$|\hat{\mathbf{L}}^{\text{field}}|^2 = (\hat{L}_x^{\text{field}})^2 + (\hat{L}_y^{\text{field}})^2 + (\hat{L}_z^{\text{field}})^2 \quad (\text{A54})$$

with eigenvalues $\hbar^2 l(l+1)$.

Orbital angular momentum is utilized in photonics and in optical trapping [132, 263–265] but has not yet been exploited fully in wireless communications. The conservation of angular momentum is a consequence of the rotational symmetry of electrodynamics.

4. Boost momentum

Due to the invariance of Maxwell's equations under Lorentz transformations, the first spatial momentum of the energy density (A1), and the linear momentum density (A10) multiplied by the elapsed time

$$\boldsymbol{\xi}(t, \mathbf{x}) = 2(\mathbf{x} - \mathbf{x}_m) u^{\text{field}} - (t - t_0) \frac{1}{\varepsilon_0} \mathbf{g}^{\text{field}} \quad (\text{A55})$$

fulfills a local (differential) conservation law. The integrated quantity

$$\mathbf{x}^{\text{ce}}(t) = \frac{\int_V d^3x \boldsymbol{\xi}(t, \mathbf{x})}{U^{\text{field}}} \quad (\text{A56})$$

is the center of energy [266]. Apparently this physical observable has not yet been exploited to any significant extent in radio or optics.

Appendix B: Hertzian dipoles

When the oscillations of an electric charge distribution $\rho^e(t', \mathbf{x}')$ are so small that their maximum amplitude (and the largest extent of the smallest volume V' that fully encloses the charge distribution) is much smaller than the wavelength of the emitted fields, we can use the multipole expansion. The lowest order contribution to the fields comes from the electric monopole (charge) scalar

$$q^e(t') = \int_{V'} d^3x' \rho^e(t', \mathbf{x}') \quad (\text{B1})$$

The second lowest contribution comes from the electric (Hertzian) dipole moment vector with respect to an arbitrary moment point \mathbf{x}'_0 ,

$$\mathbf{d}(t', \mathbf{x}'_0) = \int_{V'} d^3x' (\mathbf{x}' - \mathbf{x}'_0) \rho^e(t', \mathbf{x}') \quad (\text{B2})$$

$$= \int_{V'} d^3x' \mathbf{x}' \rho^e(t', \mathbf{x}') - \mathbf{x}'_0 \int_{V'} d^3x' \rho^e(t', \mathbf{x}') \quad (\text{B3})$$

$$= \mathbf{d}(t', \mathbf{0}) - \mathbf{x}'_0 q^e(t') \quad (\text{B4})$$

Clearly there are two cases to consider here. If $q^e(t') \neq 0$, it is always possible to choose a moment point \mathbf{x}'_0 so that $\mathbf{d}(t', \mathbf{x}'_0) = \mathbf{0}$. But if $q^e(t') = 0$, then the dipole moment is independent of the choice of the moment point \mathbf{x}'_0 . Furthermore, since \mathbf{x}'_0 is a fix point,

$$\frac{\partial[\mathbf{d}(t', \mathbf{x}'_0)]}{\partial t'} = \frac{d[\mathbf{d}(t', \mathbf{x}'_0)]}{dt'} = \frac{d[\mathbf{d}(t', \mathbf{0})]}{dt'} - \mathbf{x}'_0 \frac{dq^e(t')}{dt'} \quad (\text{B5})$$

and, according to the equation of continuity for electric charge,

$$\frac{dq^e(t')}{dt'} = \int_{V'} d^3x' \frac{\partial \rho^e(t', \mathbf{x}')}{\partial t'} = - \oint_{S'} d^2x' \hat{\mathbf{n}}' \cdot \mathbf{j}^e(t', \mathbf{x}') \quad (\text{B6})$$

If there is no net flow of electric current across the surface S' that encloses V' , it therefore follows that

$$\frac{\partial[\mathbf{d}(t', \mathbf{x}'_0)]}{\partial t'} = \frac{\partial[\mathbf{d}(t', \mathbf{0})]}{\partial t'} \quad (\text{B7a})$$

$$\frac{\partial^2[\mathbf{d}(t', \mathbf{x}'_0)]}{\partial t'^2} = \frac{\partial^2[\mathbf{d}(t', \mathbf{0})]}{\partial t'^2} \quad (\text{B7b})$$

The electric and magnetic fields from an electric Hertzian dipole, oscillating at the angular frequency $\omega = ck$, where $k = \lambda/(2\pi)$ is the wave number, λ being the wavelength in free space, and located at the origin $\mathbf{x}' = \mathbf{0}$, which is also the moment point chosen,

$$\mathbf{d}(t', \mathbf{0}) = \mathbf{d}_\omega(\mathbf{0}) e^{-i(\omega t' + \delta)} \quad (\text{B8})$$

where $\delta = \omega \Delta t'$ is an arbitrary constant phase, can be obtained from Eqns. (32).

We apply the decomposition (30) on $\mathbf{d}_\omega(\mathbf{0})$, resulting in a parallel (\parallel), and a perpendicular (\perp) component

$$\mathbf{d}_\parallel(\mathbf{0}) = [\mathbf{d}_\omega(\mathbf{0}) \cdot \hat{\mathbf{n}}'] \hat{\mathbf{n}}' \quad (\text{B9})$$

$$\mathbf{d}_\perp(\mathbf{0}) = \mathbf{d}_\omega(\mathbf{0}) - \mathbf{d}_\parallel = \mathbf{d}_\omega - [\mathbf{d}_\omega(\mathbf{0}) \cdot \hat{\mathbf{n}}'] \hat{\mathbf{n}}' \quad (\text{B10})$$

Using a spherical coordinate system (r, ϑ, φ) where $\hat{\mathbf{r}} \equiv \hat{\mathbf{n}}'$ and, from Eqn. (25), $t' = t - r/c$, the fields generated by \mathbf{d} can be written [cf. Cohen-Tannoudji *et al.* [50, Eqn. (16), p. 73]]

$$\mathbf{E}(t, \mathbf{x}) = \frac{\mathbf{d}_\parallel(\mathbf{0})}{2\pi\epsilon_0} [f_2(\delta) + f_3(\delta)] \quad (\text{B11a})$$

$$+ \frac{\mathbf{d}_\perp(\mathbf{0})}{4\pi\epsilon_0} [f_1(\delta) - f_2(\delta) - f_3(\delta)]$$

$$\mathbf{B}(t, \mathbf{x}) = \frac{\hat{\mathbf{r}} \times \mathbf{d}_\perp(\mathbf{0})}{4\pi\epsilon_0 c} [f_1(\delta) - f_2(\delta)] \quad (\text{B11b})$$

where, for convenience and compactness, we introduced the help quantities

$$f_1(\delta) \equiv f_1(\omega t', \delta) = \frac{k^2}{r} \cos(kr - \omega t + \delta) \quad (\text{B12a})$$

$$f_2(\delta) \equiv f_2(\omega t', \delta) = \frac{k}{r^2} \sin(kr - \omega t + \delta) \quad (\text{B12b})$$

$$f_3(\delta) \equiv f_3(\omega t', \delta) = \frac{1}{r^3} \cos(kr - \omega t + \delta) \quad (\text{B12c})$$

with the subscript n denoting how the component f_n in question behaves as a power of radial distance r from the dipole, *i.e.*, $\mathcal{O}(f_n) = r^{-n}$.

1. Hertzian dipoles directed along the three Cartesian axes

Let us now consider three Hertzian dipoles directed along the three Cartesian axes. We denote their (Fourier) amplitudes

$$\mathbf{d}_j(\mathbf{0}) \equiv \mathbf{d}_{j\omega}(\mathbf{0}) = d_{j\omega}(\mathbf{0}) \hat{\mathbf{x}}_j, \quad j = 1, 2, 3. \quad (\text{B13})$$

where $\hat{\mathbf{x}}_1 = \hat{\mathbf{x}}, \hat{\mathbf{x}}_2 = \hat{\mathbf{y}},$ and $\hat{\mathbf{x}}_3 = \hat{\mathbf{z}},$

a. Electric and magnetic fields The individual electric Hertzian dipoles $\mathbf{d}_j(\mathbf{0}), j = 1, 2, 3,$ generate electric and magnetic field vectors \mathbf{E}_j and $\mathbf{B}_j.$ In spherical polar coordinates they are:

$$\mathbf{E}_1(t, \mathbf{x}) = \frac{d_1(\mathbf{0})}{2\pi\epsilon_0} [f_2(\delta_1) + f_3(\delta_1)] \sin \vartheta \cos \varphi \hat{\mathbf{r}}$$

$$+ \frac{d_1(\mathbf{0})}{4\pi\epsilon_0} [f_1(\delta_1) - f_2(\delta_1) - f_3(\delta_1)] \cos \vartheta \cos \varphi \hat{\boldsymbol{\theta}}$$

$$- \frac{d_1(\mathbf{0})}{4\pi\epsilon_0} [f_1(\delta_1) - f_2(\delta_1) - f_3(\delta_1)] \sin \varphi \hat{\boldsymbol{\phi}} \quad (\text{B14a})$$

$$\mathbf{B}_1(t, \mathbf{x}) = \frac{d_1(\mathbf{0})}{4\pi\epsilon_0 c} [f_1(\delta_1) - f_2(\delta_1)] \sin \varphi \hat{\boldsymbol{\theta}}$$

$$+ \frac{d_1(\mathbf{0})}{4\pi\epsilon_0 c} [f_1(\delta_1) - f_2(\delta_1)] \cos \vartheta \cos \varphi \hat{\boldsymbol{\phi}} \quad (\text{B14b})$$

$$\mathbf{E}_2(t, \mathbf{x}) = \frac{d_2(\mathbf{0})}{2\pi\epsilon_0} [f_2(\delta_2) + f_3(\delta_2)] \sin \vartheta \sin \varphi \hat{\mathbf{r}}$$

$$+ \frac{d_2(\mathbf{0})}{4\pi\epsilon_0} [f_1(\delta_2) - f_2(\delta_2) - f_3(\delta_2)] \cos \vartheta \sin \varphi \hat{\boldsymbol{\theta}}$$

$$+ \frac{d_2(\mathbf{0})}{4\pi\epsilon_0} [f_1(\delta_2) - f_2(\delta_2) - f_3(\delta_2)] \cos \varphi \hat{\boldsymbol{\phi}} \quad (\text{B14c})$$

$$\begin{aligned} \mathbf{B}_2(t, \mathbf{x}) = & -\frac{d_2(\mathbf{0})}{4\pi\epsilon_0 c} [f_1(\delta_2) - f_2(\delta_2)] \cos \vartheta \hat{\boldsymbol{\nu}} \\ & + \frac{d_2(\mathbf{0})}{4\pi\epsilon_0 c} [f_1(\delta_2) - f_2(\delta_2)] \cos \vartheta \sin \varphi \hat{\boldsymbol{\phi}} \quad (\text{B14d}) \end{aligned}$$

$$\begin{aligned} \mathbf{E}_3(t, \mathbf{x}) = & \frac{d_3(\mathbf{0})}{2\pi\epsilon_0} [f_2(\delta_3) + f_3(\delta_3)] \cos \vartheta \hat{\mathbf{r}} \\ & - \frac{d_3(\mathbf{0})}{4\pi\epsilon_0} [f_1(\delta_3) - f_2(\delta_3) - f_3(\delta_3)] \sin \vartheta \hat{\boldsymbol{\nu}} \quad (\text{B14e}) \end{aligned}$$

$$\mathbf{B}_3(t, \mathbf{x}) = -\frac{d_3(\mathbf{0})}{4\pi\epsilon_0 c} [f_1(\delta_3) - f_2(\delta_3)] \sin \vartheta \hat{\boldsymbol{\phi}} \quad (\text{B14f})$$

b. Vector products of the fields When we want to calculate the linear and angular momenta carried by the fields radiated by Hertzian dipoles directed along the Cartesian axes, we need to evaluate expressions that involve the vector products $\mathbf{E}_j \times \mathbf{B}_k$ for various combinations of $j, k = 1, 2, 3$. Here we list a few such vector products.

$$\begin{aligned} \mathbf{E}_1 \times \mathbf{B}_1 = & \frac{d_1^2(\mathbf{0})}{16\pi^2\epsilon_0^2 c} [f_1^2(\delta_1) - 2f_1(\delta_1)f_2(\delta_1) \\ & - f_1(\delta_1)f_3(\delta_1) + f_2^2(\delta_1) \\ & + f_2(\delta_1)f_3(\delta_1)] (1 - \sin^2 \vartheta \cos^2 \varphi) \hat{\mathbf{r}} \\ & - \frac{d_1^2(\mathbf{0})}{8\pi^2\epsilon_0^2 c} [f_1(\delta_1)f_2(\delta_1) + f_1(\delta_1)f_3(\delta_1) \\ & - f_2^2(\delta_1) - f_2(\delta_1)f_3(\delta_1)] \sin \vartheta \cos \vartheta \sin^2 \varphi \hat{\boldsymbol{\nu}} \\ & + \frac{d_1^2(\mathbf{0})}{8\pi^2\epsilon_0^2 c} [f_1(\delta_1)f_2(\delta_1) + f_1(\delta_1)f_3(\delta_1) \\ & - f_2^2(\delta_1) - f_2(\delta_1)f_3(\delta_1)] \sin \vartheta \sin \varphi \cos \varphi \hat{\boldsymbol{\phi}} \quad (\text{B15}) \end{aligned}$$

$$\begin{aligned} \mathbf{E}_2 \times \mathbf{B}_2 = & \frac{d_2^2(\mathbf{0})}{16\pi^2\epsilon_0^2 c} [f_1^2(\delta_2) - 2f_1(\delta_2)f_2(\delta_2) \\ & - f_1(\delta_2)f_3(\delta_2) + f_2^2(\delta_2) \\ & + f_2(\delta_2)f_3(\delta_2)] (1 - \sin^2 \vartheta \sin^2 \varphi) \hat{\mathbf{r}} \\ & - \frac{d_2^2(\mathbf{0})}{8\pi^2\epsilon_0^2 c} [f_1(\delta_2)f_2(\delta_2) + f_1(\delta_2)f_3(\delta_2) \\ & - f_2^2(\delta_2) - f_2(\delta_2)f_3(\delta_2)] \sin \vartheta \cos \vartheta \sin^2 \varphi \hat{\boldsymbol{\nu}} \\ & - \frac{d_2^2(\mathbf{0})}{8\pi^2\epsilon_0^2 c} [f_1(\delta_2)f_2(\delta_2) + f_1(\delta_2)f_3(\delta_2) \\ & - f_2^2(\delta_2) - f_2(\delta_2)f_3(\delta_2)] \sin \vartheta \sin \varphi \cos \varphi \hat{\boldsymbol{\phi}} \quad (\text{B16}) \end{aligned}$$

$$\begin{aligned} \mathbf{E}_3 \times \mathbf{B}_3 = & \frac{d_3^2(\mathbf{0})}{16\pi^2\epsilon_0^2 c} [f_1^2(\delta_3) - 2f_1(\delta_3)f_2(\delta_3) + f_2^2(\delta_3) \\ & - f_1(\delta_3)f_3(\delta_3) + f_2(\delta_3)f_3(\delta_3)] \sin^2 \vartheta \hat{\mathbf{r}} \\ & + \frac{d_3^2(\mathbf{0})}{8\pi^2\epsilon_0^2 c} [f_1(\delta_3)f_2(\delta_3) + f_1(\delta_3)f_3(\delta_3) \\ & - f_2^2(\delta_3) - f_2(\delta_3)f_3(\delta_3)] \sin \vartheta \cos \vartheta \hat{\boldsymbol{\nu}} \quad (\text{B17}) \end{aligned}$$

$$\begin{aligned} \mathbf{E}_1 \times \mathbf{B}_2 = & -\frac{d_1(\mathbf{0})d_2(\mathbf{0})}{16\pi^2\epsilon_0^2 c} [f_1(\delta_1)f_1(\delta_2) - f_1(\delta_1)f_2(\delta_2) \\ & - f_1(\delta_2)f_2(\delta_1) - f_1(\delta_2)f_3(\delta_1) \\ & + f_2(\delta_1)f_2(\delta_2) + f_2(\delta_2)f_3(\delta_1)] (1 - \cos^2 \vartheta) \sin \varphi \cos \varphi \hat{\mathbf{r}} \\ & - \frac{d_1(\mathbf{0})d_2(\mathbf{0})}{8\pi^2\epsilon_0^2 c} [f_1(\delta_2)f_2(\delta_1) + f_1(\delta_2)f_3(\delta_1) \\ & - f_2(\delta_1)f_2(\delta_2) - f_2(\delta_2)f_3(\delta_1)] \sin \vartheta \cos \vartheta \sin \varphi \cos \varphi \hat{\boldsymbol{\nu}} \\ & - \frac{d_1(\mathbf{0})d_2(\mathbf{0})}{8\pi^2\epsilon_0^2 c} [f_1(\delta_2)f_2(\delta_1) + f_1(\delta_2)f_3(\delta_1) \\ & - f_2(\delta_1)f_2(\delta_2) - f_2(\delta_2)f_3(\delta_1)] \sin \vartheta \cos^2 \varphi \hat{\boldsymbol{\phi}} \quad (\text{B18}) \end{aligned}$$

$$\begin{aligned} \mathbf{E}_2 \times \mathbf{B}_1 = & -\frac{d_1(\mathbf{0})d_2(\mathbf{0})}{16\pi^2\epsilon_0^2 c} [f_1(\delta_1)f_1(\delta_2) - f_1(\delta_1)f_2(\delta_2) \\ & - f_1(\delta_2)f_2(\delta_1) - f_1(\delta_1)f_3(\delta_2) \\ & + f_2(\delta_1)f_2(\delta_2) + f_2(\delta_1)f_3(\delta_2)] (1 - \cos^2 \vartheta) \sin \varphi \cos \varphi \hat{\mathbf{r}} \\ & - \frac{d_1(\mathbf{0})d_2(\mathbf{0})}{8\pi^2\epsilon_0^2 c} [f_1(\delta_1)f_2(\delta_2) + f_1(\delta_1)f_3(\delta_2) \\ & - f_2(\delta_1)f_2(\delta_2) - f_2(\delta_1)f_3(\delta_2)] \sin \vartheta \cos \vartheta \sin \varphi \cos \varphi \hat{\boldsymbol{\nu}} \\ & + \frac{d_1(\mathbf{0})d_2(\mathbf{0})}{8\pi^2\epsilon_0^2 c} [f_1(\delta_1)f_2(\delta_2) + f_1(\delta_1)f_3(\delta_2) \\ & - f_2(\delta_1)f_2(\delta_2) - f_2(\delta_1)f_3(\delta_2)] \sin \vartheta \sin^2 \varphi \hat{\boldsymbol{\phi}} \quad (\text{B19}) \end{aligned}$$

- [1] Emmy Noether, “Invariante Variationsprobleme,” *Nachr. Ges. Wiss. Göttingen* **1**, 235–257 (1918), English transl.: *Invariant variation problems*, *Transp. Theor. Stat. Phys.*, **1**, 186–207 (1971).
- [2] M. Poincaré, “Sur la dynamique de l’électron,” *Rendic. Circ. Matem. Palermo* (1884–1940) **21**, 129–175 (1906).
- [3] W. I. Fushchich and A. G. Nikitin, “The complete sets of conservation laws for the electromagnetic field,” *J. Phys. A: Math. Gen.* **25**, L231–L233 (1992).
- [4] Nail H. Ibragimov, “Symmetries, Lagrangian and conservation laws for the Maxwell equations,” *Acta Applic. Math.* **105**, 157–187 (2008).
- [5] P. A. M. Dirac, “Quantised singularities in the electromagnetic field,” *Proc. Roy. Soc. London Ser. A Math. Phys. Sci.* **133**, 60–72 (1931).
- [6] Julian Schwinger, “A magnetic model of matter,” *Science* **165**, 757–761 (1969).
- [7] Julian Schwinger, Lester L. DeRaad, Jr., Kimball A. Milton, and Wu-yang Tsai, *Classical Electrodynamics* (Perseus Books, Reading, MA, USA, 1998).
- [8] John David Jackson, *Classical Electrodynamics*, 3rd ed. (Wiley & Sons, New York, NY, USA, 1998).
- [9] B. Thidé, Nicholas M. Elias, II, F. Tamburini, S. M. Mohammedi, and J. T. Mendonça, “Applications of electromagnetic OAM in astrophysics and space physics studies,” in *Twisted Photons: Applications of Light With Orbital Angular Momentum*, edited by Juan P. Torres and Lluís Torner (Wiley-Vch Verlag, Weinheim, DE, 2011) Chap. 9, pp. 155–178.
- [10] Bo Thidé, *Electromagnetic Field Theory*, 2nd ed. (Dover Publications, Inc., Mineola, NY, USA, 2011) (In press).
- [11] Heinrich Weber, *Die partiellen Differential-Gleichungen der mathematischen Physik nach Riemann’s Vorlesungen* (Friedrich Vieweg und Sohn, Braunschweig, 1901).
- [12] Ludwik Silberstein, “Elektromagnetische Grundgleichungen in bivektorieller Behandlung,” *Ann. Phys. (Leipzig)* **327**, 579–586 (1907).
- [13] Ludwik Silberstein, “Nachtrag zur Abhandlung über elektromagnetische Grundgleichungen in bivektorieller Behandlung,” *Ann. Phys. (Leipzig)* **329**, 783–784 (1907).
- [14] Ludwik Silberstein, *The Theory of Relativity* (MacMillan, London, 1914).
- [15] Harry Bateman, *The Mathematical Analysis of Electrical and Optical Wave-Motion on the Basis of Maxwell’s Equations* (Cambridge University Press, Cambridge, UK, 1915).
- [16] Iwo Białynicki-Birula and Zofia Białynicka-Birula, “Beams of electromagnetic radiation carrying angular momentum: The Riemann-Silberstein vector and the classical-quantum correspondence,” *Opt. Commun.* **264**, 342–351 (2006).
- [17] Iwo Białynicki-Birula and Zofia Białynicka-Birula, “Why photons cannot be sharply localized,” *Phys. Rev. A* **79**, 032112 (2009).
- [18] Donald H. Kobe, “A relativistic Schrödinger-like equation for a photon and its second quantization,” *Found. Phys.* **29**, 1203–1231 (1999).
- [19] Ettore Majorana, “Research notes on theoretical physics,” (2009), unpublished, deposited at the ‘Domus Galileana,’ Pisa, quaderno 2, p. 101/1; 3, p. 11, 160; 15, p. 16; 17, p. 83, 159.
- [20] J. R. Oppenheimer, “Note on light quanta and the electromagnetic field,” *Phys. Rev.* **38**, 725–746 (1931).
- [21] Otto Laporte and George E. Uhlenbeck, “Application of spinor analysis to the Maxwell and Dirac equations,” *Phys. Rev.* **37**, 1380–1397 (1931).
- [22] W. J. Archibald, “Field equations from particle equations,” *Canad. J. Phys.* **33**, 565–572 (1955).
- [23] R. H. Good, “Particle aspect of the electromagnetic field equations,” *Phys. Rev.* **105**, 1914–1918 (1957).
- [24] C. L. Hammer and R. H. Good, “Wave equation for a massless particle with arbitrary spin,” *Phys. Rev.* **108**, 882–886 (1957).
- [25] H. E. Moses, “Solution of Maxwell’s equations in terms of a spinor notation: the direct and inverse problem,” *Phys. Rev.* **113**, 1670–1679 (1959).
- [26] Behram Kurşunoğlu, “Complex orthogonal and antiorthogonal representation of Lorentz group,” *J. Math. Phys.* **2**, 22–32 (1961).
- [27] Roland H. Good, Jr. and Terence J. Nelson, *Classical Theory of Electric and Magnetic Fields* (Academic Press, London, UK, 1971).
- [28] R. Mignani, E. Recami, and M. Baldo, “About a Dirac-like equation for the photon according to Ettore Majorana,” *Lett. Nuov. Cim.* **11**, 568–572 (1974).
- [29] Asim O. Barut, *Electrodynamics and Classical Theory of Fields and Particles* (Dover Publications, New York, NY, USA, 1980).
- [30] E. Giannetto, “A Majorana-Oppenheimer formulation of quantum electrodynamics,” *Lett. Nuov. Cim.* **2**, **44**, 140–144 (1985).
- [31] J. E. Sipe, “Photon wave functions,” *Phys. Rev. A* **52**, 1875–1883 (1995).
- [32] Iwo Białynicki-Birula, “On the wave function of the photon,” *Acta Phys. Polon.* **A 86**, 97–116 (1994).
- [33] I. Białynicki-Birula, “Photon wave function,” in *Prog. Opt.*, Vol. XXXVI, edited by E. Wolf (Elsevier, Amsterdam, Holland, 1996) pp. 245–294.
- [34] S. Esposito, “Covariant Majorana formulation of electrodynamics,” *Found. Phys.* **28**, 231–244 (1998).
- [35] A. Gersten, “Maxwell equations—the one-photon quantum equation,” *Found. Phys. Lett.* **12**, 291–298 (1999).
- [36] Ole Keller, “On the theory of spatial localization of photons,” *Phys. Rep.* **411**, 1–232 (2005).
- [37] Sameen Ahmed Khan, “An exact matrix representation of Maxwell’s equations,” *Phys. Scr.* **71**, 440–442 (2005).
- [38] Daniela Dragoman, “Photon states from propagating complex electromagnetic fields,” *J. Opt. Soc. Am. B* **24**, 922–927 (2007).
- [39] B. J. Smith and M. G. Raymer, “Photon wave functions, wave-packet quantization of light, and coherence theory,” *New J. Phys.* **9**, 414 (2007).
- [40] F. Tamburini and D. Vicino, “Photon wave function: A covariant formulation and equivalence with QED,” *Phys. Rev. A* **78**, 052116(5) (2008).
- [41] A. A. Bogush, G. G. Krylov, E. M. Ovsyuk, and V. M. Red’kov, “Maxwell equations in complex form of Majorana-Oppenheimer, solutions with cylindric symmetry in Riemann S_3 and Lobachevsky H_3 spaces,” *Ricerche Mat.* **59**, 59–96 (2009).
- [42] Zhi-Yong Wang, Cai-Dong Xiong, and Qi Qiu, “Photon wave function and *Zitterbewegung*,” *Phys. Rev. A* **80**, 032118 (2009).
- [43] Peter J. Mohr, “Solutions of the Maxwell equations and photon wave functions,” *Ann. Phys. (N. Y.)* **325**, 607–663 (2010).
- [44] Andreas Aste, “Complex representation theory of the electromagnetic field,” *J. Geom. Sym. Phys.* **28**, 47–58 (2012).
- [45] V. M. Red’kov, N. G. Tokarevskaya, and George J. Spix, “Majorana-Oppenheimer approach to Maxwell electrodynamics. Part I. Minkowski space,” *Adv. Appl. Clifford Algebr.* **22**, 1129–1149 (2012).

- [46] Takuo Yamamoto, Shinji Yamashita, and Satoshi Yajima, “Wave function of a photon and the appropriate Lagrangian,” *J. Phys. Soc. Japan* **81**, 024402 (2012).
- [47] Iwo Białynicki-Birula and Zofia Białynicka-Birula, “The role of the Riemann-Silberstein vector in classical and quantum theories of electromagnetism,” *J. Phys. A: Math. Gen.* **46**, 053001 (2013).
- [48] Stephen M. Barnett, “Optical Dirac equation,” *New J. Phys.* **16**, 093008 (2014).
- [49] Justin Dressel, Konstantin Y. Bliokh, and Franco Nori, “Space-time algebra as a powerful tool for electromagnetism,” (2014), arXiv.org:1411.5002 [physics.optics].
- [50] Claude Cohen-Tannoudji, Jaques Dupont-Roc, and Gilbert Grynberg, *Photons and Atoms. Introduction to Quantum Electrodynamics* (Wiley & Sons, New York, NY, USA, 1997) Wiley Professional Paperback Edition.
- [51] Hongrui Li, “Evanescence wave of a single photon,” *Opt. Express* **52**, 074103–074103 (2013).
- [52] David L. Andrews, “Photon-based and classical descriptions in nanophotonics: a review,” *J. Nanophot.* **8**, 081599 (2014).
- [53] Freeman J. Dyson, “Why is Maxwell’s Theory so hard to understand?” in *James Clerk Maxwell Commemorative Booklet* (James Clerk Maxwell Foundation, Edinburgh, Scotland, UK, 1999) <http://www.clerkmaxwellfoundation.org/DysonFreemanArticle.pdf>.
- [54] Daniel M. Siegel, *Innovation in Maxwell’s Electromagnetic Theory: Molecular Vortices, Displacement Current, and Light* (Cambridge University Press, Cambridge, UK, 2003).
- [55] A. I. Sadovskii, “Ponderomotorniya djstvuya elektromagnitnykh’ i svtovykh’ voln’ na kristally,” *Uchen. Zapisk. Imp. Yurev. Univ.* **52**, 1–126 (1899), (English translation: Ponderomotive action of electromagnetic and light waves on crystals).
- [56] J. H. Poynting, “The wave motion of a revolving shaft, and a suggestion as to the angular momentum in a beam of circularly polarised light,” *Proc. Roy. Soc. London A* **82**, 560–567 (1909).
- [57] Max Abraham, “Der Drehimpuls des Lichtes,” *Physik. Zeitschr.* **XV**, 914–918 (1914).
- [58] H. Bateman, “The radiation of energy and angular momentum,” *Phys. Rev.* **27**, 606–617 (1926).
- [59] Walter Heitler, *The Quantum Theory of Radiation*, 3rd ed., The International Series of Monographs on Physics (Clarendon Press, Oxford, UK, 1954).
- [60] N. N. Bogolyubov and D. V. Shirkov, *Introduction to the Theory of Quantized Fields* (Interscience, New York, 1959).
- [61] Albert Messiah, *Quantum Mechanics* (North-Holland, Amsterdam, NL, 1970).
- [62] Leonard Eyges, *The Classical Electromagnetic Field* (Dover Publications, New York, NY, USA, 1972).
- [63] L. D. Landau and E. M. Lifshitz, *The Classical Theory of Fields*, Course of Theoretical Physics, Vol. 2 (Pergamon, Oxford, UK, 1975).
- [64] V. B. Berestetskii, E. M. Lifshitz, and L. P. Pitaevskii, *Quantum Electrodynamics*, 2nd ed., Course of Theoretical Physics, Vol. 4 (Pergamon Press, Oxford, UK, 1989).
- [65] Leonard Mandel and Emil Wolf, *Optical Coherence and Quantum Optics* (Cambridge University Press, New York, NY, USA, 1995).
- [66] David J. Griffiths, *Introduction to Electrodynamics*, 3rd ed. (Prentice-Hall International, London, UK, 1999).
- [67] Fritz Rohrlich, *Classical Charged Particles*, 3rd ed. (World Scientific, Singapore, 2007).
- [68] Graham Gibson, Johannes Courtial, Miles J. Padgett, Mikhail Vasnetsov, Valeriy Pas’ko, Stephen M. Barnett, and Sonja Franke-Arnold, “Free-space information transfer using light beams carrying orbital angular momentum,” *Opt. Express* **12**, 5448–5456 (2004).
- [69] B. Thidé, H. Then, J. Sjöholm, K. Palmer, J. Bergman, T. D. Carozzi, Ya. N. Istomin, N. H. Ibragimov, and R. Khamitova, “Utilization of photon orbital angular momentum in the low-frequency radio domain,” *Phys. Rev. Lett.* **99**, 087701(4) (2007).
- [70] S. Franke-Arnold, L. Allen, and M. Padgett, “Advances in optical angular momentum,” *Laser & Photon. Rev.* **2**, 299–313 (2008).
- [71] Fabrizio Tamburini, Bo Thidé, Gabriel Molina-Terriza, and Gabriele Anzolin, “Twisting of light around rotating black holes,” *Nature Phys.* **7**, 195–197 (2011).
- [72] Fabrizio Tamburini, Elettra Mari, Bo Thidé, Cesare Barbieri, and Filippo Romanato, “Experimental verification of photon angular momentum and vorticity with radio techniques,” *Appl. Phys. Lett.* **99**, 204102 (2011).
- [73] Fabrizio Tamburini, Elettra Mari, Anna Sponselli, Bo Thidé, Antonio Bianchini, and Filippo Romanato, “Encoding many channels on the same frequency through radio vorticity: first experimental test,” *New J. Phys.* **14**, 03301 (2012).
- [74] F. Tamburini, B. Thidé, E. Mari, A. Sponselli, A. Bianchini, and F. Romanato, “Reply to comment on ‘Encoding many channels on the same frequency through radio vorticity: first experimental test,’” *New J. Phys.* **14**, 118002 (2012).
- [75] F. Tamburini, E. Mari, G. Parisi, F. Spinello, M. Oldoni, R. A. Ravanelli, P. Coassini, Carlo G. Someda, B. Thidé, and F. Romanato, “Tripling the capacity of a point-to-point radio link by using electromagnetic vortices,” *Radio Sci.* **50** (2015), 10.1002/2015RS005662.
- [76] Graham Gibson, Johannes Courtial, Mikhail Vasnetsov, Stephen Barnett, and Sonja Franke-Arnold, “Increasing the data density of free-space optical communications using orbital angular momentum,” in *Free-Space Laser Communications IV*, Proceedings of SPIE, Vol. 5550, edited by Jennifer C. Rickling and David G. Voetz (Denver, CO, USA, 2004) pp. 367–373.
- [77] Jian Wang, Jeng-Yuan Yang, Irfan M. Fazal, Nisar Ahmed, Yan Yan, Hao Huang, Yongxiong Ren, Yang Yue, Samuel Dolinar, Moshe Tur, and Alan E. Willner, “Terabit free-space data transmission employing orbital angular momentum multiplexing,” *Nature Photon.* **6**, 488–496 (2012).
- [78] Natalia M. Litchinitser, “Structured light meets structured matter,” *Science* **337**, 1054–1055 (2012).
- [79] Nenad Bozinovic, Yang Yue, Yongxiong Ren, Moshe Tur, Poul Kristensen, Hao Huang, Alan E. Willner, and Siddharth Ramachandran, “Terabit-scale orbital angular momentum mode division multiplexing in fibers,” *Science* **340**, 1545–1548 (2013).
- [80] F. E. Mahmoudi and S. D. Walker, “4-Gbps uncompressed video transmission over a 60-GHz orbital angular momentum wireless channel,” *IEEE Wirel. Comm. Lett.* **2**, 223–226 (2013).
- [81] A.E. Willner, “Tb/s optical communications using orbital angular momentum,” in *Microoptics Conference (MOC), 2013 18th* (2013) pp. 1–2.
- [82] Yongxiong Ren, Long Li, Guodong Xie, Yan Yan, Yinwen Cao, Hao Huang, N. Ahemd, M.J. Lavery, Zhe Zhao, Chongfu Zhang, M. Tur, M. Padgett, G. Caire, A.F. Molisch, and A.E. Willner, “Experimental demonstration of 16 gbit/s millimeter-wave communications using MIMO processing of 2 OAM modes on each of two transmitter/receiver antenna apertures,” in *2014 IEEE Global Communications Conference (GLOBECOM)* (2014) pp. 3821–3826.
- [83] Guodong Xie, Long Li, Yongxiong Ren, Hao Huang, Yan Yan, N. Ahmed, Zhe Zhao, M.P.J. Lavery, N. Ashrafi, S. Ashrafi, M. Tur, A.F. Molisch, and A.E. Willner, “Performance metrics

- and design parameters for an FSO communications link based on multiplexing of multiple orbital-angular-momentum beams,” in *Globecom Workshops (GC Wkshps), 2014* (2014) pp. 481–486.
- [84] Yan Yan, Guodong Xie, Hao Huang, M.J. Lavery, N. Ahmed, Changjing Bao, Yongxiong Ren, A.F. Molisch, M. Tur, M. Padgett, and A.E. Willner, “Demonstration of 8-mode 32-gbit/s millimeter-wave free-space communication link using 4 orbital-angular-momentum modes on 2 polarizations,” in *2014 IEEE International Conference on Communications (ICC)* (2014) pp. 4850–4855.
- [85] Yan Yan, Guodong Xie, Martin P. J. Lavery, Hao Huang, Nisar Ahmed, Changjing Bao, Yongxiong Ren, Yinwen Cao, Long Li, Zhe Zhao, Andreas F. Molisch, Moshe Tur, Miles J. Padgett, and Alan E. Willner, “High-capacity millimetre-wave communications with orbital angular momentum multiplexing,” *Nature Commun.* **5**, 1–9 (2014).
- [86] A. E. Willner, H. Huang, Y. Yan, Y. Ren, N. Ahmed, G. Xie, C. Bao, L. Li, Y. Cao, Z. Zhao, J. Wang, M. P. J. Lavery, M. Tur, S. Ramachandran, A. F. Molisch, N. Ashrafi, and S. Ashrafi, “Optical communications using orbital angular momentum beams,” *Adv. Opt. Photon.* **7**, 66–106 (2015).
- [87] N. Papanicolaou and T. N. Tomaras, “Dynamics of magnetic vortices,” *Nucl. Phys. B* **360**, 425–462 (1991).
- [88] J. Zagrodzinski, “Vortices in different branches of physics,” *Physica C* **369**, 45–54 (2002).
- [89] Eric Yao, Sonja Franke-Arnold, Johannes Courtial, Stephen Barnett, and Miles Padgett, “Fourier relationship between angular position and optical orbital angular momentum,” *Opt. Express* **14**, 9071–9076 (2006).
- [90] A. K. Jha, B. Jack, E. Yao, J. Leach, R. W. Boyd, G. S. Buller, S. M. Barnett, S. Franke-Arnold, and M. J. Padgett, “Fourier relationship between the angle and angular momentum of entangled photons,” *Phys. Rev. A* **78**, 043810 (2008).
- [91] B. Jack, M. J. Padgett, and S. Franke-Arnold, “Angular diffraction,” *New J. Phys.* **10**, 103013 (2008).
- [92] Miles J. Padgett, Filippo M. Miatto, Martin P. J. Lavery, Anton Zeilinger, and Robert W. Boyd, “Divergence of an orbital-angular-momentum-carrying beam upon propagation,” *New J. Phys.* **17**, 023011 (2015).
- [93] Mingzhou Chen, Michael Mazilu, Yoshihiko Arita, Ewan M. Wright, and Kishan Dholakia, “Dynamics of microparticles trapped in a perfect vortex beam,” *Opt. Lett.* **38**, 4919 (2013).
- [94] Andrey S. Ostrovsky, Carolina Rickenstorff-Parrao, and Víctor Arrizón, “Generation of the “perfect” optical vortex using a liquid-crystal spatial light modulator,” *Opt. Lett.* **38**, 534–536 (2013).
- [95] Joaquín García-García, Carolina Rickenstorff-Parrao, Rubén Ramos-García, Víctor Arrizón, and Andrey S. Ostrovsky, “Simple technique for generating the perfect optical vortex,” *Opt. Lett.* **39**, 5305–5308 (2014).
- [96] Pravin Vaity and Leslie Rusch, “Perfect vortex beam: Fourier transformation of a Bessel beam,” *Opt. Lett.* **40**, 597–600 (2015).
- [97] Long Li, Guodong Xie, Yongxiong Ren, Nisar Ahmed, Hao Huang, Zhe Zhao, Peicheng Liao, Martin Lavery, Yan Yan, Bhangjing Bao, Zhe Wang, Nima Ashrafi, Solyman Ashrafi, Roger Linqvist, Moshe Tur, and Alan Willner, “Performance enhancement of an orbital-angular-momentum-based free-space optical communication link through beam divergence controlling,” in *Optical Fiber Communication Conference*, OSA Technical Digest (online) (Optical Society of America, 2015) p. M2F.6.
- [98] N. Bohr, “On the constitution of atoms and molecules,” *Philos. Mag.* **6**, **26**, 1–25 (1913).
- [99] Arnold Sommerfeld, *Atombau und Spektrallinien* (F. Vieweg & Sohn, 1921).
- [100] David Bohm, *Quantum Theory* (Dover Publications Inc., New York, 1989).
- [101] Gerard Nienhuis, “Angular momentum and vortices in optics,” in *Structured Light and its Applications: An Introduction to Phase-Structured Beams and Nanoscale Optical Forces* (Elsevier Inc., Amsterdam, NL, 2008) pp. 19–61.
- [102] M. V. Berry, “Optical vortices evolving from helicoidal integer and fractional phase steps,” *J. Opt. A: Pure Appl. Opt.* **6**, 259–268 (2004).
- [103] R. Čechovský and Z. Bouchal, “Optical implementation of the vortex information channel,” *New J. Phys.* **9**, 328 (2007).
- [104] Julio T. Barreiro, Tzu-Chieh Wei, and Paul G. Kwiat, “Beating the channel capacity limit for linear photonic superdense coding,” *Nature Phys.* **4**, 282–286 (2008).
- [105] J. B. Pors, S. S. R. Oemrawsingh, A. Aiello, M. P. van Exter, E. R. Eliel, G. W. ’t Hooft, and J. P. Woerdman, “Shannon dimensionality of quantum channels and its application to photon entanglement,” *Phys. Rev. Lett.* **101**, 120502 (2008).
- [106] P. Martelli, A. Gatto, P. Boffi, and M. Martinelli, “Free-space optical transmission with orbital angular momentum division multiplexing,” *Electron. Lett.* **47**, 972–973 (2011).
- [107] Ashok Kumar, Shashi Prabhakar, Pravin Vaity, and R. P. Singh, “Information content of optical vortex fields,” *Opt. Lett.* **36**, 1161–1163 (2011).
- [108] A. Mair, A. Vaziri, G. Weihs, and A. Zeilinger, “Entanglement of the orbital angular momentum states of photons,” *Nature* **412**, 313–316 (2001).
- [109] Andrew Watson, “New twist could pack photons with data,” *Science* **296**, 2316–2317 (2002).
- [110] J. B. Götte, K. O’Holleran, Daryl Preece, Florian Flossmann, Sonja Franke-Arnold, Stephen M. Barnett, and Miles J. Padgett, “Light beams with fractional orbital angular momentum and their vortex structure,” *Opt. Express* **16**, 993–1006 (2008).
- [111] Hsiao-Chih Huang, Yen-Ting Lin, and Ming-Feng Shih, “Measuring the fractional orbital angular momentum of a vortex light beam by cascaded Mach-Zehnder interferometers,” *Opt. Commun.* **285**, 383–388 (2012).
- [112] Tatyana A. Fadeyeva, Alexander F. Rubass, Rodion V. Aleksandrov, and Aleksander V. Volyar, “Does the optical angular momentum change smoothly in fractional-charged vortex beams?” *J. Opt. Soc. Am. B* **31**, 798 (2014).
- [113] F. Zernike, von, “Beugungstheorie des Schneidenverfahrens und seiner verbesserten Form, der Phasenkontrastmethode,” *Physica* **1**, 689–704 (1934).
- [114] K. Dholakia and T. Čížmár, “Shaping the future of manipulation,” *Nature Photon.* **5**, 335–342 (2011).
- [115] Jesús Rogel-Salazar, Juan Pablo Treviño, and Sabino Chávez-Cerda, “Engineering structured light with optical vortices,” *J. Opt. Soc. Am. B* **31**, A46–A50 (2014).
- [116] Gabriel Molina-Terriza, Juan P. Torres, and Lluís Torner, “Management of the angular momentum of light: Preparation of photons in multidimensional vector states of angular momentum,” *Phys. Rev. Lett.* **88**, 013601(4) (2002).
- [117] Lluís Torner, Juan P. Torres, and Silvia Carrasco, “Digital spiral imaging,” *Opt. Express* **13**, 873–881 (2005).
- [118] Jonathan Leach, Eric Yao, and Miles J. Padgett, “Observation of the vortex structure of a non-integer vortex beam,” *New J. Phys.* **6**, 71 (2004).
- [119] Gabriel Molina-Terriza, Liis Rebane, Juan P. Torres, Lluís Torner, and Silvia Carrasco, “Probing canonical geometrical

- objects by digital spiral imaging,” *J. Eur. Opt. Soc.* **2**, 07014(6) (2007).
- [120] Martin P. J. Lavery, Gregorius C. G. Berkhout, Johannes Courtial, and Miles J. Padgett, “Measurement of the light orbital angular momentum spectrum using an optical geometric transformation,” *J. Opt.* **13**, 064006 (2011).
- [121] Branka Vucetic and Jinhong Yuan, *Space-Time Coding* (John Wiley & Sons, UK, 2003).
- [122] Pierpaolo Boffi, P. Martelli, A. Gatto, and M. Martinelli, “Optical vortices: an innovative approach to increase spectral efficiency by fiber mode-division multiplexing,” in *Next-Generation Optical Communication: Components, Sub-Systems, and Systems I*, Proc. of SPIE, Vol. 8647 (San Francisco, CA, USA, 2013) p. 864705.
- [123] Siyuan Yu, “Potentials and challenges of using orbital angular momentum communications in optical interconnects,” *Opt. Express* **23**, 3075–3087 (2015).
- [124] Shigemi Sasaki and Ian McNulty, “Proposal for generating brilliant X-ray beams carrying orbital angular momentum,” *Phys. Rev. Lett.* **100**, 124801 (2008).
- [125] J. Courtial, K. Dholakia, L. Allen, and M.J. Padgett, “Gaussian beams with very high orbital angular momentum,” *Opt. Commun.* **144**, 210–213 (1997).
- [126] F. J. Belinfante, “On the current and the density of the electric charge, the energy, the linear momentum and the angular momentum of arbitrary fields,” *Physica* **7**, 449–474 (1940).
- [127] Davison E. Soper, *Classical Field Theory* (John Wiley & Sons, Inc., New York, NY, USA, 1976).
- [128] Clifford Truesdell, *Essays in the History of Mechanics* (Springer-Verlag, Berlin, Heidelberg, New York, 1968).
- [129] Marijan Ribarič and Luka Šušteršič, *Conservation Laws and Open Questions of Classical Electrodynamics* (World Scientific, Singapore, New Jersey, London, Hong Kong, 1990).
- [130] L. Allen, S. M. Barnett, and M. J. Padgett, *Optical Angular Momentum* (IOP, Bristol, UK, 2003).
- [131] David L. Andrews, *Structured Light and Its Applications: An Introduction to Phase-Structured Beams and Nanoscale Optical Forces* (Academic Press, Amsterdam, NL, 2008).
- [132] Juan P. Torres and Lluís Torner, *Twisted Photons: Applications of Light With Orbital Angular Momentum* (Wiley-Vch Verlag, John Wiley and Sons, Weinheim, DE, 2011).
- [133] Alison M. Yao and Miles J. Padgett, “Orbital angular momentum: origins, behavior and applications,” *Adv. Opt. Photon.* **3**, 161–204 (2011).
- [134] Richard A. Beth, “Direct detection of the angular momentum of light,” *Phys. Rev.* **48**, 471 (1935).
- [135] Richard A. Beth, “Mechanical detection and measurement of the angular momentum of light,” *Phys. Rev.* **50**, 115–125 (1936).
- [136] A. H. S. Holbourn, “Angular momentum of circularly polarised light,” *Nature* **137**, 31–31 (1936).
- [137] Nello Carrara, “Torque and angular momentum of centimetre electromagnetic waves,” *Nature* **164**, 882–884 (1949).
- [138] P. J. Allen, “A radiation torque experiment,” *Am. J. Phys.* **34**, 1185–1192 (1966).
- [139] S. Carusotto, G. Fornaca, and E. Polacco, “Radiation beats and rotating systems,” *Nuov. Cim.* **53**, 87–97 (1968).
- [140] Soo Chang and Sang Soo Lee, “Optical torque exerted on a homogeneous sphere levitated in the circularly polarized fundamental-mode laser beam,” *J. Opt. Soc. Am. B* **2**, 1853–1860 (1985).
- [141] K. S. Vul’fson, “Angular momentum of electromagnetic waves,” *Sov. Phys. Usp.* **30**, 667–674 (1987).
- [142] M. Kristensen, M. W. Beijersbergen, and J. P. Woerdman, “Angular momentum and spin-orbit coupling for microwave photons,” *Opt. Commun.* **104**, 229–233 (1994).
- [143] H. He, M. E. J. Friese, N. R. Heckenberg, and H. Rubinsztein-Dunlop, “Direct observation of transfer of angular momentum to absorptive particles from a laser beam with a phase singularity,” *Phys. Rev. Lett.* **75**, 826–829 (1995).
- [144] M. E. J. Friese, J. Enger, H. Rubinsztein-Dunlop, and N. R. Heckenberg, “Optical angular-momentum transfer to trapped absorbing particles,” *Phys. Rev. A* **54**, 1593–1596 (1996).
- [145] H. Then and B. Thidé, “Mechanical properties of the radio frequency field emitted by an antenna array,” (2008), arXiv.org:0803.0200 [physics.class-ph].
- [146] K. Helmersen, M. F. Andersen, P. Cladé, V. Natarajan, W. D. Phillips, A. Ramanathan, C. Ryu, and A. Vaziri, “Vortices and persistent currents: Rotating a Bose-Einstein condensate using photons with orbital angular momentum,” *Topologica* **2**, 002–1–002–12 (2009).
- [147] Miles Padgett and Richard Bowman, “Tweezers with a twist,” *Nature Phys.* **5**, 343–348 (2011).
- [148] A. Ramanathan, K. C. Wright, S. R. Muniz, M. Zelan, W. T. Hill, C. J. Lobb, K. Helmersen, W. D. Phillips, and G. K. Campbell, “Superflow in a toroidal Bose-Einstein condensate: An atom circuit with a tunable weak link,” *Phys. Rev. Lett.* **106**, 130401 (2011).
- [149] Nicholas M. Elias, II, “Photon orbital angular momentum and torque metrics for single telescopes and interferometers,” *Astron. Astrophys.* **541**, A101 (2012).
- [150] Olivier Emile, Christian Brousseau, Janine Emile, Ronan Niemiec, Kouroch Madhjoubi, and Bo Thidé, “Electromagnetically induced torque on a large ring in the microwave range,” *Phys. Rev. Lett.* **112**, 053902(4) (2014).
- [151] B. Thidé, “Nonlinear physics of the ionosphere and LOIS/LOFAR,” *Plasma Phys. Contr. Fusion* **49**, B103–B107 (2007).
- [152] J. T. Mendonça, B. Thidé, J. E. S. Bergman, S. M. Mohammadi, B. Eliasson, W. Baan, and H. Then, “Photon orbital angular momentum in a plasma vortex,” (2008), arXiv.org:0804.3221 [physics.plasm-ph].
- [153] J. T. Mendonça, B. Thidé, and H. Then, “Stimulated Raman and Brillouin backscattering of collimated beams carrying orbital angular momentum,” *Phys. Rev. Lett.* **102**, 185005(4) (2009).
- [154] F. Tamburini, A. Sponselli, B. Thidé, and J. T. Mendonça, “Photon orbital angular momentum and mass in a plasma vortex,” *Europhys. Lett.* **90**, 45001 (2010).
- [155] F. Tamburini and B. Thidé, “Storming Majorana’s Tower with OAM states of light in a plasma,” *Europhys. Lett.* **96**, 64005 (2011).
- [156] J. T. Mendonça, “Twisted waves in a plasma,” *Plasma Phys. Contr. Fusion* **54**, 124031 (2012).
- [157] M. Ibanescu, Y. Fink, S. Fan, E. L. Thomas, and J. D. Joannopoulos, “An all-dielectric coaxial waveguide,” *Science* **289**, 415–419 (2000).
- [158] A. N. Alexeyev, T. Fadeyeva, A. V. Volyar, and M. S. Soskin, “Optical vortices and the flow of their angular momentum in a multimode fiber,” *Semicond. Phys. Quant. Electron. Optoelectron.* **1**, 82–89 (1998).
- [159] Charles Brunet, Pravin Vaity, Younès Messaddeq, Sophie LaRochelle, and Leslie A. Rusch, “Design, fabrication and validation of an OAM fiber supporting 36 states,” *Opt. Express* **22**, 26117–26127 (2014).
- [160] R. de Melo e Souza, M. V. Cougo-Pinto, C. Farina, and M. Moriconi, “Multipole radiation fields from the Jefimenko equation for the magnetic field and the Panofsky-Phillips equa-

- tion for the electric field,” *Am. J. Phys.* **77**, 67–72 (2009).
- [161] Julius Adams Stratton, *Electromagnetic Theory* (McGraw-Hill Book Co., New York, NY, USA, 1941).
- [162] Wolfgang K. H. Panofsky and Melba Phillips, *Classical Electricity and Magnetism*, 2nd ed. (Addison-Wesley Publishing Company, Reading, MA, USA, 1962).
- [163] Oleg D. Jefimenko, *Electricity and Magnetism. An introduction to the theory of electric and magnetic fields* (Appleton-Century-Crofts, New York, NY, USA, 1966).
- [164] Mark A. Heald and Jerry B. Marion, *Classical Electromagnetic Radiation*, 3rd ed. (Saunders College Publishing, Fort Worth, TX, USA, 1995).
- [165] B. Thidé, J. Lindberg, H. Then, and F. Tamburini, “Linear and angular momentum of electromagnetic fields generated by an arbitrary distribution of charge and current densities at rest,” (2010), arXiv.org:1001.0954 [physics.class-ph].
- [166] B. Thidé, F. Tamburini, H. Then, C. G. Someda, E. Mari, G. Parisi, F. Spinello, and F. Romanato, “Angular momentum radio,” in *Complex Light and Optical Forces VIII*, Proceedings of SPIE, Vol. 8999, The International Society for Optical Engineering (SPIE, San Francisco, CA, USA, 2014) pp. 89990B–89990B–11.
- [167] José A. Heras, “Radiation fields of a dipole in arbitrary motion,” *Am. J. Phys.* **62**, 1109–1115 (1994).
- [168] Konstantin Y. Bliokh, Aleksandr Y. Bekshaev, and Franco Nori, “Dual electromagnetism: helicity, spin, momentum and angular momentum,” *New J. Phys.* **15**, 033026 (2013).
- [169] Arthur Stanley Eddington, *The Nature of the Physical World* (Kessinger Publishing, 2010).
- [170] H. Dieter Zeh, *The Physical Basis of The Direction of Time*, 4th ed. (Springer, 2001).
- [171] John Archibald Wheeler and Wojciech Hubert Zurek, eds., *Quantum Theory and Measurement*, Princeton Legacy Library (Princeton University Press, Princeton, NJ, USA, 2014).
- [172] G. H. Brown, “Turnstile aerials,” *Electronics* **9**, 14–17 (1936).
- [173] Carlo G. Someda, *Electromagnetic Waves*, 2nd ed. (CRC, Boca Raton, FL, USA, 2006).
- [174] Matt M. Coles, Mathew D. Williams, Kamel Saadi, David S. Bradshaw, and David L. Andrews, “Chiral nanoemitter array: A launchpad for optical vortices,” *Laser & Photon. Rev.* **7**, 1088–1092 (2013).
- [175] Mathew D. Williams, Matt M. Coles, David S. Bradshaw, and David L. Andrews, “Direct generation of optical vortices,” *Phys. Rev. A* **89**, 033837 (2014).
- [176] N. Gagnon, A. Petosa, and D.A. McNamara, “Thin microwave quasi-transparent phase-shifting surface (PSS),” *IEEE Trans. Ant. Prop.* **58**, 1193–1201 (2010).
- [177] M.A. Salem and C. Caloz, “Precision orbital angular momentum (OAM) multiplexing communication using a metasurface,” in *2013 7th International Congress on Advanced Electromagnetic Materials in Microwaves and Optics (METAMATERIALS)* (2013) pp. 94–96.
- [178] Li Cheng, Wei Hong, and Zhang-Cheng Hao, “Generation of electromagnetic waves with arbitrary orbital angular momentum modes,” *Sci. Rep.* **4** (2014), 10.1038/srep04814.
- [179] Xinlu Gao, Shanguo Huang, Yongfeng Wei, Wensheng Zhai, Wenjing Xu, Shan Yin, Jing Zhou, and Wanyi Gu, “An orbital angular momentum radio communication system optimized by intensity controlled masks effectively: Theoretical design and experimental verification,” *Appl. Phys. Lett.* **105**, 241109 (2014).
- [180] Peter Schemmel, Giampaolo Pisano, and Bruno Maffei, “Modular spiral phase plate design for orbital angular momentum generation at millimetre wavelengths,” *Opt. Express* **22**, 14712–14726 (2014).
- [181] Nanfang Yu and Federico Capasso, “Flat optics with designer metasurfaces,” *Nature Mater.* **13**, 139–150 (2014).
- [182] X. Hui, S. Zheng, Y. Hu, C. Xu, X. Jin, H. Chi, and X. Zhang, “Ultralow reflectivity spiral phase plate for generation of millimeter-wave OAM beam,” *IEEE Ant. Wirel. Prop. Letter.* **14**, 966–969 (2015).
- [183] Juan P. Treviño, Omar López-Cruz, and Sabino Chávez-Cerda, “Segmented vortex telescope and its tolerance to diffraction effects and primary aberrations,” *Opt. Express* **52**, 081605–081605 (2013).
- [184] A. Bennis, R. Niemiec, C. Brousseau, K. Mahdjoubi, and O. Emile, “Flat plate for OAM generation in the millimeter band,” in *7th European Conference on Antennas and Propagation (EuCAP)* (2013) pp. 3203–3207.
- [185] Mario Krenn, Robert Fickler, Matthias Fink, Johannes Handsteiner, Mehul Malik, Thomas Scheidl, Rupert Ursin, and Anton Zeilinger, “Communication with spatially modulated light through turbulent air across Vienna,” *New J. Phys.* **16**, 113028 (2014).
- [186] Joerg Bochmann, Amit Vainsencher, David D. Awschalom, and Andrew N. Cleland, “Nanomechanical coupling between microwave and optical photons,” *Nature Phys.* **9**, 712–716 (2013).
- [187] H. Shi and M. Bhattacharya, “Mechanical memory for photons with orbital angular momentum,” *J. Phys. B: Atom. Mol. Opt. Phys.* **46**, 151001 (2013).
- [188] H. Shi and M. Bhattacharya, “Coupling a small torsional oscillator to large optical angular momentum,” *J. Mod. Opt.* **60**, 382–386 (2013).
- [189] R. W. Andrews, R. W. Peterson, T. P. Purdy, K. Cicak, R. W. Simmonds, C. A. Regal, and K. W. Lehnert, “Bidirectional and efficient conversion between microwave and optical light,” *Nature Phys.* **10**, 321–326 (2014).
- [190] M. Aspelmeyer, S. Gröblacher, K. Hammerer, and N. Kiesel, “Quantum optomechanics—throwing a glance,” *J. Opt. Soc. Am. B* **27**, A189 (2010).
- [191] Markus Aspelmeyer, Tobias J. Kippenberg, and Florian Marquardt, “Cavity optomechanics,” *Rev. Mod. Phys.* **86**, 1391–1452 (2014).
- [192] T. Bagci, A. Simonsen, S. Schmid, L. G. Villanueva, E. Zeuthen, J. Appel, J. M. Taylor, A. Sørensen, K. Usami, A. Schliesser, and E. S. Polzik, “Optical detection of radio waves through a nanomechanical transducer,” *Nature* **507**, 81–85 (2014).
- [193] Keye Zhang, Francesco Bariani, Ying Dong, Weiping Zhang, and Pierre Meystre, “Proposal for an optomechanical microwave sensor at the subphoton level,” *Phys. Rev. Lett.* **114**, 113601 (2015).
- [194] Pradip Kumar Mondal, Bimalendu Deb, and Sonjoy Majumder, “Angular momentum transfer in interaction of Laguerre-Gaussian beams with atoms and molecules,” *Phys. Rev. A* **89**, 063418 (2014).
- [195] S. A. Wolf, D. D. Awschalom, R. A. Buhrman, J. M. Daughton, S. von Molnár, M. L. Roukes, A. Y. Chtchelkanova, and D. M. Treger, “Spintronics: A spin-based electronics vision for the future,” *Science* **294**, 1488–1495 (2001).
- [196] Shuichi Murakami, Naoto Nagaosa, and Shou-Cheng Zhang, “Dissipationless quantum spin current at room temperature,” *Science* **301**, 1348–1351 (2003).
- [197] Jairo Sinova, Dimitrie Culcer, Q. Niu, N. A. Sinitsyn, T. Jungwirth, and A. H. MacDonald, “Universal intrinsic spin hall effect,” *Phys. Rev. Lett.* **92**, 126603 (2004).
- [198] Igor Žutić, Jaroslav Fabian, and S. Das Sarma, “Spintronics: Fundamentals and applications,” *Rev. Mod. Phys.* **76**, 323–410

- (2004).
- [199] Alina M. Deac, Akio Fukushima, Hitoshi Kubota, Hiroki Maehara, Yoshishige Suzuki, Shinji Yuasa, Yoshinori Nagamine, Koji Tsunekawa, David D. Djayaprawira, and Naoki Watanabe, “Bias-driven high-power microwave emission from MgO-based tunnel magnetoresistance devices,” *Nature Phys.* **4**, 803–809 (2008).
- [200] B. Andrei Bernevig, Taylor L. Hughes, and Shou-Cheng Zhang, “Orbitronics: The intrinsic orbital current in *p*-doped silicon,” *Phys. Rev. Lett.* **95**, 066601 (2005).
- [201] A. Dussaux, B. Georges, J. Grollier, V. Cros, A. V. Khvalkovskiy, A. Fukushima, M. Konoto, H. Kubota, K. Yakushiji, S. Yuasa, K. A. Zvezdin, K. Ando, and A. Fert, “Large microwave generation from current-driven magnetic vortex oscillators in magnetic tunnel junctions,” *Nature Commun.* **1**, 8 (2010).
- [202] Andrei Kirilyuk, Alexey V. Kimel, and Theo Rasing, “Ultrafast optical manipulation of magnetic order,” *Reviews of Modern Physics* **82**, 2731–2784 (2010).
- [203] I. V. Tokatly, “Orbital momentum Hall effect in *p*-doped graphane,” *Phys. Rev. B* **82**, 161404 (2010).
- [204] S. S. Verma, “Atomtronics trying to replace Electronics,” *Electronics For You* **43**, 60–64 (2011).
- [205] Sadamichi Maekawa, Hiroto Adachi, Ken-ichi Uchida, Jun’ichi Ieda, and Eiji Saitoh, “Spin current: Experimental and theoretical aspects,” *J. Phys. Soc. Japan* **82**, 102002 (2013).
- [206] Fabio Stucchi Vannucchi, Áurea Rosas Vasconcellos, and Roberto Luzzi, “Emission of monochromatic microwave radiation from a nonequilibrium condensation of excited magnons,” *Appl. Phys. Lett.* **103**, 072401 (2013).
- [207] Peng Yan, Akashdeep Kamra, Yunshan Cao, and Gerrit E. W. Bauer, “Angular and linear momentum of excited ferromagnets,” *Phys. Rev. B* **88**, 144413 (2013).
- [208] Arne Brataas and Kjetil M. D. Hals, “Spin-orbit torques in action,” *Nature Nanotech.* **9**, 86–88 (2014).
- [209] Timo Kuschel and Günter Reiss, “Spin orbitronics: Charges ride the spin wave,” *Nature Nanotech.* **10**, 22–24 (2015).
- [210] Andreas Vogel, Michael Martens, Markus Weigand, and Guido Meier, “Signal transfer in a chain of stray-field coupled ferromagnetic squares,” *Appl. Phys. Lett.* **99**, 042506 (2011).
- [211] Masahito Mochizuki, “Spin-wave modes and their intense excitation effects in skyrmion crystals,” *Phys. Rev. Lett.* **108**, 017601 (2012).
- [212] J. F. Pulecio, P. Warnicke, S. D. Pollard, D. A. Arena, and Y. Zhu, “Coherence and modality of driven interlayer-coupled magnetic vortices,” *Nature Commun.* **5** (2014), 10.1038/ncomms4760.
- [213] G. F. Quinteiro and J. Berakdar, “Electric currents induced by twisted light in quantum rings,” *Opt. Express* **17**, 20465–20475 (2009).
- [214] K. Köksal and J. Berakdar, “Charge-current generation in atomic systems induced by optical vortices,” *Phys. Rev. A* **86**, 063812 (2012).
- [215] J. V. Nieminen, O. Vänskä, I. Tittonen, S. W. Koch, and M. Kira, “Accessing orbital angular momentum of quantum-ringing excitons via directional semiconductor luminescence,” *New J. Phys.* **17**, 033046 (2015).
- [216] H. Nyquist, “Certain topics in telegraph transmission theory,” *AIEE Trans.* **47**, 617–644 (1928).
- [217] C.E. Shannon, “Communication in the presence of noise,” *Proceedings of the IRE* **37**, 10–21 (1949), 05728.
- [218] A.J. Jerri, “The Shannon sampling theorem—its various extensions and applications: A tutorial review,” *Proc. IEEE* **65**, 1565–1596 (1977).
- [219] H. Then, B. Thidé, J. T. Mendonça, T. D. Carozzi, J. E. S. Bergman, W. A. Baan, S. Mohammadi, and B. Eliasson, “Detecting orbital angular momentum in radio signals,” (2008), arXiv.org:0805.2735 [astro-ph].
- [220] J. Sjöholm and K. Palmer, *Angular Momentum of Electromagnetic Radiation. Fundamental physics applied to the radio domain for innovative studies of space and development of new concepts in wireless communications*, Master’s thesis, Uppsala University, Uppsala, SE (2009), arXiv.org:0905.0190 [physics.class-ph].
- [221] Siavoush M. Mohammadi, Lars K. S. Daldorff, Jan E. S. Bergman, Roger L. Karlsson, Bo Thidé, Kamyar Forozesh, and Tobia D. Carozzi, “Orbital angular momentum in radio—a system study,” *IEEE Trans. Ant. Prop.* **58**, 565–572 (2010).
- [222] O. Edfors and A.J. Johansson, “Is orbital angular momentum (OAM) based radio communication an unexploited area?” *IEEE Trans. Ant. Prop.* **60**, 1126–1131 (2012).
- [223] Lingling Huang, Xianzhong Chen, Holger Mühlenbernd, Guixin Li, Benfeng Bai, Qiaofeng Tan, Guofan Jin, Thomas Zentgraf, and Shuang Zhang, “Dispersionless phase discontinuities for controlling light propagation,” *Nano Lett.* **12**, 5750–5755 (2012).
- [224] A. Tennant and B. Allen, “Generation of OAM radio waves using circular time-switched array antenna,” *Electron. Lett.* **48**, 1365–1366 (2012).
- [225] Qiang Bai, A. Tennant, B. Allen, and M.U. Rehman, “Generation of orbital angular momentum (OAM) radio beams with phased patch array,” in *Antennas and Propagation Conference (LAPC), 2013 Loughborough* (2013) pp. 410–413.
- [226] M. Barbuto, A. Toscano, and F. Bilotti, “Single patch antenna generating electromagnetic field with orbital angular momentum,” in *2013 IEEE Antennas and Propagation Society International Symposium (APSURSI)* (2013) pp. 1866–1867.
- [227] Changjiang Deng, Wenhua Chen, Zhijun Zhang, Yue Li, and Zhenghe Feng, “Generation of OAM radio waves using circular Vivaldi antenna array,” *Int. J. Ant. Prop.* **2013** (2013), 10.1155/2013/847859.
- [228] Xinlu Gao, Shanguo Huang, Jing Zhou, Yongfeng Wei, Chao Gao, Xukai Zhang, and Wanyi Gu, “Generating, multiplexing/demultiplexing and receiving the orbital angular momentum of radio frequency signals using an optical true time delay unit,” *J. Opt.* **15**, 105401 (2013).
- [229] Zhengyi Li, Y. Ohashi, and K. Kasai, “Quasi-LoS MIMO wireless communication with twisted radio wave,” in *Microwave Conference (EuMC), 2013 European* (2013) pp. 577–580.
- [230] H. Weber, “Angular momentum of low frequency electromagnetic fields,” *Optik—Intern. J. Light Electron Opt.* **124**, 4313–4314 (2013).
- [231] Q. Bai, A. Tennant, and B. Allen, “Experimental circular phased array for generating OAM radio beams,” *Electron. Lett.* **50**, 1414–1415 (2014).
- [232] Mirko Barbuto, Fabrizio Trotta, Filiberto Bilotti, and Alessandro Toscano, “Circular polarized patch antenna generating orbital angular momentum,” *Progr. Electromagn. Res.* **148**, 23–30 (2014).
- [233] E. Cano, B. Allen, Qiang Bai, and A. Tennant, “Generation and detection of OAM signals for radio communications,” in *Antennas and Propagation Conference (LAPC), 2014 Loughborough* (2014) pp. 637–640.
- [234] K.A. Opare and Yujun Kuang, “Performance of an ideal wireless orbital angular momentum communication system using multiple-input multiple-output techniques,” in *2014 International Conference on Telecommunications and Multimedia (TEMU)* (2014) pp. 144–149.

- [235] Xudong Bai, Ronghong Jin, Liang Liu, Junping Geng, and Xianling Liang, "Generation of OAM radio waves with three polarizations using circular horn antenna array," *Int. J. Ant. Prop.* **2015**, e132549 (2015).
- [236] Kwasi A. Opare, Yujun Kuang, Jerry J. Kponyo, Kenneth S. Nwizege, and Zhang Enzhan, "The degrees of freedom in wireless line-of-sight OAM multiplexing systems using a circular array of receiving antennas," in *2015 Fifth International Conference on Advanced Computing Communication Technologies (ACCT)* (2015) pp. 608–613.
- [237] Kang Liu, Yongqiang Cheng, Zhaocheng Yang, Hongqiang Wang, Yuliang Qin, and Xiang Li, "Orbital-angular-momentum-based electromagnetic vortex imaging," *IEEE Ant. Wirel. Prop. Lett.* **14**, 711–714 (2015).
- [238] Yohai Roichman, Bo Sun, Yael Roichman, Jesse Amato-Grill, and David G. Grier, "Optical forces arising from phase gradients," *Phys. Rev. Lett.* **100**, 013602(4) (2008).
- [239] Gregorius C. G. Berkhout, Martin P. J. Lavery, Johannes Courtial, Marco W. Beijersbergen, and Miles J. Padgett, "Efficient sorting of orbital angular momentum states of light," *Phys. Rev. Lett.* **105**, 153601(4) (2010).
- [240] Siavoush M. Mohammadi, Lars K. S. Daldorff, Kamyar Forozesh, Bo Thidé, Jan E. S. Bergman, Brett Isham, Roger Karlsson, and T. D. Carozzi, "Orbital angular momentum in radio: Measurement methods," *Radio Sci.* **45**, RS4007 (2010).
- [241] Martin P. J. Lavery, David J. Robertson, Anna Sponselli, Johannes Courtial, Nicholas K. Steinhoff, Glenn A. Tyler, Alan E. Willner, and Miles J. Padgett, "Efficient measurement of an optical orbital-angular-momentum spectrum comprising more than 50 states," *New J. Phys.* **15**, 013024(7) (2013).
- [242] J. Wang, J. Y. Yang, I. M. Fazal, N. Ahmed, Y. Yan, B. Shamee, A. E. Willner, K. Birnbaum, J. Choi, and B. Erkmen, "Demonstration of 12.8-bit/s/hz spectral efficiency using 16-QAM signals over multiple orbital-angular-momentum modes," in *Optical Communication (ECOC), 2011 37th European Conference and Exhibition on* (2011) pp. 1–3.
- [243] Fabrizio Tamburini, Bo Thidé, Elettra Mari, Giuseppe Parisi, Fabio Spinello, Matteo Oldoni, Roberto A. Ravanelli, Piero Coassini, Carlo G. Someda, and Filippo Romanato, " N -tupling the capacity of each polarization state in radio links by using electromagnetic vorticity," (2013), arXiv.org:1307.5569 [physics.optics].
- [244] Francis E. Low, *Classical Field Theory. Electromagnetism and Gravitation* (John Wiley & Sons, New York, NY, USA, 1997).
- [245] Nuri Ünal, "A simple model of the classical *Zitterbewegung*: Photon wave function," *Found. Phys.* **27**, 731–746 (1997).
- [246] Donald H. Kobe, "*Zitterbewegung* of a photon," *Phys. Lett. A* **253**, 7–11 (1999).
- [247] C. C. Leary and Karl H. Smith, "Unified dynamics of electrons and photons via *Zitterbewegung* and spin-orbit interaction," *Phys. Rev. A* **89**, 023831–1–11 (2014).
- [248] A. Einstein and W. J. deHaas, "Experimental proof of the existence of Ampère's molecular currents," *Proc. Kon. Akad. Wetensch. Amsterdam* **18**, 696–708 (1915).
- [249] Michael R. Andrews, Partha P. Mitra, and Robert deCarvalho, "Tripling the capacity of wireless communications using electromagnetic polarization," *Nature* **409**, 316–318 (2001).
- [250] R. Essiambre and R. W. Tkach, "Capacity trends and limits of optical communication networks," *Proc. IEEE* **100**, 1035–1055 (2012).
- [251] S. O. Arik, D. Askarov, and J. M. Kahn, "Effect of mode coupling on signal processing complexity in mode-division multiplexing," *J. Lightw. Technol.* **31**, 423–431 (2013).
- [252] F. Tamburini, B. Thidé, V. Boaga, F. Carraro, M. del Pup, A. Bianchini, C. G. Someda, and F. Romanato, "Experimental demonstration of free-space information transfer using phase modulated orbital angular momentum radio," (2013), arXiv.org:1302.2990 [physics.class-ph].
- [253] Ivan Fernandez-Corbaton, Xavier Zambrana-Puyalto, and Gabriel Molina-Terriza, "Helicity and angular momentum: A symmetry-based framework for the study of light-matter interactions," *Phys. Rev. A* **86**, 042103 (2012).
- [254] T. G. Philbin, "Lipkin's conservation law, Noether's theorem, and the relation to optical helicity," *Phys. Rev. A* **87**, 043843 (2013).
- [255] In certain disciplines a non-standard convention is sometimes used in which the term Lorentz force density denotes only the second term in the RHS of Eqn. (A14b). We follow the standard convention.
- [256] S. J. van Enk and G. Nienhuis, "Commutation rules and eigenvalues of spin and orbital angular momentum of radiation fields," *J. Mod. Opt.* **41**, 963–977 (1994).
- [257] In fact, the surface integral may also be a vector that is (at most) a function of time t .
- [258] See in particular Section V.5: "Daniel Bernoulli and Euler on the Dependence or Independence of the Law of Moment of Momentum in 1744."
- [259] Dwight E. Neuenschwander, *Emmy Noether's Wonderful Theorem* (Johns Hopkins University Press, Baltimore, MD, 2011).
- [260] Konstantin Y. Bliokh, Justin Dressel, and Franco Nori, "Conservation of the spin and orbital angular momenta in electromagnetism," *New J. Phys.* **16**, 093037 (2014).
- [261] E. Leader, "The angular momentum controversy: What's it all about and does it matter?" *Phys. Part. Nucl.* **44**, 926–929 (2013).
- [262] Iwo Białynicki-Birula and Zofia Białynicka-Birula, "Canonical separation of angular momentum of light into its orbital and spin parts," *J. Opt.* **13**, 064014 (2011).
- [263] L. Allen, M. J. Padgett, and M. Babiker, "The orbital angular momentum of light," in *Prog. Opt.*, Vol. XXXIX, edited by E. Wolf (Elsevier, Amsterdam, Holland, 1999) pp. 291–372.
- [264] Sonja Franke-Arnold, Stephen M. Barnett, Eric Yao, Jonathan Leach, Johannes Courtial, and Miles Padgett, "Uncertainty principle for angular position and angular momentum," *New J. Phys.* **6**, 1–8 (2004).
- [265] Gabriel Molina-Terriza, Juan P. Torres, and Lluís Torner, "Twisted photons," *Nature Phys.* **3**, 305–310 (2007).
- [266] Timothy H. Boyer, "Illustrations of the relativistic conservation law for the center of energy," *Am. J. Phys.* **73**, 953–961 (2005).